UNIVERSIDADE
BEIRA INTERIOR

Numerical Analysis of a Single Droplet Combustion: Jet-A1, N-Dodecane, N-Hexadecane

(Versão corrigida após defesa)

Francisco José Ramos Dias

Tese para obtenção de grau de Mestre em
Engenharia Aeronáutica
(ciclo de estudos integrado)

Orientador: Prof. Doutor André Resende Rodrigues da Silva

Covilhã, Abril de 2022

Acknowledgements

Firstly, I would like to thank my supervisor, Professor André Resende Rodrigues da Silva, for his valuable guidance and support throughout the development of this research. His motivation and enthusiasm allowed the performance of this research with interest and rigor. I feel grateful for having the opportunity to develop my dissertation in AEROG - Aeronautics, and Astronautics Research Center, which allowed knowledge acquisition to perform and conclude the dissertation. Furthermore, I would like to thank my colleagues of AEROG, Sullivan Gonçalves, Daniela Ribeiro, and Daniel Rodrigues, for the countless hours passing in joyful times and helping the improvement of the learning process that further allowed the finalization of this dissertation. I would like to be especially grateful to Inês Ferrão, who aided me throughout all the research steps, trying its best to help me concerning every doubt that could have originated throughout this research. Without her help, the main goals of this dissertation investigation would reveal much more complicated tasks. I also would like to thank all my friends that I have met during my university life with whom I had the most memorable and enjoyable moments. Due to the contribution of these people, the student life was an enriching experience and a period that allows the formation of durable and strong friendships. Lastly, I would like to thank all my family members who believed in my skills and helped me in the most variable ways during this academic period. I would like to thank my girlfriend, parents, and grandparents for their persistence and guidance, which carried immense importance in my life.

Resumo

As preocupações relativamente ao planeta Terra e os seus recursos naturais têm vindo a aumentar nas últimas décadas. A dependência de combustíveis fósseis provocou um problema delicado, visto que o transporte atualmente é essencialmente abastecido por fontes de energia tradicionais e não sustentáveis. A crise climática originada devido à utilização de combustíveis fósseis exige ações da humanidade, especificamente no que se refere à pesquisa de formas inovadoras de abastecer os atuais meios de transporte. A implementação de biocombustíveis nos transportes atuais, desperta o interesse dos cientistas e engenheiros como uma opção viável entre os distintos possíveis caminhos para se desenvolver opções de combustíveis sustentáveis. O estudo de fenómenos como a injeção, a colisão de gotas, a evaporação e a combustão permite a melhoria das características de queima de um determinado combustível dentro da câmara de combustão, porém o estudo da combustão e da evaporação revela ser a forma mais eficiente para reduzir as emissões e melhorarando significativamente o desempenho da queima.

Este estudo pretende simular numericamente a evaporação e combustão de gotículas de combustível dentro de um forno tubular com capacidade de variar a temperatura ambiente. A abordagem numérica simplifica os fenómenos físicos, empregando uma abordagem Euler-Lagrange realizada com auxílio de um *software* de Dinâmica de Fluidos Computacional (DFC). A fase contínua é calculada recorrendo a um modelo de turbulência, enquanto a fase dispersa é calculada separadamente utilizando um modelo de fase discreta. O cálculo do fenómeno de combustão está profundamente relacionado à evaporação da fase discreta empregando posteriormente o modelo de combustão fornecida pelo *software* utilizado. Adicionalmente, existe uma simplificação 2D do domínio e a respetiva discretização das equações matemáticas em conformidade com o acoplamento pressão-velocidade do modelo numérico.

Neste trabalho o fenómeno de queima de gotas é simulado para gotas isoladas de n-dodecano, jet fuel e n-hexadecano. Os resultados obtidos relativamente à evolução temporal do diâmetro da gota mostram concordância com a lei d^2 e respetivos dados obtidos experimentalmente. Os resultados adquiridos também permitem uma correlação das características da combustão e a dinâmica das gotas, apresentando uma redução entre velocidade das gotas e a respetiva redução do diâmetro das gotas. Esta relação ocorre para diferentes temperaturas do meio continuo e utilizando diferentes combustíveis, sugerindo uma associação física. Além dessa interpretação, a variação da velocidade inicial da gota não afeta os resultados das características de combustão. Durante o estudo é demonstrada uma relação entre a temperatura ambiente do forno tubular e a indução do processo de combustão bem como as propriedades de queima da gota. Além disso, as composições químicas dos combustíveis utilizados aparenta influenciar as características de combustão da gota e o seu desempenho global na câmara de combustão. De uma forma geral, a simulação numérica poderá ser optimizada em trabalhos futuros e aproximar a simulação ao fenómeno fisico, permitindo assim o desenvolvimento de conhecimentos nesta temática.

Palavras-chave

Combustíveis Alternativos, Jet Fuel, Combustão de Gota Isolada, Simulação Numérica, Euler-Lagrange

Abstract

There has been an increase in concerns about the planet earth and its resources throughout the past decades. The dependency on fossil fuels created a critical dilemma since transportation is currently fueled by traditional, not sustainable power sources. The originated climate crisis on fossil fuels demands action from mankind, specifically concerning the research on alternative ways of fueling the current methods of transportation. The implementation of Biofuels in transportation encourages future scientists and engineers as a realistic option among other different paths constructed to develop sustainable fuels. The study of the injection, impinging, evaporation, and combustion allows the improvement of the burning characteristics assuming a specific fuel within a combustion chamber. These investigations of the combustion and evaporation procedures improve the burning droplet performance and thus reduce the emitted emissions under the same circumstances.

This study intends to numerically simulate the single droplet evaporation and combustion of fuel droplets in a drop tube furnace (DTF) that has the capacity of varying the ambient temperature. The numerical approach simplifies the physical phenomena by employing an Eulerian-Lagrangian approach, considering a discrete and a continuous phase, which is further accomplished while running in a CFD software. The continuous phase is computed recurring to a turbulence modeling, while the dispersed phase is separately computed using the discrete phase model. The computation of the combustion phenomenon is deeply related to the evaporation of the discrete phase employing the non-premixed combustion provided by the operating software. There is a 2D planar simplification of the 3D axisymmetric experimental cylinder followed by the respective discretization of the mathematical equations and pressure-velocity coupling.

This work numerically simulates the burning phenomenon of n-dodecane, jet fuel, and n-hexadecane single droplets. The obtained results of the droplet size reduction relating to time display agreement with the d^2 law and respective experimentally obtained data. The acquired outcomes also allow the establishment of correlations between the combustion characteristics and the droplet physics properties, such as velocity, displaying a reduction of the droplet velocity alongside the shrink of the droplet diameter. This information is visible for different temperature environments and fuels, suggesting a physical association. Besides this interpretation, the imposed droplet initial velocity variations ($1.0\ m/s$ until $1.3\ m/s$) do not affect the combustion characteristics outcomes. This study demonstrates a precise relation between the ambient temperature of the drop tube furnace (DTF) and the improvement of the combustion process and burning properties. Additionally, the chemical composition of the fuels influences the combustion characteristics and their performances. Overall, the numerical performed simulation can be improved and thus approximate the implemented simulation to the occurring physical event, allowing the development of the additional knowledge in this thematic.

Keywords

Alternative Fuels, Jet Fuel, N-Alkanes, Single Droplet Combustion, Numerical Simulation, Eulerian–Lagrangian

Contents

List of Figures

List of Tables

Nomenclature

a	Sound Velocity Constant	[m/s]
A_{3D}	Inlet Area	[m^2]
A, B, C, D	Dependent Constants	[-]
B_q, $B_{o,q}$	Transfer, or Spalding Number	[-]
$C_{\varepsilon-3}$	Empirical Constant	[-]
C_μ, $C_{\varepsilon-1}$, $C_{\varepsilon-2}$	Dimensionless Model Constant	[-]
C_D	Drag Coefficient	[-]
C_g, C_d	Turbulent Combustion Model Constants	[-]
c_p	Specific Heat	[$J \cdot kg^{-1} \cdot K^{-1}$]
D_0	Initial Droplet Diameter	[mm]
d_p	Dispersed Phase Particle Diameter	[m]
E	Energy Transfer due to Conduction	[J]
f	Mixture Fraction	[-]
g	Gravity Acceleration	[m/s^2]
H	Instantaneous Enthalpy	[J/ Kg]
h	Sensible Enthalpy	[J/ Kg]
h_f	Heat of Vaporization	[J/Kg]
H_I	Height of the Inlet	[m]
I	Turbulent Intensity	[%]
I_w	Wobbe Index	[MJ/Nm^3]
$\overrightarrow{J_j}$	Diffusion Flux of Species	[mol m^{-2} s^{-1}]
K	Evaporation/Combustion Rate	[mm^2/s]
k	Thermal Conductivity	[$W/(m \cdot K)$]
k_{eff}	Effective Conductivity	[$W/(m \cdot K)$]
K_B	Basset Force Constant in Particle Momentum Equation	[-]
K_m	Virtual Mass Force Constant in Particle Momentum Equation	[-]
k_t	Turbulent Kinetic Energy	[m^2/s^2]
L_{ref}	Characteristic Length	[m]
l_e	Characteristic Dimension of an Eddy	[m]
$\dot{m}$	Mass Flow	[Kg/s]
m_p	Particle Mass	[Kg]
$n_{1:j}$	Unit vector of the Direction	[m]
Nu	Nusselt Number	[-]
p	Pressure	[atm]

Pr	Prandtl Number	[-]
Pr_t	Turbulent Prandtl Number	[-]
R	Correlation Coefficient	[-]
r_s	Droplet Radius	[m]
Re	Reynolds Number	[-]
Re_{D_H}	Hydraulic Reynolds Number for Tubular Geometries	[-]
s	Distance Between Droplets	[m]
S_m, $S_{\overline{U_i}}$, S_H, S_k, S_ε, S_ϕ, S_{user}	Interphase Source Terms	[-]
Sc	Schmidt Number	[-]
Sc_t	Turbulent Schmidt Number	[-]
Sh	Sherwood Number	[-]
T	Temperature	[K]
$\overline{T}$	Average Temperature of the Film	[K]
T_ω	Time Scale of the Considered PDF Function	[s]
t_{cm}	Time taken for the drop height to go from its maximum value of D_0 to 0	[s]
t_d	Droplet Lifetime	[s]
T_e	Eddy Lifetime	[s]
t_i	Amount of Time Considered in the Turbulent Analysis of Mixture Fraction	[s]
t_{ig}	Ignition Time	[s]
t_{int}	Eddy-Droplet Interaction Time	[s]
U_1, U_2	Random Sampled Velocities	[m/s]
U_T	Flow Friction Velocity	[m/s]
U,u	Velocity	[m/s]
$\dot{V}$	Volumetric Flow	[m^3/s]
y^+	Non-Dimensional Distance	[-]
y_p	Distance Between a Specific Mesh Cell Center and the Wall	[m]
Z	Elemental Mass Fraction	[-]
Z_T	Convenience evaporation Operator	[m · s /Kg]

Greek Letters

Γ	Effective Diffusion Coefficient
δ_{ij}	Kronecker Delta
Δ	Standard Variation
ε	Rate of Dissipation of Turbulent Kinetic Energy
ε_{ijk}	Third-order Tensor
μ	Dynamic Viscosity
μ_t	Turbulent Dynamic Viscosity
ρ	Volumetric Mass
$\sigma_k, \sigma_\varepsilon$	Turbulence Model Constants
τ_{eff}	Viscous Dissipation
τ_p	Droplet Relaxation Time
υ	Direction Versor Energy Equation
ϕ	Standard Property
ω	Angular Velocity

Subscripts

∞	Freestream or Far-Removed from Surface
0	Initial Condition
2D	2 Dimensional Geometry
3D	3 Dimensional Geometry
boil	Boiling Point
c	Continous Phase
d	Droplet
f	Flame
F	Fuel Vapour
g	Gas Phase
i, j, k,	Cartesian Versor
l	Liquid
m	Number of Hydrogen Atoms
n	Number of Carbon Atoms
Ox, ox	Oxidant
p	Particle
s	Surface
x, y, z	Cartesian Directions

Superscripts

$\overline{\cdot}$	Mean Averaged Value
$'$	Fluctuation

Acronyms and Abbreviations

2D	Two-Dimensional
3D	Three-Dimensional
AEROG	Aeronautics and Astronautics Research Center
ANSYS	Analysis of Systems
BW	Black and White
CAD	Computer Assisted Drawing
CCD	Charge-Coupled Device
CFD	Computer Fluid Dynamics
CHEMKIN	Chemical Kinetics
DFS	Deterministic Separated Flow
DPM	Discrete Phase Model
DPSF	Discrete Particle Separated Flow
DRW	Discrete Random Walk
DTF	Drop Tube Furnace
FAE	Fatty Acid Ester
FT	Fischer-Tropsch
HAP	Hazard Air Pollutants
HVO	Hydrotreated Vegetable Oil
IC	Internal Combustion
ICAO	International Civil Aviation Organization
JF	Jet Fuel
LCV	Lower Calorific Value
LHV	Lower heating value
PDF	Probability Density Function
QUICK	Quadratic Upstream Interpolation for Convective Kinetics
RF	Radiative Forcing
SG	Specific Gravity
SIMPLE	Semi-Implicit Method for Pressure-Linked Equations
SSF	Stochastic Separated Flow
UHC	Unburned Hydrocarbon
VOC	Volatile Organic Compounds
VOF	Volume of Fluid

Chapter 1

Introduction

The main aim of this dissertation is to numerically simulate the single droplet combustion phenomenon. The present chapter will present a brief introduction to the theme and the main motivations and objectives of this dissertation.

The first section of the chapter intends to introduce the motivations of the present study implemented throughout the dissertation. The second section enumerates the central objectives of this work, while the third exhibits the employed structure of this dissertation.

1.1 Motivation

Throughout the past decades, the concerns over the future of our planet and its resources have been increasing. Due to this fact, fossil fuels were assumed as a crucial concern within the world of transportation since they do not represent a sustainable way of leading the transport evolution. Therefore, the research on alternative possibilities to power the current transports fleet has been increasing to discover greener fuels that pollute less while performing the required tasks. However, the implementation of these alternatives brings several concerns about the economic viability of these fuels. Nonetheless, the pursuit of new ways of mitigating climate change and achieving carbon neutrality relies on scientific research, which will never end while is still an intention to continue on this path.

One of the biggest challenges of our generation is the achievement of carbon neutrality coupled with improving the environmental degradation of the atmosphere [1]. The nonrealization of this goal might indicate irreversible jeopardy to future generations. This problem may have been urged by the evident increase in dependency on fossil fuels by the air transportation fleet for the last 50 years [2]. The worldwide existing aircraft fleet suffered a substantial increase in order to comply with the demand of the current trade globalization. Hence, the majority of airlines searched for fuel options that could protrude a high energy efficiency while remaining relatively cheap. Then, jet fuel for most of the air services providers was the chosen option due to the affordable price and high energetic power, yet there is a substantial environmental impact associated with its utilization. Nowadays, pollutant emissions are originated from the utilization of derived fossil fuels, such as jet fuel. Specifically, the air industry predominantly fuelled by jet fuel is responsible for $2-3\ \%$ of global carbon emissions with a predicted growth of $4.7\ \%$ per year. The evident environmental damage demonstrates the demand of the current and future generations in the search for renewed sustainable forms of power the air mobility. Therefore, biofuels might be glimpsed as a reasonable alternative

to conventional fossil fuels. These alternative fuels have a sustainable feedstock provided by commonly vegetable or biomass sources [3]. The usage of these fuels in the aircraft industry demands previous certifications, which will verify if the fuel possesses the minimal requirements to be utilized in aviation. For instance, the alternative fuel should provide similar energy power to the minimal demand by the advisable aviation organizations [4]. Consequently, the employment of these fuels could be noticed as a complex infrastructure transformation, yet several advantages can be highlighted besides the beneficial environmental impact. The production of biofuels would require the development of additional agriculture activity, which could contribute to the development of weaker economies in fragile countries [5].

The alternative fuels are a plausible possibility for future utilization, highlighting the importance of guaranteeing their efficiency while powering the forthcoming aircraft fleet. For this reason, it is of paramount importance to research their behavior throughout the different processes within an aviation gas turbine. Innumerous processes define the combustion procedure in a combustion chamber. The fuel suffers injection, atomization, and evaporation until it starts the combustion phenomenon, which is among the ones that develop more interest in scientists. There had been experimental investigations that intended to assimilate more knowledge regarding this physical occurrence. However, the numerical studies are classified as a valuable complement to the information provided in the experimental researches. Through the numerical analyses, the phase equations are computed depicting the illustration of the physical phenomenon. Specifically, multiphase flows require the implementation of specific approaches that ensure an accurate representation of the replicated reality. The increased expense of the experimental facilities and the problematic conditions designed to be replicated in experimental facilities are, amidst other issues, factors that benefit the numerical research. Recently, an increase of scientific works aided the understatement of the physical phenomena of combustion. Pacheco et al. [6], and Ferrão et al. [7–9] aim to understand the combustion characteristics of falling droplets in a drop tube furnace (DTF). The fuels tested were jet fuel and biofuel mixtures to measure the impact of the emissions that result from the combustion processes of these fuels in the aviation sector [6]. In this respect, the present work aims to simulate numerically the single droplet combustion in the experimentally used drop tube furnace. The numerically obtained data is then compared to the experimental data, ensuring a well-balanced addition of information about this thematic. Therefore the work performed throughout this dissertation can be utilized as a valuable complement in the development of new alternatives to traditional fossil fuels, likewise, the investigations of Rodrigues [10], Abrantes [11], Ribeiro [12], Pinto [13] and Cardoso [14]

1.2 Objectives

The present work intends to simulate the phenomenon of single droplet combustion in a drop tube furnace numerically. Suitable implementations of multiphase models that characterize the combustion and evaporation of fuel droplets contribute to a more reasonable

understanding of the procedure. The objectives of this dissertation attempt to accurately simulate the phenomena supplied in Ferrão et al. [7–9] and Pacheco et al. [6] employing an Euler-Lagrange approach. Their experiments were performed in a drop tube furnace further replicated in a 2D representation of the domain. The accurate replication of the phenomena requires the fulfilling of the following purposes:

- Numerical simulation of the airflow conditions within the drop tube furnace;
- Validation and verification of the mathematical model and Euler-Lagrange approach respectively;
- Numerical simulation of the combustion of single fuel droplets of jet fuel and n-alkanes;
- Comparison between the numerical and the experimental results of the burning characteristics of the fuel droplets, in terms of the influence of ambient temperature, initial droplet velocity, and fuel chemical composition;

1.3 Overview

This dissertation comprises the following sections: Introduction, Literature Review, CFD Methodology, Results and Discussion, Conclusions and Future Work.

In the first and current chapter, there is an introduction to the structure of the dissertation. Through the motivation, it is introduced the interest in biofuels and their implication in reducing pollutant emissions. Additionally, the objectives related to the thesis investigation and the overview of the dissertation structure are mentioned.

The second section extensively exhibits the bibliography review concerning the usage of alternative fuels, the historical evolution of the droplet evaporation physics understanding, and further single droplet combustion experiments. Firstly, the seriousness of aviation emissions is remarked and the evident necessity of reducing their impact on the environment. This issue requires solutions that are studied and comprised with the gathered information concerning biofuels and their usage and benefits compared with traditional fossil fuels. Furthermore, a historical review of the phenomena associated with single droplet evaporation is detailed, in line with the physical events that concern the combustion of single droplets and its modeling. Succeeding the modeling description of evaporation and combustion, it is relevant to detail the different external influences associated with the single droplet phenomena. This exposition is performed through the specification of similar researches investigating single droplet evaporation and combustion.

The third chapter describes the physical concepts that support the replicated phenomenon occurring in the numerical simulation. Besides depicting the physical models associated with the reproduced process, there is a mathematical formulation of the domain and discretiza-

tion of the mathematical equations. Additionally, the CFD modeling requires the adoption of models that allow the approximation of reality through mathematical approaches and domain simplifications. This chapter depicts the approaches employed and the respective explicative accuracy in representing the physical phenomenon. Lastly, there is the corresponding grid independence analysis.

The fourth chapter presents the results of the numerical simulation. The obtained outcomes are extensively compared with the experimentally provided data in order to certify the accuracy of the implemental mathematical models. It is verified the obtained flow continuous phase, the droplet lifetime regarding the different implemented fuels, and respective analysis of the burning characteristics.

The final chapter presents the conclusions drawn through this research and the prospective future work regarding the theme of this dissertation.

Chapter 2

Literature Review

The current section describes a review of the most relevant information and studies concerning the degeneration of the environment due to fuel emissions and the usage of biofuels as a prospective solution to deal with the nowadays environmental concerns. This analysis is further coupled with a review focused on comparing the alternative biofuels with traditional fuels. Furthermore, it is specified the modeling of the droplet evaporation and combustion phenomena, with the consequent elaboration of a literature review regarding the combustion of single droplets for distinct environments and n-alkanes. In order to sustain the exhibited information, a historical review of this thematic is presented alongside describing the respective physical models. Subsequently, it is detailed the various external factors that could influence the characteristics of the analyzed phenomena while presenting investigation works regarding these single droplet events.

The importance of this work regarding the combustion emissions is correlated with the fact that studying the improvement of combustion characteristics of the single droplet phenomenon aids the consequent reduction of the process emissions.

2.1 Environmental impact of the aircraft emissions

The demand for aviation fuel is constantly increasing and has become apprehensive due to the depletion of fossil fuels. The utilization of petroleum sourced fuels as an energy source in the air transportation industry concerns an unsustainable alternative involving the shortage of environmental resources. This problem induced a reaction from humanity in aiming to reduce greenhouse and pollutant emissions since fossil fuels result in severe environmental damage, loss of environmental quality, and human life. However, the aviation industry accounts for a significant fraction of global carbon emissions, being portrayed as a sector that might assume a substantial implication on global warming alongside several environmental problems [3].

The pollutant emissions from the transportation industry carry relevance within the production of air pollution. Hence, several pollutants emitted from aircraft engines aid the damage increase in the air quality and consequent development of environmental issues. In addition, these pollutants potentially affect human health and the quality of life of the populations. The origin of these damaging pollutants is in the combustion procedure inside most gas turbines. The combustion process aims to produce energy through a chemical process that mixes air and fuel while igniting and burning in order to release heat. In reality, this process is not con-

sidered ideal, which provokes hundreds of intermediate reactions and multi-step procedures that will produce additional emissions. Figure 2.1 exhibits the preeminent emissions from aviation operations alongside the respective atmospheric processes that consequently lead to harming environment processes and climate change [15]. The products of ideal complete combustion are CO_2, water vapor, N_2, O_2, and SO_2, depending on the fuel composition, as depicted in Figure 2.1. Nevertheless, in most cases, the optimal combustion process does not exist, and additional products are considered, such as CO, UHC, soot, and complementary types of sulfur oxides (SO_2, SO_3, commonly named as SO_x) and nitrogen oxides (frequently referred to as NO_x). The non-ideal nature of most combustion procedures and the appearance of the additional toxic elements justify the pollutant nature of the combustion.

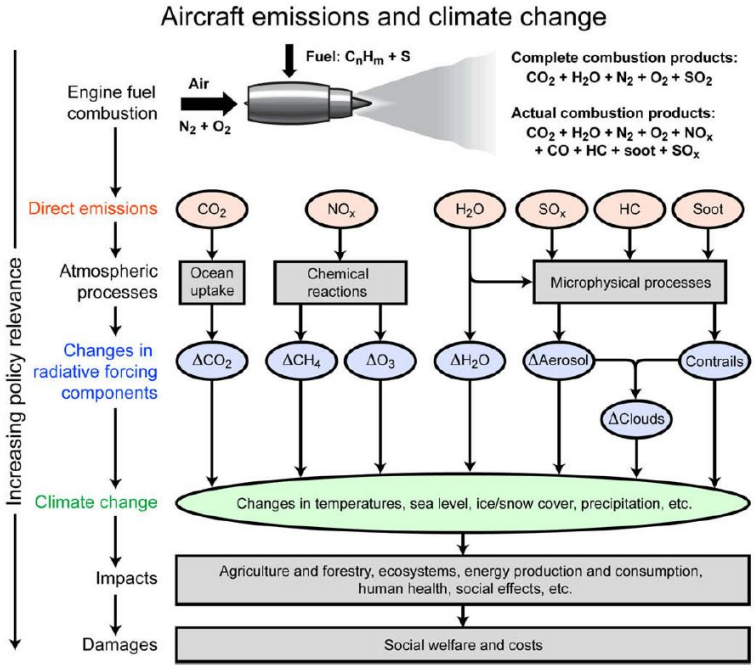

Figure 2.1: Schematic regarding the main processes related to the predominant emissions resulting from aircraft engine combustion. The Radiative Forcing measures may lead to changes in climate change as measured by temperatures and sea levels. Figure adapted from [1].

Organizations, such as ICAO (International Civil Aviation Organization) [16] intend to regulate the emissions on the local level making restrictions on the levels of NO_x, CO, UHC, and smoke. The task of reducing emissions is complex, and it appears like it will not possess a solution briefly. For instance, there is still a lack of regulations on aviation emissions, yet the international institutions and initiatives had been urged to implement supplementary legislation. However, there has been a growth in the concern regarding emission species that potentially can harm health and posses toxic impacts on the populations. These initiatives accomplished the implementation of additional efforts in establishing restrictions on the emissions of these pollutants. These species are commonly called HAPs (Hazard Air Pollutants), which are part of VOC (Volatile Organic Compounds) [17].

Regarding the environmental concerns, the working conditions of the combustion chamber

affect the production and emission of pollutants. In the literature, the variation of operating conditions such as the temperature of the combustion chamber, air-fuel ratios, speed of the engine (in the cases of IC engines), and type of mixture originate different values of emissions from the ones visualized in normal operating conditions [18, 19]. These studies report the possibility of reducing engine emissions by regulating the temperature of the combustion chamber and promoting blends of gasoline and biofuels, which are conceivable to control by the engineers. Ultimately, the emissions commonly emitted by combustion engines require specific analysis to understand how damaging they are to the environment.

Concerning the various types of emissions, it is relevant to notify and detail the particularities that distinguish the pollutants and their respective origins. Specifically, the impact of NO_x emissions on the environment carries some debatable questions on this topic since it is possible to find favorable and unfavorable consequences from NO_x emissions. Regarding the negative impacts, NO_x emissions (after the chemical reactions that will suffer) remain an active member of the formation of tropospheric ozone (O_3), proving the crucial role of NO_x emissions within the environmental degeneration. Nonetheless, the emissions of NO_x are also correlated to a long-term reduction in the lifetime of methane molecules (CH_4) through liberating OH radicals which reduce the lifetime of greenhouse gases such as methane [1]. Regardless, there are yet studies in the literature supporting the premise that NO_x emissions directly influence the reduction of air quality in several regions of the globe [20].

Concerning the emissions of CO_2, it is essential to remark that this pollutant is widely known for its contribution to the greenhouse effect. In addition, some studies and reports acknowledge the impact of the presence of CO_2 particles in the air and the damage that these emissions bring to the oceans, precipitation, and water quality supplies [21]. The excess of carbon dioxide in the atmosphere also results in several damages in the world sea life as well as a prime role in the acidification process of the oceans [22].

Conversely to common knowledge, water vapor yields importance on the increment of greenhouse effects. Even though the contribution of the water emission from the aviation sector is negligible compared to the influence of the natural hydrologic cycle of water, it might be considered as a subject in the contribution of the greenhouse effects and global warming [3]. The contribution is explained by the absorption and re-emission of the longwave radiation in the clouds formed by the contrails from the engine exhaust at high altitudes when the water crystalizes [23]. The water vapor relevance in the greenhouse effects has been increasing, which is supported by several studies in the literature [23].

UHCs and CO are pollutants that result from incomplete combustion. Due to maintaining the type of combustion more common in real life, these emissions will subsequently represent a big problem in atmospheric pollution. Moreover, these pollutants represent an active member in climate change, adding to the fact that their emission degrades the life span of the engine turbine. Currently, several strategies are implemented in the gas turbines to decrease the amount of these emissions. The implemented techniques could be regarding improving

the combustion performance or the installation of filtration devices that reduce the emitted amount of UHCs, and CO [24].

There are yet additional pollutants that generate negative impacts on the earth atmosphere. However, in order to analyze the overall effect considering the aggregation of emissions, the literature commonly recurs the concept of Radiative Forcing (RF). This notion measures the perturbation of the Earth-atmosphere energy budget since 1750, which results from changes in trace gases and particles in the atmosphere and other effects such as changed albedo. Regarding the conceptualization of the term, it can be classified as positive when it quantifies a net warming effect, whereas it could have negative values when it shows a cooling effect.

2.2 Liquid Fuels

As previously mentioned, greenhouse gas and pollutant emissions are deeply related to the aviation industry will induce global warming and environmental damage. For instance, in order to understand better this topic is necessary to remark the implication of the variety of fuels employed and thus examine the individual properties.

Consequently, the attribute that liquid fuels contain different properties indicates distinct outcomes of emissions. Concerning the properties of the liquid fuels and their different classification, it is possible to distinguish them by the predominance and the type of hydrocarbons possessed by brute oil [25]. Hence, the classifications attributed to a specific fuel besides its compounds will subsequently imply the level of emission that it will emit.

In particular, paraffinic components are considered a compound for the bulk of the clean fuels used in air transportation which implies the importance of their study. These saturated hydrocarbons are described by the formulae C_nH_{2n+2}. The paraffinic hydrocarbons are a primary component of natural gas, petroleum, low index octane gasoline, high-quality kerosene, and diesel with good combustion characteristics. Nevertheless, several studies reveal that paraffinic fuels can be glimpsed as a clean alternative [26]. Additionally, other characteristics certify paraffinic fuels as appealing, such as being high-quality fuels made from a wide variety of feedstocks, standing fungible, and the possibility of being utilized at any blending rates in current diesel engines. Hence, whenever it is considered the development of fuel alternatives, the usage of paraffins encourages the debate on this theme alongside further relevant researches [25].

Similar to paraffinic components, naphthenic hydrocarbons have relevant importance within the theme of fuel emissions. They stand as a classification of organic biomolecules composed of carbon and hydrogen, with the particularity of containing one or more saturated cyclic (ring) structures. These compounds have general formulae defined as C_nH_{2n}. For instance, naphthenic compounds are frequently called naphthenes, cycloparaffins, or hydrogenated benzenes. Naphtha is a refined petroleum fraction that contains a high percentage of naphthenics and gasoline with a high level of octane and asphaltic residues. Additionally, when

considering drilling fluids, particularly oil-based muds, the number of naphthenics in the "muds" can be a relevant parameter in the performance of these drilling oils [25] .

Moreover, the importance of the aromatics compounds is remarkable in the aircraft emissions analysis nowadays. This significance is justified by the high level of environmental damage linked to the presence of aromatics. Above all, aromatics are described as similar o naphthenes, whereas defined with the formula, C_nH_{2n-6}. On the contrary to the naphthenes, these compounds contain at least one resonance stabilized unsaturated ring core. This benzene ring is very stable and does not crack into smaller components. Nevertheless, aromatics are not a preferred utilized feedstock due to their molecules fragility tending to crack. This phenomenon mainly involves breaking off the side chains resulting in excess fuel gas yield [25,27]. Most fuels include aromatics in their composition. These compounds have at the very least a high level of controversy, requiring regulated impositions on the percentage of aromatics that a specific fuel can possess [28]. Consequences such as the increase in the emissions of pollutants and the emanation of particles in aviation justify the imposed restrictions performed by the regulatory authorities. A high percentage of aromatics in the composition of the fuel also conducts to the formation of soot. As mentioned before, this combustion outcome is an emission that harms the turbine lifetime, yet this phenomenon is more likely to occur whenever it is reached the smoke point [15]. Nowadays, the fuels predominantly used in the aviation sector still possess aromatics as one of the most relevant components of their mixtures. This fact undoubtedly reveals that the efforts to reduce pollutant emissions in aviation are still not sufficient compared to what could be performed. Nevertheless, there were still produced several signs of progress to achieve net-zero carbon dioxide emissions. For instance, as an alternative to conventional fuels, it has been made a vital work in improving the technology and characteristics of alternative fuels throughout the past years. Through the usage of biofuels or by combining them with traditional fuels, it is possible to perform a significant reduction of carbon dioxide pollutants and soot emissions in the combustion chambers [29].

2.2.1 Jet Fuel

Nowadays, the type of fuels intended to utilize in air transport should possess specific parameters that enable combustion to occur in a certain way. Aviation turbine fuel or jet fuel is commonly the preferred option for the majority of aircraft owners. This type of fuel is a distillate descendant of the widely known kerosene designed for applications in the aeronautical industry. Equivalent to kerosene, their properties are similar, and thus their composition is typically formed of paraffins, naphthenes, cycloparaffins, and aromatics compounds along with small amounts of olefins and other compounds. Additionally, several quantities of sulfur are present in mercaptans, sulfites, disulfides, and thiophenes, yet currently limited to 3000 ppm by the specification [30]. Jet fuel is also enriched with several additives that aim to inhibit the hazard of static charges, reducing the oxidizing and corrosive potentials, while increasing the lubricity and improving the cold flow properties. The presence of these additives in the fuel, even notified in parts per million represents the main differences between

jet fuel and kerosene.

Concerning the specific composition of the jet fuel, it is necessary to mention that jet fuel, more precisely jet-A1 is composed of a carbon chain with the length of C8-C16, implying that from 70 % up to 85 %, is composed of paraffin constituents. These paraffin compounds can be straight-chain, branched-chain isoparaffins, and cycloparaffins, which are complemented by naphthenes that are already present in this fuel composition [4]. Concerning how the molecules of paraffin dispose of variable, this circumstance depends on the raw crude employed in the refinement process. The presence of high hydrogen to carbon ratios for n- and iso-paraffins ensures a higher heat-to-weight proportion maintaining a cleaner burn. This is explained due to the highest levels of heat capacity being obtained in pure hydrogen (H_2) combustion, which further decreases with the increment of the presence of carbons in the molecular chain of the fuel. Alternatively, the cycloparaffins reduce the hydrogen to carbon ratio and reduce the heat release per unit weight. Hence, their deficiency in the level of hydrogen suggests that they have high heat content per unit volume but lower heat content per unit mass compared to paraffins with the same carbon number. These characteristics mean a significant impact on the optimization of fuel properties [3]. Besides these compounds, it is also present in the jet fuel constitution, aromatics components, known for their damaging characteristics. These components represent up to 25 % of the jet fuel constitution. As a consequence of the wide variety of components present in the Jet Fuel used nowadays, it will subsequently lead to an increase in the complexity of modeling its combustion by the combustion engineers.

Analyzing the properties that form jet fuel, it is visible the presence of intermediate values of vapor pressure and octane number, which result as the best values for the stable combustion under extreme conditions of the turbine engine. Possessing an acceptable value of vapor pressure indicates that the fuel will not be volatile in the harsh conditions of the turbine engine while having an acceptable value of octane number suggests that auto-ignition will not be enhanced at the normal soft conditions of the turbine engine. The control of these parameters will allow the turbine to work in harsh conditions. Moreover, it is relevant to note that the high flash point will reduce the explosion hazard, while the low freeze and wax points allow the airplane that uses this fuel to fly at high altitudes [25].

2.2.2 Alternative Fuels

Following the analysis of the damaging role of fuel emissions in preserving the world as a livable place, it is recommended to realize the origins of the harmful pollutants. Furthermore, by utilizing the information on the components that threaten the environment, it is possible to research refreshed alternatives that could enable a better livable planet, allowing a sustained decrease in the usage of fossil fuels until achieving a complete decarbonization objective. Concerning the research aiming at alternative types of fuel for aviation, most engine producers require specific general characteristics within the fuel to allow the combustion to occur smoothly. Hence, primarily the researched and developed fuels must fulfill these pre-

cise requirements. The requirements ensure that the fuel can become a suitable substitute to the current solutions while having a good performance in aviation. Several studies in the literature summarized the main characteristics that should be considered in the research of new alternatives [3, 4]. According to Blakey 1998 [3], some of the suggested properties are enumerated below:

1. High heat content for maximum range or payload. This can mean high mass specific energy.
2. Good atomization.
3. Rapid evaporation.
4. Good burning characteristics, including relight capability at altitude.
5. Low explosion risk.
6. High specific heat capacity.
7. Free from contaminants.
8. Minimum carbon formation.
9. Low viscosity and high lubricity - good storage and pumping characteristics, including low freezing point to facilitate altitude operation.
10. Good thermal stability/chemical stability.
11. Wide availability and acceptable cost.
12. Products of combustion acceptable environmentally.
13. Good ground storage and handling characteristics.

Besides the mentioned characteristics, studies within the literature correlated distinct parameters and discovered the best suitable fuel candidates. In the literature, some works [31, 32] enounce that can be made a correlation between different factors such density, Wobbe Index, and LCV (Lower Calorific Value) in order to find the most promising alternative jet fuel. Regarding the importance of the Wobbe index, an indicator of the interchangeability of fuel gases describes how distant from the design fuel an alternative fuel can be classified. This index is detailed in Equation 2.1. Usually, the values of the Wobbe index for jet fuel alternatives will be comprised between 0.95 and 1.05 of the jet fuel average value, as shown in Figure 2.2. Additionally, the parameters of LCV, known as the measure of available thermal energy produced by combustion of fuel, and density are also a matter of immense importance

whenever it is being studied as a fuel alternative since there is a minimum of lower calorific value that a fuel shall have to power an aircraft engine. Lastly, the fuel density should be also comprised of specific values since a high density is desirable until a certain point when it does not compromise the weight [3].

$$I_w = \frac{LCV}{\sqrt{SG}} \quad (2.1)$$

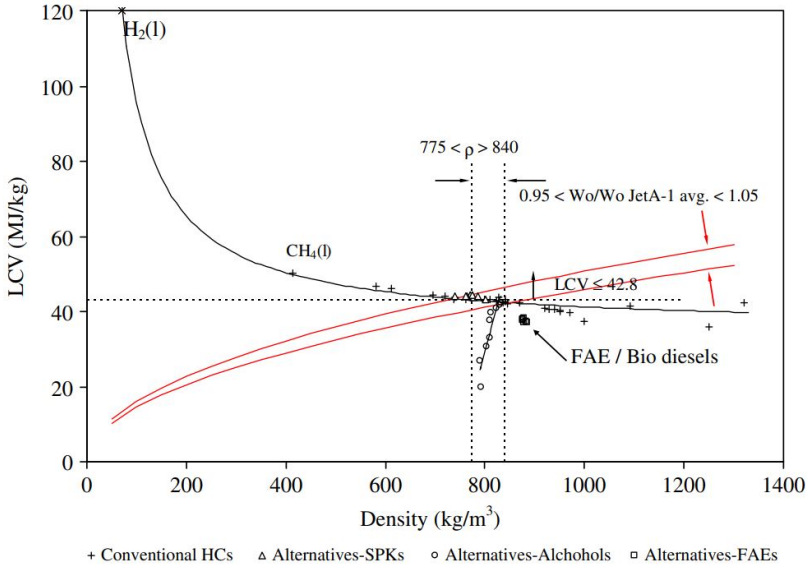

Figure 2.2: Relationship between the several parameters for range of the liquid fuels showing limits of jet-A1 specifications, adapted from [3].

The study of eco-friendly fuels increased extensively throughout the last couple of decades. Therefore it is relevant to perform a brief review regarding which alternatives might protrude a valid option over the currently used fuels.

Fatty acid ester (FAEs) fuels can also be named biodiesel and originated from the transesterification process of vegetable oils, animal fats, or waste cooking oils. In this process, it is feasible to produce a mixture of fatty acids ester, and alcohol by a reaction occurring between the glyceride and alcohol in the presence of a catalyst, as exhibited in Figure 2.3. As mentioned previously, several materials are suitable for the production of this type of fuel. Remarkably, the production of biodiesel is relatively simple and already widely studied. Whenever it is used methanol in the transesterification procedure, it will simultaneously separate the glycerol, which stands as an advantage in the process due to the consequent reduction of complexity. However, the utilization of ethanol throughout the process requires the existence of a low level of water content to achieve a simple glycerol separation. The consequent products of the chemical reaction will be the raw biodiesel and the raw glycerol, usually employed in the cosmetic industry after being purified [33].

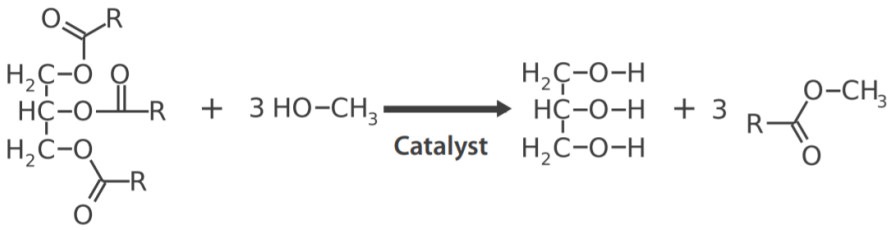

Figure 2.3: Equation of the process of transesterification [33].

Regarding the usage of this type of fuel in aviation, it is visible through the literature several arguments that support that a transition to biodiesel with different properties or phases, would be achieved through minimal and justified engine modifications in the currently used combustion apparatuses. Nonetheless, presently there are also disadvantages, such as the ineffectiveness that the fuel systems would face in comparison to the jet fuel based systems. There is also the disadvantage associated with the bio-degradable characteristics of the fuel, which subsequently means the growth of biological components in their storage. Overall, these disadvantages outweigh the advantages, which suggests that this type of fuel might not be a prone solution to use in the future of aviation [34].

Additionally, the usage of Fischer-Tropsch (FT) fuels should be mentioned within the spectrum of the alternatives to the conventionally used fuels. Conversely to the refinement of biodiesel, the Fischer-Tropsch fuels refinery process is quite different since this type of fuel can be reassembled to the crude and is not considered a suitable product unless it is refined to the consumer product. There is the possibility of utilizing solid carbon sources (coal, biomass, and waste) as the feedstock of Fischer-Tropsch fuels since the feed material commonly required for synthesis gas is H_2, and CO in the production of any variety of carbon sources. Nevertheless, depending on the type of feedstock associated with the procedure, the creation of syngas is whether a net consumer (when it is employed coal) or a producer(whenever it is employed natural gas) of water [3]. The synthesis gases are relevant due to the feed used in the liquid conversion process [35]. The FT process is essentially characterized by the carbon chain building that requires the implementation of the syngas fabricated in the previous phase. In this procedure, depending on the product requirements, it is possible to favor the production of long chains of paraffin as is represented in Equation 2.2 [36].

$$nCO + (n + \frac{m}{2})H_2 \rightarrow C_nH_m + nH_2O \quad (2.2)$$

Subsequently, the product of the reaction is further refined and treated to acquire specific characteristics allowing the fuel composition to increase performance upon desired molecular chain lengths. This fact permits the combustion engineers to control the type of out-

put carbon numbers considering specific combustion parameters such as temperature, pressure, and syngas composition of the initial reaction. Suscently, the general procedures of the process are depicted in Figure 2.4. Generally, the process offers some advantages, such as controlling the output carbon process and thus the type of final result, yet the process is frequently costly. These disadvantages indicate that the benefits of this fuel can not outweigh the disadvantages related to the economic costs, which are potentialized due to the inefficiency of the refinement procedure [3, 35].

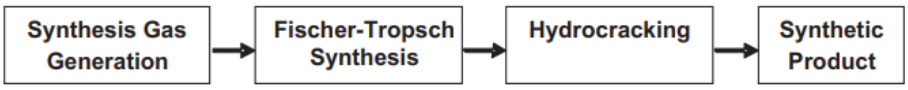

Figure 2.4: Synthetic product production process that could be aviation fuel [37] .

Despite the ineffectiveness of different biofuels in replacing the current aviation alternatives, there is still room for improvement whenever it is examined the ample research performed in the hydrotreated vegetable oils [38]. These types of fuels consist in a high regard alternative to the commonly used fossil fuels since the level of emissions is consistently low and their production as its basis on biomass and renewable origins. Their usage of feedstock is mainly portrayed by recurring to existing plant oils such as camelina oil, jatropha oil, and algae crops leading to a controversial question concerning the environmental impact on the soil and water sources of the mass production envisaged by these alternatives [39].

The process that leads to the fabrication of this alternative fuel is known as hydroprocessing. Initially, a triglyceride that has its origin in a biomass compound will be subjected to hydrotreatment to convert the existing biomass into a brand of paraffin. In this procedure, the oxygen is removed via hydrodeoxygenation in the presence of excess hydrogen, alongside the oxygen. Besides this, it can also be removed compounds such as nitrogen, sulfur, and residual metals [40]. Furthermore, while submitting the product of hydrodeoxygenation to high temperatures alongside the acidic character of the support, it is possible to lead to more selective production of kerosene-like paraffin since the hydrocracking phenomena is the further step of the procedure suitable for optimization in these conditions. In addition, isomerization reactions, which are defined by the conversion of paraffin into more compact isoparaffins, can also be favored, producing a high-quality biofuel. This reaction will lead to the reduction of hydrocarbon blend freeze and flashpoints. Hence, by finalizing the refinement procedures, a synthetic product is obtained as a hydro-processed fuel from a biomass vegetable oil [3]. A brief scheme of this process is presented in Figure 2.5.

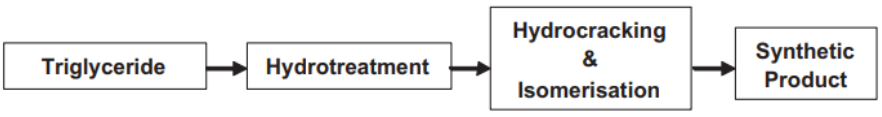

Figure 2.5: Hydroprocessing of Vegetable oil classified as Synthetic Product [40].

Regarding the usage of hydrotreated vegetable oil (HVO), the most frequently used in avia-

tion has the commercial name NExBTL. There are considerable works in the literature that promote a better understanding of this fuel. The researches performed by Ribeiro [12] allowed the understanding of the properties of this fuel and evident influences on the impinging processes while comparing it with the traditional jet fuel. Subsequently, this work was numerically simulated utilizing a VOF (Volume of Fluid) approach in the studies of Rodrigues [10] and further compared the different outcomes experimentally and numerically. Furthermore, regarding the combustion properties of this fuel. Pacheco et al. [6], compares the burning properties of this fuel with the traditional jet fuel, and the intends of Ferrão et al. [7–9] in optimizing the combustion properties of NExBTL by adding nanoparticles to the utilized blends. This variety of HVO possesses a remarkably similar density to the widely known jetA1, besides being composed of a straight-chain and branched paraffin known as the most elementary configurations that could originate the hydrocarbons. NExBTL has regularly in its composition alkanes that possess between 15 and 18 carbon numbers and are practically free of aromatics, which are compounds that are known for increasing dangerous emissions [3]. This fuel also maintains satisfactory characteristics concerning microbiological growth, which has minimal occurrences in normal combustion usage and storage. Generally, it can be used HVO as a blending component that can incorporate mixes with the currently utilized fuels such as jet fuel, diesel, and kerosene. This initiative requires regulation, developed by regulatory agencies demanding the companies willing to implement fuel alternatives on their fleet [41]. Investing in these initiatives, Japan airlines pushed significant actions into the feedstock independence of hydroprocessed jet fuel through an experimental flight conducted in 2009 utilizing one of its Boeing 747-300 aircraft out of Tokyo [42]. The experiment consisted of using a fuel mixture in one of the aircraft engines that contained a blend of conventional jetA1 with a hydroprocessed biomass feedstock containing Camelina (42%), Jatropha (8%), and Algae ($< 0.5\ \%$). The test has revealed a success and proved the importance of biofuel alternatives in achieving carbon neutrality in the airline industry. The fuel blend employed would not require further modifications to the conventional aircraft combustion chambers and any significant transformation in the infrastructures needed for airplane maintenance. However, the blending process would add a new layer of complexity to the fuel production while presumably decreasing the overall combustion efficiency process due to the characteristics of the biofuel. Ultimately, HVO and its derivatives, with evident research regarding its implementation, might originate well-sustained alternatives to the current aviation fuels.

2.3 Evaporation and Combustion of the Droplet

The concept of droplet evaporation encloses several applications in engineering. Such a process motivated extensive analysis and research throughout the past decades since it is a crucial process in fuel burning. Besides this, atomization and conventional combustion of liquid fuels within combustion engines or aviation turbines also reveal immense relevance in the mechanism. The advancements in the research of this theme can imply that it might be possible to achieve better performances in the evaporation and combustion systems. These im-

provements result in optimizing the burning fuel process and evidently, reduce the produced pollutants.

Specific topics should be highlighted to comprehend the phenomenon of evaporation. Firstly, it is highly relevant to develop an accurate method that could predict evaporation rates and their properties variation through the process. Furthermore, there is a distinguishment between the concept of vaporization and boiling. The evaporation event is the conversion (liquid to vapor) when the liquid is already above boiling temperature and does not require the heating process to achieve the boiling point. However, boiling is the phenomenon when the liquid is surrounded by a higher temperature gas and it has to be heated to complete the transition phase. Both phenomena imply mass and heat transfer between both phases modeled to predict the evaporation rate. Equally, it is crucial to account for different droplet properties. The modeling of the evaporation completes its process with the addition of the surrounding gas characteristics. These topics shall be resolved in order to develop a mathematical model of evaporation and evident fulfillment of the model intentions.

2.3.1 Droplet model for vaporization

The physical phenomena that involve evaporation are rather complex. As a consequence, the literature essentially describes the phenomenon as extensive. One of the first studies intended to understand the natural phenomenon of evaporation was developed by Godsave [43]. At this point, several assumptions interpreted the droplet as a spherical body and the consequent boiling point of pure fuel as a well-known variable. From this study emerged one of the first formulations of the so-called d^2 *law*, widely utilized in analyzing the droplet fuel burning performances. Besides this study, Spalding [44], as well known as one of the predecessors of the evaporation analysis, developed extensive work in fuel combustion and evaporation. From such studies derived the concept of the Spalding number, which describes the mass transfer process of droplet evaporation. This variable possesses ample research afterwards and still retains crucial importance nowadays, whenever considering approaches with mass transfer phenomena in evaporation.

The development of the $d^2\ law$ turned the case more prone to analysis. Thus, the phenomena emerge easier to understand mathematically, leading to extensive research, both experimentally and numerically. Researchers such as Williams [45], Faeth [46], Law and King [47], Sirignano [48], and Lefebvre et al. [49] contributed to the development of the knowledge on this theme. The concept of droplet evaporation and combustion is further simplified with the definition of boundary conditions that ensure great accuracy whenever validating numerical results with experimental data. Such experimental data and works allowed the validation of the theory behind the physical and mathematical models. The authentication of these researches achieves higher significance in similar studies to those executed by Ranz and Marshall [50, 51], where it emerged as one of the first Euler-Lagrange approaches to analyze the droplet fuel evaporation within a hotter environment.

Concerning the literature, Sirignano [52] analyzed different prospective models of droplet evaporation that would consider distinct circumstances. This innovation allowed the usage of the model in specific cases that could not be modeled until that moment. One of these models is the addition of convection and flow effects into the evaporation model, which led to a whole new type of analysis.

Furthermore, the coupling of the different works and research conducted to create the simple model for droplet evaporation stands still widely utilized nowadays. This model has its fundamental foundation in the application of the historical Stefan problem [53] into a spherical coordinates reference. The appliance of this model into a single fuel droplet assumes the existence of mass and heat transfer between the liquid droplet phase and the surrounding gas environment. The physical processes, consider the absorption of heat until the droplet reaches the boiling point and then assume mass transfer after being initiated in the evaporation procedure. Such heat and mass transfers occur alongside the mathematical formulations required to understand the nature of the process. The assumptions employed in the development of the model are then certified with the experimental research and works assuring further validation of the model.

The further modeling of the phenomenon assumes that mass and heat transfer are constantly occurring. Hence, the droplet temperature is assumed as having the droplet liquid boiling point, and the evaporation rate is established by the heat-transfer rate from the ambient to the droplet surface as depicted in Figure 2.6. This is a satisfactory approximation of the physical phenomenon since it shows good agreement with the experimental data [43,44,49]. Consequently, a mathematical description of the occurring phenomena might stand as the most suitable approach to employ in engineering calculations.

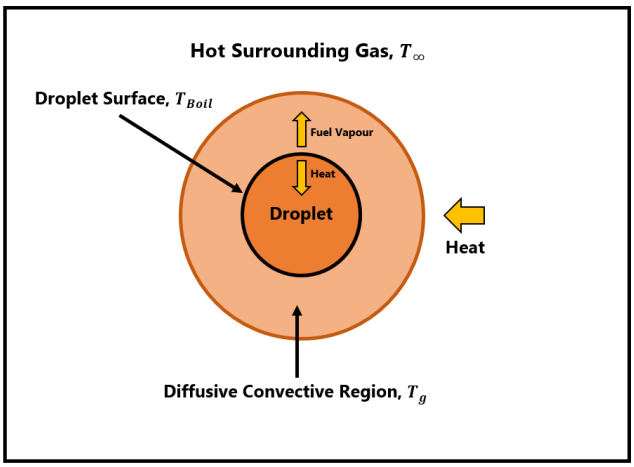

Figure 2.6: Schematic of droplet evaporation process.

Whenever a droplet is involved within a warmer gas, there is a droplet core temperature increment and consequent formation of fuel vapor at the droplet surface. This occurrence reveals that part of the heat provided is further used to supply the vaporization of the fuel.

Such a fact results in the uniformization of the droplet temperature. Tendentially, this stage is when all the heat provided to the droplet is utilized as the heat of vaporization. Consequently, after the droplet stabilizes, its temperature achieves the denominated by "steady-state".

The droplet evaporation model guarantees its efficiency by assuming the idea of a spherical droplet, the fact that the boiling point is an assumed premise, and the negligence of heat transfer by radiation. Consequently, when the droplet reaches a specific temperature at the liquid boiling point, it will be considered a nearly steady-state where all the energy supplied to the droplet is employed in the evaporation process of the droplet, likewise in Williams, [54] The employment of these model assumptions aids the development of the simple model of droplet evaporation. The further implementation of detailed mass and heat balances according to the thermodynamic properties between both phases leads to the temperature distribution specified in Equation 4.2. The comprehension of the temperature phenomena onto the droplet is reached in the studies of Hall [55], Hiroyasu et al. [56] and Matlosz et al. [57].

$$T(r) = \frac{(T_\infty - T_{boil})exp(-Z_T\dot{m}/r) - T_\infty exp(-Z_T\dot{m}/r_s) + T_{boil}}{1 - exp(-Z_T\dot{m}/r_s)} \quad (2.3)$$

Where, for convinience Z_T is considered $Z_T = c_{p:g}/4\pi k$ and $\dot{m}$ accounts for the mass flux occurring during the evaporation process.

Additionally, determining the parameters directly related to the evaporating process allows the researchers to evaluate the phenomena. Given this, it will arrive at the well-known expression called "d^2 $evaporation$ law" (Equation 2.4) [43], where is visible the relationship between the time and the diminishing of the droplet diameter. The visualization of the mathematical function is shown in Figure 2.7.

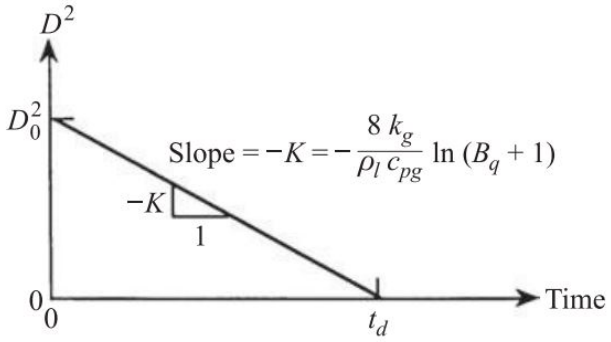

Figure 2.7: The D^2 law for droplet evaporation resulting from the simplified analysis [53].

$$D_0^2 - D(t)^2 = Kt \quad (2.4)$$

Where the parameter K, measured in mm^2/s, can be characterized in Equation 3.7 as the evaporation constant given by:

$$K = \frac{8k_g}{\rho_l c_{p:g}} ln(1 + B_q) \quad (2.5)$$

Which $c_{p:g}$ accounts for the specific heat at constant pressure, whereas the parameter k_g provides the thermal conductivity of the gaseous phase. Generally, these parameters are constants whenever during analysis is adopted the simple model of the droplet evaporation. However, they might vary considerably throughout the phenomena from the droplet surface to the freestream conditions. Therefore, frequently applies the approach followed by Law and Williams [58] for burning droplets, described in Equations 2.6 and 2.7.

$$c_{p:g} = c_{p:F}(\overline{T}) \quad (2.6)$$

$$k_g = 0.4k_F(\overline{T}) + 0.6k_\infty(\overline{T}) \quad (2.7)$$

Where the subscript F accounts for the fuel vapor and the subscript ∞ represents the free stream, regarding the term $\overline{T}$ is the average of the fuel boiling point temperature and the free stream. The definition of the averaged temperature of the film is then exhibited in Equation 2.8.

$$\overline{T} = (T_{boil} + T_\infty)/2 \quad (2.8)$$

The B_q parameter is a crucial dimensionless number, such as Reynolds number, that has special significance in combustion and is commonly referred to by those knowledgeable in the fuel combustion field. The number can be named Spalding Number or Transfer Number since it was firstly mentioned in the investigation performed by Spalding [44]. The definition of B_q (Equation 2.9) applies only to the set of assumptions that validate the simple evaporation model. Nevertheless, further definitions might appear depending on the functional form depending on the assumptions made, as it is yielded in the literature [53].

$$B_q = \frac{c_{p:g}(T_\infty - T_{boil})}{\Delta H_{vap}} \quad (2.9)$$

Essentially, this information represents a valuable resource since it allows the researchers to analyze the relationship between the heat, the evaporation process, and the steps of the process. Therefore, whenever the initial droplet diameter is known as well as the properties that enable the computation of the evaporation constant (K). Hence is capable to predict the droplet evaporation time or, as it is more known in the literature, the droplet lifetime (t_d) (Equation 2.10) :

$$\text{If } \; D^2(t_d) = 0 \; \text{ then } t_d = \frac{D_0^2}{K} \quad (2.10)$$

Lastly, according to the previously mentioned expressions, predicting time for full evaporation is a straightforward process. However, the K and its computation depend on the physical constants and parameters such as gas-phase specific heat ($c_{p:g}$) and thermal conductivity (k_g). In the simple model, they are considered constant, yet they vary significantly from the droplet surface until the freestream conditions. In order to solve the dilemma, different approaches are assuring the achievement of an average value of these parameters, revealing accurate predictions. Such premise is justified with a comparison with the experimental analysis. For instance, the work developed by Hubbard et al. [59], where is compared different property modeling, and which the one-third rule model (developed by Sparrow and Gregg [60]) achieves good agreement with the experimental data.

2.3.2 Droplet model for combustion

The phenomenon of combustion is alongside evaporation among the most relevant events that occur during the process of obtaining energy from fuels. The understanding of these phenomena possesses immense importance in the concern of reducing the emissions produced by the engines. Figure 2.8 shows a chronological schematic of a working industrial combustor that intends to utilize the chemical energy provided from the combustion of the fuel. Hence, the modeling of processes like combustion ensures the comparison of the numerical results for fuel combustion with the experimental data. Such comparison supplements credibility and knowledge in the study of new fuel alternatives, likewise it is performed in this specific research.

In order to analyze the combustion phenomenon, there are specific processes accounted for in the study. Firstly, it is significant to remark that the definition of combustion is the event that occurs between a specified fuel and an oxidant [62]. This process leads to the formation of combustion products result of the chemical reaction. The fuels used in the combustion vary widely depending on the results intended with the procedure. The oxidant more commonly used is the air, which possesses a significant amount of oxygen standing as the process catalyst. In general aviation, the bulk of fuels utilized delivers their injection as a liquid spray with further atomization and production of a stream of fuel droplets [53]. The subsequent droplets will experience the vaporization process originating in a gaseous phase constituted

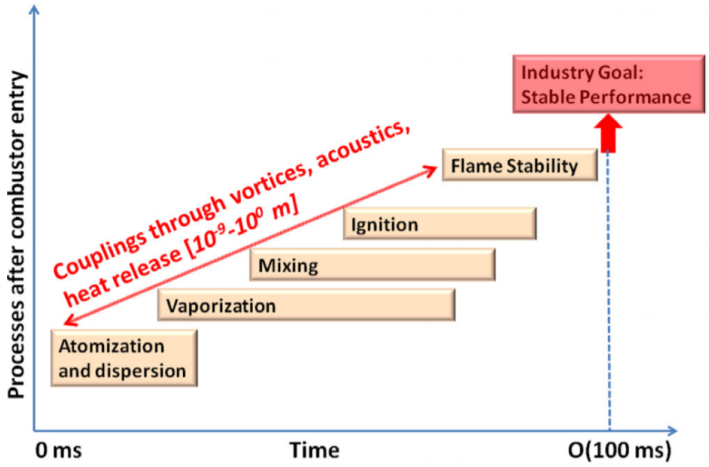

Figure 2.8: Schematic of the key processes in a liquid fuelled combustion chamber, adapted from [61].

by the gaseous state of the fuel. This gaseous phase is the combustible of the chemical reaction and, along with the oxidant enables the combustion occurrence. Figure 2.9 displays a schematic of the presence of the combustion process contributor compounds throughout the droplet domain.

The combustion model suggested in this dissertation is the liquid fuel droplet combustion model since the analysis occurs for single spherical droplets within a drop tube furnace DTF [63] . Generally, this model is an extension of the evaporation model. This model involves the inference of certain assumptions and the modeling of the physical equations describing the phenomenon, considering the combustion properties. Similarly to the evaporation model, several conditions influence the performance of the combustion, such as the multicomponent nature of the droplet, and the convection ambient conditions. Alternatively, there are concerns where the combustion model diverges from the evaporation mode. In the combustion modeling, it is expected the occurrence of a flame assumed as an infinitesimally thin sheet where the fuel vapor that results from the evaporating droplet reacts instantaneously with the oxidizer [53]. This boundary promotes combustion resulting in combustion products that might stand as pollutant emissions. Likewise to the evaporation problem, the mathematical modeling requires the definition of appropriate combustion properties, in this circumstance, the parameters $c_{p:g}$, k_g, and ρ_l, currently computed supposing the considered flame and burning properties. Employing the model ensures the prediction of combustion characteristics such as the droplet burning rate, flame radius, droplet surface, flame temperatures, and vapor concentration at the droplet surface [63].

The Figure 2.9 provided by Brennen 2005 [63] depicts the schematic of single droplet combustion model. There is a representation of the liquid fuel droplet phase, the gaseous phase that results from the evaporation surrounding the liquid droplet, the flame front boundary between phases, and the surrounding hotter environment. Concerning the occurrence of several mass fractions for each combustion compound in every considered phase is then feasible to analyze its variation of quantities. The presence of the combustion products mass fraction

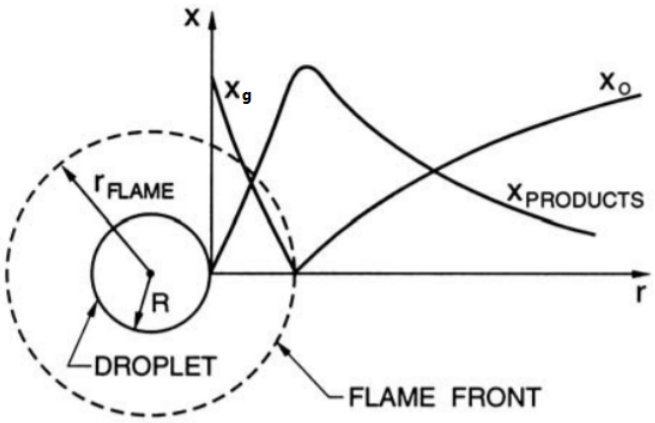

Figure 2.9: Schematic of single droplet combustion indicating the radial distributions of fuel/vapor mass fraction x_g, oxidant mass fraction, x_{Ox} and the combustion mass fraction products, $x_{products}$ [63].

is increasing in the gaseous fuel phase until reaching the flame front, where it suffers a further presence decrease throughout the hotter gas environment. Considering the presence of the evaporated mass fraction of the fuel it is maximum at the droplet radius suffering an evident decrease until reaching the droplet flame front with further diminishing to a negligible quantity and converted into the presence of oxidant mass fraction. Consequently, this property will increase its presence in the hotter environment.

The computation of the gaseous phase mixture properties utilizes the simple model of the droplet combustion enounced in the book by Turns [53]. Similar to what was perceptible in the evaporation droplet model, the parameters $c_{p:g}$, k_g, and ρ_l enable the calculation of burning and combustion properties that are important to analyze the fuel combustion performance. One of such properties is considered the burning rate (K) of a specific fuel droplet is relevant to investigate the combustion characteristics, and its definition is exhibited in Equation 2.11, which is measured in mm^2/s.

$$K = \frac{8k_g}{\rho_l c_{p:g}} ln(1 + B_{o,q}) \quad \textbf{(2.11)}$$

The obtained burning rate alongside the information of the droplet initial diameter ensures the computation of the droplet combustion lifetime (t_d) in a process similar to the detailed in the evaporation modeling. In order to calculate the burning rate and the droplet lifetime, it is necessary the implementation of empiricism regarding the fuel mixture parameters, defining the properties through the process suggested by Law and Williams [58] and further depicted in Equations 2.12, 2.13, and 2.14.

$$c_{p:g} = c_{p:F}(\overline{T}) \quad (2.12)$$

$$k_g = 0.4k_F(\overline{T}) + 0.6k_{Ox}(\overline{T}) \quad (2.13)$$

$$\rho_l = \rho_l(T_s) \quad (2.14)$$

Concerning the temperatures employed in Equations 2.12, 2.13, and 2.14, the property $\overline{T}$ represents the average temperature of the film represented in Equation 2.15, which is an averaged temperature that accounts for the temperature of the surface of the droplet and the flame temperature. The parameter T_s portrays the temperature of the droplet radius equivalent to the boiling temperature of the fuel and the T_f as the flame temperature. The droplet combustion model derives from the evaporation model due to assuming distinct particularities in the assumptions performed to represent the physical phenomenon. Ultimately, the modeling of the required parameters, $c_{p:g}$, k_g, and ρ_l, demands the assumption of properties regarding the kinetic events of the oxidant, flame, and products of the combustion. Therefore, the flame temperature used to compute the average temperature suggests an iterative considering the combustion chemical models instead of the boiling point of the fuel as utilized in the evaporation model [25].

$$\overline{T} = (T_f + T_\infty)/2 \quad (2.15)$$

Following the state of art exposition regarding the evaporation and combustion modeling of fuel droplets, it is thus relevant to acknowledge the external effect that might assume influence in these physical phenomena, performed alongside mentioning the studies that allow the improvement of the knowledge of these modelings.

2.3.3 Effects of ambient temperature

Commonly, the evaporation problem has to consider the temperature of the gas phase since this will be the principal heat producer to the evaporation phenomenon. Given this, the gas temperature highly influences the evaporation and combustion of the droplet. This characteristic is often modified to confirm the importance of its modification and what it indicates to the evaporation and combustion experiments. Hence, this parameter frequently yields influences in the burning characteristics of the droplet, such as evaporation rates, ignition time, and total lifetime.

Initially, one of the first studies carried to remark the importance of this property is the re-

search of Lefebvre et al. [49]. Throughout the studies, there is a relation between the increase of the evaporation/combustion rates and the rise of the ambient temperature. Furthermore, in the studies of Wang et al. [64], different fuel droplets and subsequent mixtures suffer a free fall within a furnace that changes the average temperature. Even though not all fuels and mixtures used demonstrated a similar tendency to increase the ambient temperature. Generally, it was verified that the increase in the ambient temperature meant a decrease in the ignition delay time. This phenomenon occurs due to a casualty effect reaction between both parameters since the increase of the environment temperature tends to increase the environment volatility, which tendentially favors and enhances the evaporation and combustion, triggering the ignition to occur earlier

Additionally, through the studies performed by Kotake et al. , [65], burning a different variety of fuels, the influence of the temperature in the droplet burning rate was evident. This fact is prominent in higher burning rate coefficients registered with the increase of the ambient temperatures. More recently, it was visible in the experimental research developed by Pacheco et al. [6] a strong dependence between the ambient temperature and the combustion of the droplet. This study executed experiments with jet fuel, HVO, and mixtures between the last two. The results inferred that the increase of the ambient temperature means a decrease in the droplet lifetime and an evident increase in the burning rate. The research of Awasthi et al. [66] investigates the effects of the ambient temperature and initial diameter in droplet combustion considering a numerical model. The computations are performed on an isolated droplet of n-heptane in a transient numerical simulation with defined ambient conditions. The obtained results follow the d^2 law and suggest a dependency between the combustion characteristics and the ambient temperature. The increase of the ambient temperature indicates an increase in the droplet burning rates, alongside the decrease of the droplet lifetime.

Figure 2.10 depicts the effect of ambient temperature in the ignition delay for the n-heptadecane droplet. This graph is adapted from the studies of Saitoh et al. [67] which suggests that high temperature ambients promote droplet combustion by enhancing the heat transfer to the droplet surface and ensuring the faster evaporation of the droplet content. This phenomenon is visible with the reduction of the ignition time of the fuel droplet.

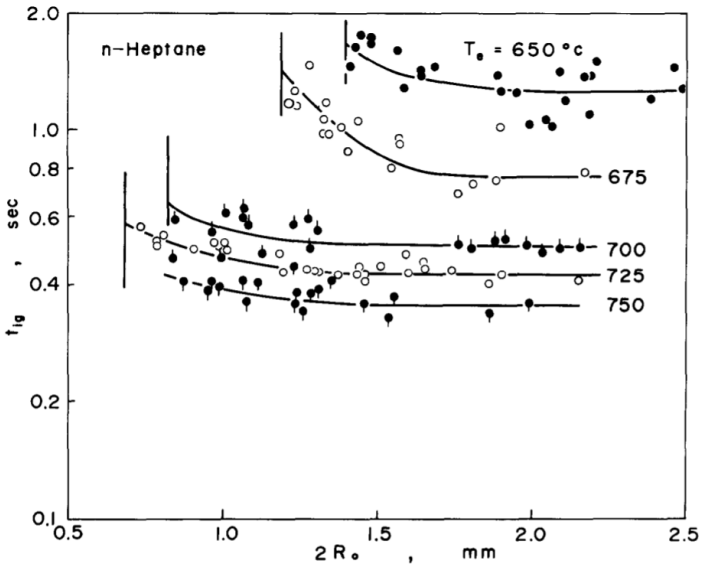

Figure 2.10: Measured ignition delay of the fuel droplet versus droplet diameter for n-heptane droplets throughout the different analyzed ambient temperatures [67].

2.3.4 Effects of the Convection

Concerning the droplet evaporation and combustion and the conditions of the environment, there are external effects that affect these phenomena throughout the droplet's lifetime within the domain. Specifically, in engineering applications, such as simulations of combustion chambers or gas turbines and the influence of convection. Hence, the commonly visualized crossflows or forced swirls can be considered in the heat and mass transfer phenomena between the droplet and the involving environment.

The convection affects the droplet ignition delay and consequently the droplet lifetime by increasing the mass and heat transfer between both phases. The experiments of Chen et al. [68], performed droplet suspension experiments of n-decane, toluene, and butanol subjected to different convection velocities. Generally, the droplet evaporation rate increased with the increase of the convection velocity. This occurs due to the Reynolds number increase with the rose of the convection velocity, which implies a higher intensity and mass diffusion coefficient increase. The authors also state that the rise of the convective velocity has less influence on the increase of the evaporation rate than the increase of the ambient temperature.

Furthermore, it is relevant to mention the modeling made to incorporate the convection effect in the droplet evaporation. Generally, the most accepted theory in the literature is the fact that the convection flow will affect adimensional numbers that describe the process, such as Re (Reynolds), Sc (Schmidt), Pr (Prandtl). Regarding each adimensional number, the Reynolds number accounts for a ratio between the inertial forces, and viscous forces within a fluid, the Schmidt number considers the ratio of the momentum diffusivity to the molecular diffusion coefficient, and the Prandtl, which is defined as the ratio of momentum diffusivity to thermal diffusivity. Consequently, many investigators suggested that these numbers could

form correlations capable of modeling the convection within the droplet evaporation models. These investigations indicate a relation between the standard spherical droplet evaporation case and an evaporation model that accounts for the convection utilizing the correlation with adimensional numbers as shown in Equation 2.16.

$$\dot{m}_{convection} = \dot{m}_{spherical} \cdot f(Re, Pr\ or\ Sc) \quad (2.16)$$

In respect to this expression, $f(Re, Pr\ or\ Sc)$ affords the correction factor that allows representing the effect of the convection in the adimensional numbers. Frequently, the correlations are utilized to account for the impact of the convection in the modifications in the heat and mass transfer processes. In order to proceed with the correlations, there is a need to regard an adimensional number like the Nusselt Number, Nu, known as the ratio of convective to conductive heat transfer at a boundary in a fluid, and Sherwood number,Sh, representing the ratio of the convective mass transfer to the rate of diffusive mass transport. The usage of these numbers allows the creation of correlations and respective representations of the convection. Given this, it is possible for the development of new relations of these numbers (Equation 2.17 and Equation 2.18) considering both convective effect and the conditions in a non-convective flow.

$$Sh = A + BRe_d^{1/2}Sc^{1/3} \quad (2.17)$$

$$Nu = A + BRe_d^{1/2}Pr^{1/3} \quad (2.18)$$

In these Equations, 2.17 and 2.18, Re_d accounts for the droplet Reynolds number, while A and B represent the coefficients that allow the correlations and that are further modified to model the convection in the evaporation phenomenon. There are different approaches to the computation of these constants, yet it is possible to summarize the most relevant methodologies of the convection phenomenon and its investigations as is visible in Table 2.1.

Authors Approaches	Equations	A	B	Validity Range
Frossling [69]	2.17 and 2.18	2	0.552	$10 < Re_d < 1800$
Ranz and Marshall [50, 51]	2.18	2	0.6	$Re_d > 300$
Faeth [70]	2.18	$\frac{2}{\sqrt{1+\frac{1.232}{Re_d Pr^{4/3}}}}$	$\frac{0.552}{\sqrt{1+\frac{1.232}{Re_d Pr^{4/3}}}}$	$Re_d < 1800$

Table 2.1: Summary of the coefficients in the Equations 2.17 and 2.18 adapted from [71].

Generally, the correlation adopted by Ranz and Marshall [50,51] is frequently used in several CFD codes, one notorious example is the algorithm employed in ANSYS Fluent ®2021 R1. Equation 2.19 exhibits the fuel evaporation resulting mass flow within a convective gas field, utilizing the convective correlation adopted by Ranz and Marshall [50, 51].

$$\dot{m}_F = 2\pi D_0 \frac{k_g}{c_{p:g}} ln(1+B)(1+0.30Re_d^{1/2}Pr^{1/3}) \quad (2.19)$$

2.3.5 Effects of the Droplet Velocity

The evaporation/combustion phenomenon of the droplet influences the velocity of the droplet throughout the occurrence of the procedure. In the investigation of this event, is conceivable the effect of the droplet initial velocity in the droplet diameter reduction and the related droplet velocity variation. Hence, the analysis of the influences of the initial droplet velocity in the evaporation and combustion procedure reveal relevant to analyze the combustion performance and evident variation of the droplet velocity.

Some studies analyze the evolution of the droplet velocity throughout the evaporation phenomenon of liquid droplets suggesting a decrease of the droplet velocity with the reduction of the droplet diameter. This might be explained by the decrease of mass of the fuel droplets provoked by the evaporation process, which considering Newtonian physics and a case of a free-falling droplet, the reduction of mass by the droplet results in a decrease in the droplet acceleration and consequent velocity. The studies performed by Roth et al. [72], implement a technique that intends to scatter the droplet just after being released into the observation channel that is further detected by a CCD camera. The studies analyze the reduction of the droplet diameter due to the evaporation of different liquids such as n-alkanes, while also evaluating the evolution of the droplet velocity. Throughout the evaporation process is visible the decrease of the droplet velocity in comparison with the initial velocity. The numerical research of Xie et al. [73] regarding liquid droplets expelled from the mouth in the thematics of respiratory diseases also suggests that the contraction of the droplet diameter due to the evaporation provokes a decrease in the droplet falling velocity during the evaporation process. Lastly, there are the numerical studies of Sharma et al. [74] where it is studied the

droplet characteristics within internal combustion (IC) engines and how it affects the performance of the engine. This research utilizes a PDF cloud distribution to analyze the distribution of gasoline droplets in the domain and study their velocities. The obtained distribution shows lower droplet velocities for smaller droplets assuming that the study does not consider the analysis of the droplet throughout the domain in a Lagrangian approach. This fact suggests that the smaller droplets already suffered evaporation and thus reveals a decrease in the droplet velocity alongside the evaporation.

Concerning the effects of the initial droplet velocity in the evaporation characteristics, Chen et al. [75] analyzes the evaporation of water droplets at high temperatures to investigate the extreme flash evaporation in superheated fluids. Throughout this study, it was analyzed the influence of the initial droplet velocity in the evaporation efficacy considering the thermal utilization property. The study suggests a higher thermal utilization for droplets with a lower initial velocity. This indicates faster evaporation while increasing the evaporation efficacy. However, assuming a case with a minimal variation of the initial droplet velocity at a relatively low-speed range, the study suggests that the effect can be negligible.

2.3.6 Droplet Multicomponents

Concerning the usage of multicomponents in droplet evaporation and combustion modeling, it is relevant to analyze its applicability in physical phenomena. Generally, the knowledge available about droplet evaporation and combustion is related to the information on single component droplets such as n-heptane and n-dodecane. However, the fuels that should be the aim of study from the combustion engineers are not always composed of single components droplets, increasing the complexity of the analysis. For instance, as examples of multicomponent fuels that are frequently studied, there is the case of jet fuel or the fuels that might appear as an alternative in the future, likewise the HVO.

The phenomenon of multicomponents evaporation possesses an increased extent of complexity since the different components that compose the bulk of the droplet own distinct properties that subsequently induce the vaporization of the compounds at different rates, creating concentration gradients throughout the droplet and causing mass-diffusion phenomena in the liquid phase [44]. The most volatile species tend to vaporize faster and consequently diffuse until the droplet surface, increasing their concentration at the film with further evaporation of these species happening as well. Other species with lower volatilities indicate to obey the same tendency, which induces the controlled mass diffusion in the liquid phase. Hence, some properties hold significant relevance whenever it is analyzed the multicomponents droplet, such as its volatility and the mass diffusion rates. Concerning this topic, the studies developed by Makino and Law [76] demonstrated the overall importance of the Peclet number (Pe) in this process as opposed to the previously predominantly used Lewis Number. In order to analyze this study is relevant to consider the Peclet number as the ratio of the rate of advection of a physical quantity by the flow to the rate of diffusion of the same quantity driven by an appropriate gradient and the Lewis number as the ratio of

thermal diffusivity to mass diffusivity. Therefore, the theory affirms that the Peclet number is preferred over the Lewis number since the Lewis number does not represent the diffusion resistance, whereas the Peclet number accounts for the ratio of mass and mass diffusion.

The studies performed by Ghassemi et al. [77] contain significant relevance in understanding the evaporation behavior of multicomponent fuel droplets. The kerosene is employed in this research, classified as multicomponent fuel, widely utilized in the industry. The kerosene droplets in the procedure were subjected to distinct environmental conditions to understand the nature of the evaporation process for different ambient pressures and temperatures. In spite of the multicomponent nature of the kerosene, it is visible that the evaporation follows the traditional $d^2\ law$. There are heavy components and lighter components, portraying distinct volatilities in their composition, which thus induce vaporization at different rates. This fact origins concentration gradients, forming around the droplet. When the droplets are tested at low environmental temperatures, the rate of heat diffusion into droplets is comparable to the rate of mass diffusion. Therefore, the heat diffusion will bear significant relevancy in the vaporization process of the droplet. However, whenever considering high environmental temperatures, heat diffusion is much faster than mass diffusion, due to this assumption the temperature inside the droplet throughout the evaporation process will be relatively constant, leading to the condition where the concentration gradient controls the evaporation rate. Additionally, as well as in the case of a single component droplet, it was visible that the evaporation rate of the multicomponents droplets will increase monotonically with the increase of the ambient temperature.

There is a considerable contribution to this theme in the numerical studies performed by Bhattacharya et al. [78] on the evaporation of multicomponent liquid fuel droplets. Through this investigation, the evaporation process is analyzed in droplets with components that possess different volatilities as well as distinct molecular weights. During the evaporation of the multiple component droplets, the numerical simulation on this research reveals that the more volatile compound evaporates first from the surface, which oversteps the less volatile components. Nevertheless, the remaining constituents will possess distinct weights alongside different massic fractions. Therefore, the evaporation behavior and the droplet lifetime are controlled by the component holding a higher percentage of the fuel droplet composition due to being the component with a higher molecular weight. The phenomenon of admitting an isolated compound as the leading responsible for the evaporation behavior has significant relevance in numerical simulations, where it is habitually challenging to simulate the evaporation of all the compounds of the droplet due to a lack of computational resources.

2.3.7 Infuence of Fuel Composition

Several fuels reveal appealing results that might have significance to the alternative sustainable fuels theme. Consequently, relevant to study experimental researches of combustion procedures produced in the literature on distinct types of fuels in different environments and analyze their various combustion characteristics and properties. The variation of these

properties is thus researched regarding the chemical composition and the environmental conditions.

Shang et al. [79] investigates the experimental phenomenon of the combustion and microexplosion characteristics of different n-alkanes droplets, which fuels that yield more appeal for this dissertation are n-dodecane and n-hexadecane. The analyzed d^2 curves assume a relationship between the square of the normalized droplet diameter with normalized time. Initially, there is a heating phase until the droplets achieve the boiling point, resulting in the beginning of the evaporation process and an evident decrease of the droplet diameter over time (Figure 2.11).

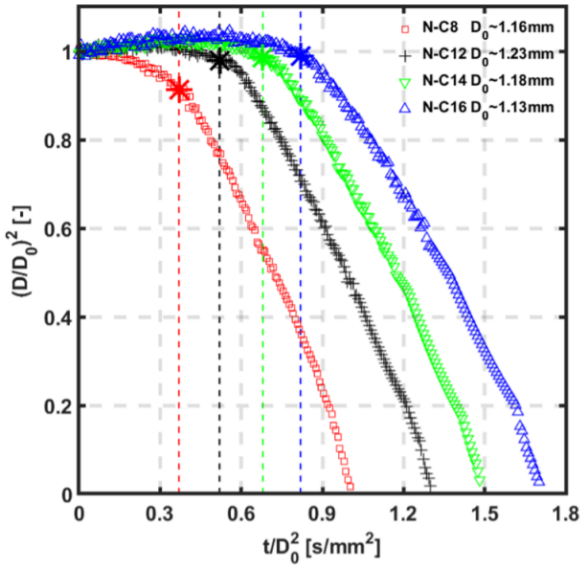

Figure 2.11: Evolution of the square of the normalized droplet diameter with normalized time for single component fuels; the vertical dashed line with an asterisk corresponds to the time of ignition, adapted from [79].

Throughout the study, the single component n-alkanes exhibited similar d^2 curves, while the fuel droplet has experienced evaporation and consequent combustion. The study bears a tendency between the burning rate obtained constant and the size of the carbon chain of the fuel. The increase in the number of carbons in the fuels molecular chain suggests a decrease in the burning constant and an increase in the droplet ignition time. This evidence indicates a relationship between the carbons of the fuel and the droplet lifetime. The reduction of the boiling point alongside higher vapor pressure verified by fuels with lower carbons within their molecular chains may justify these occurrences. Due to the evidence gathered from this article [79], is then expected that n-dodecane possesses a higher droplet lifetime, ignition time, and burning constant in comparison with n-hexadecane. Figure 2.12 depicts the obtained relationship between the number of carbons in the molecular chain, the burning rate of the fuel, and the adimensional droplet lifetime.

The analytical and experimental research performed by Faeth and Olson [80] assisted the understanding of the influences of the n-alkanes nature, ambient temperature, and ambient flow conditions in the resulting combustion characteristics of the fuel droplets. This work

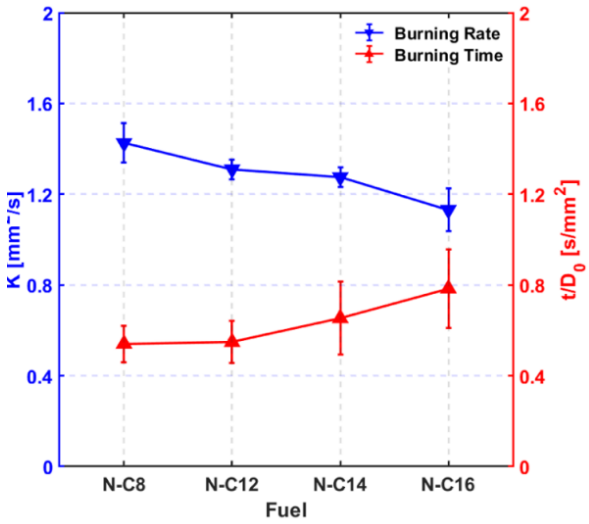

Figure 2.12: Evolution of the mean burning rates (left, blue) and normalized combustion duration (right, red) with four single component n-alkane droplets adapted from [79].

aims to develop an analytical model that replicates the ignition of single fuel droplets in the air considering the influence of these time-varying conditions. The experimental performed work validates the constructed numerical model and aids further acquired knowledge of the phenomenon. The research utilized an experimental apparatus expected to reproduce the phenomenon of a single free-falling droplet within a combustion chamber. The utilization of ignition constants of the different fuels to model the ignition of the distinct fuels enables the determination of the ignition times depending on the droplet size. This correlation is performed for the employed fuels and further calculates the critical (minimum) diameters that enable the occurrence of ignition and combustion. Figure 2.13 shows the gathered results that are then comprised, depicting remarkable similarities for all the distinct fuels. The study refers that the results require careful analyses due to the specificities of the experimental conditions. However, the results ensure a relationship between ignition time and the size of the droplet, allowing the creation of ignition and non-ignition regions. The separate regions allow the correlation of different fuels within the combustion conditions, varying depending on the fuel characteristics and the ambient temperature. The utilization of this data might satisfy the analysis of these fuels for distinct ignition conditions within the range of these characteristics. This information is helpful in the further research of n-hexadecane for the different temperatures tested in the simulations of this dissertation.

According to the experimental study performed by Xu et al. [81], there is a significant influence on the combustion characteristics and soot production between jet fuel and algae-derived biofuel. Throughout the studies, the droplets are assumed as spherical and ejected in a free-falling environment, where is achieved similar operating conditions to the combustion chambers. During the experiment, there is the intention of varying the composition of the droplets where it is analyzed the combustion characteristics of pure jet fuel, pure algae-derived biofuel, and respective mixtures. It is incorporated into 25%, 50%, and 75% of an alga-derived biofuel into the original jet fuel. Noteworthy, the jet fuel utilized in this exper-

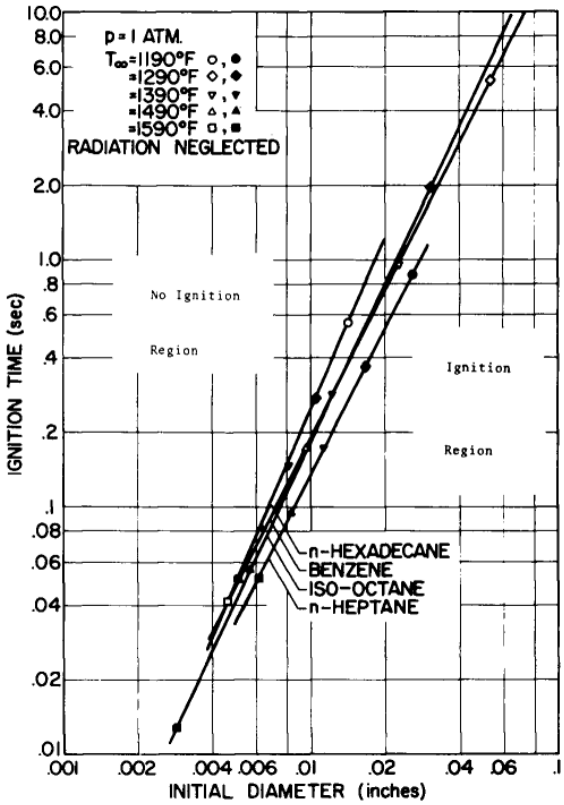

Figure 2.13: Computed ignition limits for the different fuels while correlating with the droplet diameters, adapted from [80].

iment possesses approximately 16% aromatics while the algae-derived biofuel contains no aromatics. This fact will imply different behaviors in the combustion process besides the variation in the emissions of pollutants. Through an analysis of the quantitative measurements of the tests, the time of evaporation of the jet fuel droplets will be greater in comparison with the utilized biofuel as well as with all the blends. Besides this, was reported the increase in the burning rate with the addition of the Algae-Derived biofuel, since the experiment with a lower burning rate corresponds to pure jet fuel droplets. Both of these parameters are important with the intent of reduction of pollutant emissions. However, the analysis of the presence of soot in each test has a more direct evaluation of the combustion emissions. In this experiment, the presence of soot is performed while recurring to images of the soot "shell" in BW images. During this study, it was visualized an increase of soot with the increment of the presence of jet fuel in the tested droplet blends, this fact was expected since the algae-directed biofuel, which is blended with jet fuel, has virtually no components that generate soot pollutants, such as aromatics. The experimental results indicate that this algae-derived biofuel can be an attractive additive to the commonly employed aviation fuels.

In the study performed by Muelas et al. [82], similar conclusions were achieved concerning the combustion properties of jet fuel. The experiment conditions were identical to the ones previously mentioned, yet rather than being used Algae-Derived biofuel fuel, it is utilized butanol. Butanol can also be portrayed as an alternative fuel, due to its sustainable nature. In this case, it is studied the combustion of pure jet fuel, its blend with 10%, 20%, and 50% of

butanol, and pure butanol for the same combustion conditions. Conversely to what was visualized previously the evaporation curves and the burning rates of the jet fuel and its blends are similar. In contrast, pure butanol displays a distinct behavior likely explained due to its higher latent heat of vaporization. Nevertheless, it was also seen a reduction in the presence of soot with the increase of the percentage of butanol in the fuel droplets. The results obtained are relevant since the butanol addition to the mixture does not suggest the reduction of the combustion efficacy and correspondent modifications on the burning characteristics.

Regarding the importance of the comparison of biofuels and fossil fuels, it is significant the study performed by Pacheco et al. [6]. Pacheco et al. investigated the influence of the presence of HVO and jet fuel within the combustion characteristics of the fuel droplets. The absence of aromatics in the constitution of the HVO, implying lower quantities of soot that should be emitted in comparison with jet fuel, justifies the utilization of this fuel in this research. Throughout the process, it was analyzed the combustion and the d^2 law of jet fuel and HVO and the correspondent blends of 25%, 50%, and 75%, further analyzed considering different temperatures of the facility. The droplets of pure jet fuel present the highest burning rate, and droplets of pure jet fuel have the shortest burning time, increasing the lifetime with the increment of the quantity of HVO in the mixture. This might occur due to the higher volatility of the aromatic components present in jet fuel composition meaning the increased volatility of jet fuel. Subsequently, the droplet burning time increases with the temperature of the air decreases. Whichever analyzed combustion property, it is significant to remark its importance within the implementation of biofuels in aviation nowadays. The experimental results indicate that the blending of alternative fuels into the airplane burning mixtures does not decrease significantly the efficacy levels of engine combustion originally intended for jet fuel.

Chapter 3

Numerical Modeling and Methodology

This chapter introduces the CFD modeling supported by clarifying the physical events intended to simulate. Furthermore, there is an explanation of the physical models that are incorporated and respective mathematical formulations. In the previous section, it was mentioned the relevancy of combustion within the field of fuels. After explaining this thematic, there is paramount importance in describing the type of events intended to replicate in the simulation. A proper simulation requires thus information about the experimental facilities and conditions of the phenomena reproduced.

The second section describes both physical and mathematical models employed to represent the physical phenomena. Throughout this section, the concepts of the Euler-Lagrange approach are presented. This fact implies the explanation of the continuous and discrete phase, and subsequent assumptions and models. The numerical process involved in combustion modeling is also described.

The third section comprises the description of the procedure within the operated software ANSYS®Fluent 2021 R1. The geometry, meshing, boundary conditions, and respective computation and discretization methods are described. Throughout the section, the case is specified and further exhibited the mathematical approaches utilized to solve the equations and achieve a reasonable solution.

Lastly, there is a display of the grid independence study for the numerical model. This study assumes a relevant role to reach coherent data. This parameter is only achieved when meshes do not affect the numerical solution.

3.1 Introduction and Physical Phenomenon

The combustion bears as a phenomenon of importance within the improvement of fuel utilization in transportation like was previously illustrated. The relevancy of combustion was further exemplified recurring to studies and researches that highlight the development between the combustion of fossil alkane fuels and novel biofuels. Therefore, this dissertation goal is the investigation of fuel burning characteristics when injected with spherical shape into the combustion chamber. Consequently, the present work aims to numerically simulate the phenomenon of single droplet combustion in a DTF. Numerical studies contain a valuable complement to experimental research due to the increased problems in performing the experimental works. The high cost of the experimental rigs and the difficult conditions

to replicate in experimental facilities benefit an increment in numerical research. Recently, studies performed by Pacheco et al. [6] and Ferrão et al. [7, 8] aim to understand the combustion characteristics of falling droplets in a DTF.

The combustion facility was firstly employed in Pacheco et al. [6] investigations on combustion o biofuel droplets and then utilized in Ferrão et al. [7–9] studies. The drop tube furnace (DTF) possesses an electrically heated coil and a vertical quartz tube with an inner diameter of $6.6\ cm$ and a length of $82.6\ cm$. It can achieve wall temperatures up to 1200 °C that are monitored by two type-S thermocouples. The DTF has two opposed rectangular windows, with $2\ cm$ width and $20\ cm$ height, placed in the heating zone, where the coils are located, which is $30\ cm$ long. Figure 3.1 exhibits the experimental setup intended to simulate, which contains inside the representation of the heated quartz tube pictures of burning fuel droplets and their flame, representing a schematic of the distinct phases of the combustion procedure.

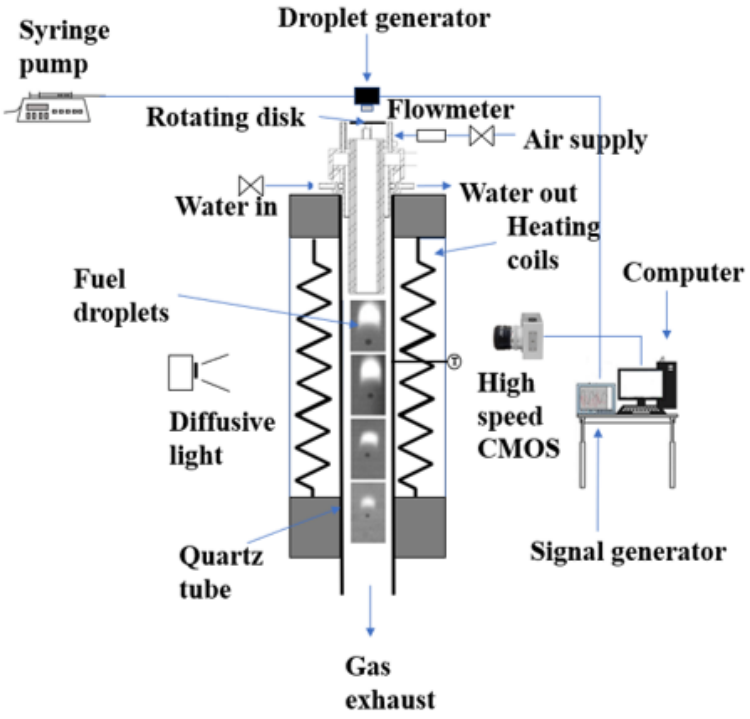

Figure 3.1: Schematic of the experimental setup, adapted from [6–9].

The phenomenon intended to simulate is the single droplet combustion within a drop tube furnace. There is the injection of fuel single droplets in a hot air environment which promotes the combustion of the droplets. The air supply is constant and $5.7 L/min$ which guarantees stable laminar airflow inside the DTF. On the contrary, the drop tube furnace temperature varies, ensuring the analysis of the temperature variation in the combustion event. This particularity generates the divergence of the air characteristics for each aimed temperature within the DTF, which requires further analysis in the results section. The numerical simulation intends to reproduce the combustion of n-dodecane, jet fuel, and n-hexadecane. These fuel droplets experiment with the burning in two distinct temperature environments performed by Pacheco et al. [6], and Ferrão et al. [7–9]. The two ambient temperatures de-

signed to simulate are 800 °C and 1000 °C.

Concerning the fuels tested in this research, the usage of Jet-A1 is justified since it is the main source of air transportation. Additionally, n-dodecane was also tested since it is a single component surrogate fuel of jet fuel for which reliable data on its properties is available in the literature [83]. Furthermore, there is the intention to simulate n-hexadecane [78, 84, 85] considering that it is one of the main components of the HVO, a possible replacement for jet fuel. Table 3.1 depicts the information of the experimentally employed fuels considering the suppliers information from previous works [12–14, 86]. The information regarding jet fuel and HVO are held from the experimental research of Pacheco et al. [6], while the n-dodecane information is withdrawn from the literature [53, 87]. The experimentally obtained information represents a reliable reference to assess the accuracy of the models employed in the numerical computations. Hence, the experimental data utilized to validate de numerical models are obtained from the laboratory facilities and conditions extensively depicted.

Parameter	**Jet-A1**	**n-Dodecane**	**HVO**
Density at 20 °C $[Kg/m^3]$	798	749.5	780.6
Viscosity at 40 °C $[mm^2/s]$	1.2	1.34	2.98
Aromatics $[wt\ \%]$	13.8	-	0.2
Distillation at 10 vol % $[C]$	169.9	-	262
Final Boiling Point $[C]$	237.2	216.2	300
Sulfur $[wt\ \%]$	0.3	-	≈ 0
Cloud Point (C)	-26	-	-30
LHV $[MJ/kg]$	43.4	44.47	43.9
LHV $[MJ/L]$	34.6	33.75	34.2
Hydrogen Mass Content	14.5	0.25	15.4
Carbon Mass Content	85.5	85.0	84.6
H/C Ratio	1.99	2.16	≈ 2.18
Average Chemical Composition	$C_{10.8}H_{21.8}$	$C_{12}H_{26}$	$C_{15}H_{32}$–$C_{18}H_{38}$

Table 3.1: Summary of properties of the fuels employed experimentally [6, 53, 87].

3.2 Mathematical and Physical Models

The employment of physical and mathematical models aids the depiction of an experimental phenomenon in a numerical simulation. The representation of a particular phenomenon requires the knowledge of the physical events which occur alongside an illustration of the procedure in mathematical assets. The accurate selection of a specific approach to represent an experimental phenomenon like the one intended in this dissertation ensures the acquisition of compatible data with the laboratory outcomes. Furthermore, there is an extensive explanation of the best-fitted approach to simulate the intended single droplet combustion process.

3.2.1 Euler-Lagrange Approach

There is the necessity to define a model that can simplify the physical phenomena of droplets falling in a hot furnace tube. Therefore, the case can be scrutinized into the simplified occurrence of droplets falling within an air domain. Although the phenomenon is rather complex, this multiphasic approach can simplify the analysis. Generically, two types of numerical models describe multiphase fluids problems. In an Eulerian model, both phases are treated as a continuum, and respective time-averaged equations are calculated for both phases. However, there is tracking and analysis of a certain dispersed phase particle within a fluid in a Lagrangian model. The computation and tracking of the path of the particle follow the lagrangian dynamic of the particle. This specific case implies the phenomenon of single droplets within a hot air domain [6–9]. The literature formed by Shirolkar et al. [88] and Yuan and Crowe [89] suggests a formulation that might be adequate for this problem known as Euler-Lagrange. In this schematic, the single droplets represent a particle dispersed phase, while the hot air that involves the domain depicts a continuous phase. The continuum phase computation requires solving the time-averaged equations of the properties of the fluid recurring to discretization methods. The discrete phase treats the fluid differently, where the droplet properties are condensed in a particle, and the path is determined considering the Lagrangian dynamic of the particle. The interactions of both phases are not negligible, being considered a two-way-coupling system, and assume relevant importance in this case since the modeling of combustion depends on this process.

3.2.1.1 Continuous phase

The Euler-Lagrange approach requires the definition of a continuous phase. This flow of air that involves the experimental facility assumes the role of a continuous domain. It is appropriate to regard air as a continuum at a macroscopic length scale where the microscopic molecular structure and matter are ignored as a discrete phase. Consequently, several properties such as density, dynamic viscosity, thermal conductivity are constant throughout the domain. These assumptions ensure the simplification of the model. The consequent validation is ensured by comparing the experimental and numerical temperature development within the DTF.

The representation of the air in the mathematical description helps gather the gas properties in each location and respective properties. These equations result from the continuity, momentum, and energy equations represented in the form of time-averaged partial differential equations. The usage of these equations corresponds to the necessity of implementing a model that accounts for the fluctuations of velocity originated in a turbulent source. The performed experiment demands accounting for the turbulence that might occur in the experimental apparatus even if it is considered a nearly laminar situation in the DTF. Equations 3.1, 3.2, and 3.3 denote the continuity, momentum, and energy Reynolds Averaged Navier Stokes equations that represent the flow in a Cartesian tensor. The implementation of these models was previously considered in Markatos et al. [90].

$$\frac{\partial \rho}{\partial t} + \frac{\partial \left(\rho \overline{U_i}\right)}{\partial x_i} + S_m = 0 \quad (3.1)$$

$$\frac{\partial \overline{U_i}}{\partial t} + \frac{\partial \left(\rho \overline{U_i} \overline{U_j}\right)}{\partial x_j} = -\frac{\partial \overline{p}}{\partial x_j} + \frac{\partial}{\partial x_j}\left[\mu\left(\frac{\partial \overline{U_i}}{\partial x_j} + \frac{\partial \overline{U_j}}{\partial x_i} + -\frac{2}{3}\delta_{ij}\frac{\partial \overline{U_l}}{\partial \overline{x_l}}\right)\right] + \frac{\rho \overline{U_i' U_j'}}{\partial x_j} + S_{\overline{U_i}} \quad (3.2)$$

$$\frac{\partial}{\partial t}(\rho E) + \nabla \cdot \left(\overrightarrow{v}(\rho E + p)\right) = \nabla \cdot \left[k_{eff} \nabla T - \sum_j h_i \overrightarrow{J_j} + \left(\overline{\overline{\tau}}_{eff} \cdot \overrightarrow{v}\right)\right] + S_H \quad (3.3)$$

In the continuity and momentum equations (3.2 and 3.1), ρ accounts for the density of the fluid, μ assumes the parameter of the continuous phase viscosity, $\overline{U_i}$ represents the mean velocity of the fluid in a certain direction, $\overline{p}$ portrays the mean pressure and δ_{ij} is the kronecker delta. Concerning the energy equation 3.3, E accounts for the energy transfer due to conduction, h represents the sensible enthalpy, k_{eff} is the effective conductivity, $\overrightarrow{J}$ portrays the diffusion flux of species, $\overline{\tau}_{eff}$ represents the viscous dissipation and T is the static temperature. The various represented S parameters account for the distinct source terms for each considered equation.

The term $\rho \overline{U_i' U_j'}$, known as stress Reynolds, is commonly modeled recurring to the Boussinesq Hypothesis, developed by Lauder and Spalding [91]. The method depicted in Equation 3.4 computes the value of the Reynolds Stresses of a specific flow by relating this parameter with the mean rates of deformation:

$$\rho \overline{U_i' U_j'} = -\mu_t \left(\frac{\partial \overline{U_i}}{\partial x_j} + \frac{\partial \overline{U_j}}{\partial x_i}\right) + \frac{2}{3}\rho k_t \delta_{ij} \quad (3.4)$$

In which k_t stands for the kinetic turbulent energy. In this case, due to the two-dimensional nature of the flow, there are only two components depicted in Equation 3.5.

$$k_t = \frac{1}{2}\sqrt{\overline{U_i'^2} + \overline{U_j'^2}} \quad (3.5)$$

In this particular computation, where two distinct phases exist the source terms assume particular relevancy. These terms exhibit the interactions between the continuum fluid and the particulate material accounted through the source terms(S_m, S_{U_i} and S_H) for the flow equa-

tion. Typically, for a general variable property per unit mass, ϕ, the source term is portrayed as S_ϕ. Despite the previously mentioned expressions, continuous phase modeling requires the usage of additional equations that compute the transport and evolution of the different occurring phenomena throughout the domain. This event is accomplished by assuming a specific scalar, ϕ, that might be either the energy, mixture fraction, or enthalpy, among others, which are further applied in the respective transport equation depicted in Equation 3.6. Examples of these properties can be the species transport and combustion modeling parameters.

$$\frac{\partial(\rho\phi)}{\partial t} + \frac{\partial(\rho\phi U_i)}{\partial x_i} = \frac{\partial}{\partial x_i}\left[\Gamma_\phi \frac{\partial \phi}{\partial x_i}\right] + S_\phi \quad (3.6)$$

Equation 3.6 possesses as the first term the temporal term, followed by the convective term. This first part of the equation is equalized to a diffusive term including the parameter , Γ, portraying the effective diffusion coefficient for quantity ϕ and the respective source term.

The k-ε approach of Lauder and Spalding [91] is a widespread turbulence model since allows the representation of turbulence for various applications and cases. The turbulence is extremely complex due to the dissipated nature, and momentum exchanged by small-scale fluctuations. These processes are inconceivable to simulate at their full complexity with regular computational resources. Hence, it urges the necessity of utilizing turbulence models to aid the representation of these phenomena. There are numerous cases of turbulence models that vary in level of complexity and thus are required for a different combination of analysis. The k-ε model is a two equations model which will determine a certain turbulent length and time scale by solving two distinct transport equations. The two additional equations that are solved describe the evolution of the turbulence kinetic energy k_t and dissipation rate ε throughout the flow. Generally, these equations are depicted in Equations 3.7 and 3.8. The inclusion of the turbulence model characteristic equations defined as k_t and ε in the algebraic system formed by Equations 3.1, 3.2 and the variations of Equation 3.6 allows the computation of the flow attributes and evident turbulent properties. Hence, it is possible to obtain the development of the flow and perform a proper analysis of the flow properties within the domain.

$$\begin{aligned}\frac{\partial}{\partial t}(\rho k_t) + \frac{\partial}{\partial x_i}(\rho k_t U_i) = \frac{\partial}{\partial x_j}\left[\left(\mu + \frac{\mu_t}{\sigma_k}\right)\frac{\partial k_t}{\partial x_j}\right] - \rho\overline{U_i' U_j'}\frac{\partial U_j}{\partial x_i} - g_i\frac{\mu_t}{\rho Pr_t}\frac{\partial \rho}{\partial x_i} - \\ \rho\varepsilon - 2\rho\varepsilon\left(\sqrt{\frac{k_t}{a^2}}\right)^2 + S_k\end{aligned} \quad (3.7)$$

$$\frac{\partial}{\partial t}(\rho\varepsilon) + \frac{\partial}{\partial x_i}(\rho\varepsilon U_i) = \frac{\partial}{\partial x_j}\Big[\Big(\mu + \frac{\mu_t}{\sigma_\varepsilon}\Big)\frac{\partial \varepsilon}{\partial x_j}\Big] + C_{\varepsilon-1}\frac{\varepsilon}{k_t}(\rho\overline{U_i'U_j'}\frac{\partial U_j}{\partial x_i}) + C_{\varepsilon-3}\Big(g_i\frac{\mu_t}{\rho Pr_t}\frac{\partial \rho}{\partial x_i}\Big) - C_{\varepsilon-2}\rho\frac{\varepsilon^2}{k_t} + S_\varepsilon \tag{3.8}$$

The implementation of the turbulence model results in the appearance of several constants. The constants are initially unknown, yet possess relevancy to the simulation. Lauder and Spalding [91] studied the determination of the constants based on the analysis of experimental data to reproduce a numerical simulation capable of reliable outcomes. The constants given in Table 3.2 allow the resolution of the equations system and an evident illustration of the turbulent flow. Overall, this model has been widely used throughout the past decades, which revealed its efficiency in reproducing turbulent flows.

$C_{\varepsilon-1}$	$C_{\varepsilon-2}$	$C_{\varepsilon-3}$	σ_k	σ_ε	Pr_t	Sc_t	Pr	Sc
1.44	1.92	1.1	1.0	1.3	0.6	0.85	$\mu\frac{C_p}{k}$	$\frac{\mu}{\rho}C_d$

Table 3.2: Coefficents of the "k- ε" turbulence model calculated from Lauder and Spalding studies [91].

Essentially, the implementation of this turbulence model is sustained by its simplicity and versatility. The model does not require much further analysis and applies to a wide variety of situations. The experimental work intended to simulate describes the internal flow of the laboratory facility as similar to laminar. This evidence results in a numerical simulation where a relatively low prevalence of turbulence is expected. A situation with low levels of turbulence requires the utilization of a simple turbulence model that is adaptable for different cases. Consequently, the usage of k -ε reveals to be sufficient to obtain reliable outcomes in this research. After describing the calculation of the continuous phase, there is a need to characterize the discrete phase and mention the required assumptions.

3.2.1.2 Dispersed phase

The approach utilized to regard the discrete phase is acknowledged as a Lagrangian approach. The droplets are described as material particle that is tracked and labeled as it moves and adapts their properties throughout the domain. This approach requires distinctive assumptions and formulations that are necessary to develop a reliable computation of this phase. Essentially, there are mainly two different procedures to define the Lagrangian discrete phase treatment. It is possible to employ the Taylor fluid particle dispersion model and the models based on the particle momentum equation. The model suggested by Shirolkar et al. [88] assumes that the particle trajectories of the representative samples are obtained by solving the momentum equation of the particle while immersed within an Eulerian fluid velocity field. The Eulerian fluid velocity can be acquired by solving the averaged Navier-Stokes equations recurring to a turbulence model, such as $k-\varepsilon$, providing the time-averaged

Eulerian fluid velocity. This property at the specific location of the particle enables the calculation of the particle momentum equation. In order to calculate the particle attributes it is also relevant to account for the correspondent fluctuating component of the velocity at every particle location throughout the computational domain. The determination of the fluid velocity information suggests that the computation of the particle trajectory requires previous knowledge of the flow that involves the droplet, such as considered in a two-way-coupling scheme.

The models based on particle momentum equation are also known as discrete particle separated flow (DPSF) and as suggested previously, they treat the carrier phase and discrete phase separately considering the finite interphase transport rates. Researches like Gosman and Ionnides [92], Shuen et al. [93], Yuan et al. [89] researched this approach, yet Shirolkar et al. [88] referred to which type of phenomena might be analyzed recurring to this modeling. The research suggests that these models elegantly account for several complex phenomena, such as vaporization and combustion of a discrete phase similar to what is demanded in this case. DPSF mainly differs according to how the trajectories of the particles are determined. Additionally, the dispersive effects of turbulence can be incorporated into the particle motion by using the Monte Carlo approach [94]. This method possesses a stochastic nature that involves the computation of numerous particle trajectories to obtain statistical information that characterizes the particle behavior. The schematic assumes relevancy in work developed by Wang and Stock [95]. Generally, the DPSF models that involve the Monte Carlo simulation are also referred to as stochastic separated flow (SSF). These models determine the fluctuating instant fluid velocity at the particle location needed to calculate the total velocity and then solve the particle equation of motion. The procedure utilized to determine the fluctuating fluid velocity assumes particular importance in the discrimination of the method. In this research, it is employed a deterministic tracking model with these characteristics.

Considering the SSF model assertions, it is required to compute the particle equation. The trajectory followed by the particle can be determined by solving the equation of motion of the particle deduced from Newton second law of motion. The definition of the discrete trajectory requires the quantification of all the forces that act on the particle, which is enounced in Shirolkar et al. [88]. The equation of the particle motion was firstly derived by Basset [96], Boussinesq [97], and Oseen [98] and is represented in Equation 3.9. The formulation of this equation led to the description of the respective moving forces further divided into Basset, Virtual mass, and Magnus forces. Basset forces describe the transitory nature of the particle mainly influenced by the history of the particle trajectory. The virtual mass force originates in the difference in acceleration between both phases in motion, being more present whenever there is a significant difference between the densities of the fluid and the particle. Lastly, the Magnus force results from the rotating process of the particle. Additionally, the Staffman force may be considered whenever an environment of uniform shear flows is present. This force describes a lift force that results from the local gradients.

$$\underbrace{m_p \frac{\partial U_{p:i}}{\partial t}}_{\text{Inertia Force}} = \underbrace{3\pi\mu_c d_p f(U_{c:i} - U_{p:i})}_{\text{Steady-state Draft Force}} + \underbrace{K_B d_p^2 \sqrt{\pi\rho_c\mu_c} \int_{t_0}^{t} \frac{\frac{\partial}{\partial t}(U_{c:i} - U_{p:i})}{\sqrt{t-t'}} dt'}_{\text{Basset Force}}$$
$$+ \underbrace{K_m \rho_p \frac{\pi}{6} d_p^3 \frac{\partial}{\partial t}(U_{c:i} - U_{p:i})}_{\text{Virtual Mass Force}} + \underbrace{\frac{\pi}{8} \rho_c d_p^3 \omega_p \varepsilon_{ijk} n_{1:j} (U_{c:i} - U_{p:i})}_{\text{Magnus Force}} \tag{3.9}$$
$$+ \underbrace{m_p g_i}_{\text{Body Gravity Force}} - \underbrace{\rho_c \frac{\pi}{6} d_p^3 g_i}_{\text{Buoyancy Force}}$$

The obtained expression couples all the forces present in the motion of the particle and possesses great complexity. However, several assumptions can be employed, such as assuming the droplet as spherical body geometry, considering the particle-particle collision negligible, and supposing the particle density to be much larger than the surrounding fluid density. In terms of spherical body geometry, the particle drag may be considered similar to a sphere due to the low static pressure gradient. Following the intention of the simulation of replicating the single droplet event, it is considered that the droplets will not suffer from collision interaction. The presence of single fuel droplets within hot air presumably assumes that the density of the dispersed phase is much higher than the revealed by the continuous phase. The further verification of a difference between the fluid densities being a ratio greater than 200 justifies the employment of the simplification. These assumptions result in neglecting several fluid forces such as Basset, virtual mass, Magnus, and Staffman lift forces. The resulting expression is Equation 3.10, where the steady-state drag term is yet not neglected due to the importance of this force applied on the particle.

$$\frac{\partial U_{p:i}}{\partial t} = \frac{1}{\tau_p}(U_{c:i} - U_{p:i}) + g_i \tag{3.10}$$

The simplified equation allows determining the particle velocity, $U_{p:i}$, considering the fluid mean velocity, $U_{c:i}$, the externally applied forces g_i and τ_p perceived as the particle relaxation time. This property describes the response rate of the particle acceleration to the relative velocity between the particle and the respective carrier fluid. Whenever the droplet is dense enough, the inertial force at the fluid-particle interface will dampen the fluctuations in its velocity compared to the fluctuations observed in the surrounding fluid. This reduction in its root means square (rms) fluctuating velocity in a time scale perceives an inertia effect. Therefore, the droplet relaxation time is relevant in the discretization of the particle path and the respective definition exhibited in Equation 3.11.

$$\tau_p = \frac{24\rho_p d_p^2}{18\mu_c C_D Re_p} \quad (3.11)$$

Where Re_p represents the particle Reynolds described as:

$$Re_p = \frac{\rho|U_{p:i} - U_{c:i}|d_p}{\mu} \quad (3.12)$$

Moreover, the consequent Equation that defines the drag coefficient, C_D, is enounced as:

$$C_D = \begin{cases} \frac{24}{Re_p}(1 + 0.5Re_p^{0.687}), & Re_p < 1000. \\ 0.44, & Re_p \geq 1000. \end{cases} \quad (3.13)$$

Furthermore the association of Equations 3.12 and 3.13 result in Equation 3.11. This equation reveals a novel way of characterizing the particle relaxation time in Equation 3.14.

$$\tau_p = \frac{m_p}{3\pi\mu d_p}\frac{1}{1 + 0.15Re_p^{0.687}} \quad (3.14)$$

The determination of the particle information through the passage of time accounts for the newtonian physics and respective dynamics represented in Equation 3.10. This expression demands integration over small time steps (Δt), resulting in Equation 3.15, where is included the fluid mean velocity and the droplet relaxation time that were earlier estimated. The utilization of the different particle velocities for each position alongside the evident discretization ensures the creation of an expression that describes the droplet trajectory represented in Equation 3.16. Hence, the employed process to determine the droplet properties is considered iterative requiring information from the previous time steps.

$$U_{p:i}^{NEW} = U_{c:i} + (U_{p:i}^{OLD} - U_{c:i})e^{\frac{\Delta t}{\tau_p}} + g_i\tau_p(1 - e^{\frac{-\Delta t}{\tau_p}}) \quad (3.15)$$

$$x_{p:i}^{NEW} = x_{p:i}^{OLD} + \frac{\Delta t}{2}(U_{p:i}^{NEW} + U_{p:i}^{OLD}) \quad (3.16)$$

The utilization of Equations 3.15 and 3.16 applied to the different cartesian coordinates ensures the computation of the particle trajectory at each time step. The utilized software computes the velocity of the fluid regarding the Equation 3.15 and uses an analytical discretization scheme [99]. The result is the respective velocity of the particle at each location of the path that is further used to calculate the new position. The schematic employed is the trapezoidal discretization. The trapezoidal schematic of determining the velocity at each position is exhibited in Equation 3.17. Furthermore, the analytical trapezoidal schemes provided by the software employ Equation 3.16 to determine the new position of the particle.

$$U_{p:i}^{NEW} = \frac{U_{p:i}^{OLD}\left(1 - \frac{1}{2}\frac{\Delta}{\tau_p}\right) + \frac{\Delta}{\tau_p}\left(U_{c:i}^{OLD} + \frac{1}{2}\Delta t U_{p:i}^{OLD} \cdot \nabla U_{c:i}^{OLD}\right) + (\Delta t) g_i}{1 + \frac{\Delta t}{\tau_p}} \quad (3.17)$$

The stochastic model used is denominated as discrete random walk (DRW) model or "eddy lifetime" model. This model defines the particle trajectory in a turbulent flow as an interaction between the particle and a succession of discrete stylized fluid phases with turbulent eddies. This model accounts for the characterization of each eddy by a gaussian distribution (as a probability density function) random velocity fluctuation and time scale. There are parameters essential for the model computed by the utilized software [99]. The only requirement for the DRW model implementation is a value for the integral time scale constant and the choice of the method to predict the eddy lifetime. In order to implement the model, there is a possibility to utilize either an obtained constant value or a random value as the employed constant. The calculation of the respective values for eddy lifetime and eddy size requires the understanding of the turbulent flow of the continuous phase. These parameters differ at each particle location and are required to determine each particle further interaction time with the respective eddy. Ideally, the eddy lifetime, t_e, and the integral time scale, l_e, are obtained from the Kolmogorov length scale and described in Equations 3.18 and 3.19. These procedures follow the studies developed by Shirolkar [88] and Gosman and Ioannides [92].

$$t_e = C\frac{k_t}{\varepsilon} \quad (3.18)$$

$$l_e = D\frac{k_t^{3/2}}{\varepsilon} \quad (3.19)$$

The interaction time can be deducted from the minimum between the eddy lifetime previously determined, t_e, and the minimum time (t_{cm}) that a particle would take to cross an eddy with a specific characteristic dimension l_e. Equation 3.20 describes the determination of the interaction time.

$$t_{int} = \Delta t = min(t_e, t_{cm}) \quad (3.20)$$

The minimum time (t_{cm}) that a particle would require to cross an eddy with a specific characteristic dimension l_e is defined in Equation 3.21.

$$t_{cm} = \frac{l_e}{|U_d|} \quad (3.21)$$

Shirolkar [88] suggested Equation 3.22 to describe the eddy transit time considering a simplified and linearized equation of motion of the particle in a uniform flow. The expression assumes ($|U_{c:i} - U_{p:i}|$) as a relative velocity between the particle and the fluid through the eddy interaction approximated at the start of each iteration. Whenever $l_e > \tau_p|U_{c:i} - U_{p:i}|$ is verified, the expression has no solution in the physical domain, suggesting that the particle is smaller than the eddy size. Therefore, Gosman and Ioannides [92] and Shuen et al. [93] indicate that the particle is trapped within the eddy and the interaction time assumed as the eddy lifetime.

$$t_{cm} = -\tau_p \cdot ln\left(1 - \frac{l_e}{\tau_p|U_{c:i} - U_{p:i}|}\right) \quad (3.22)$$

Furthermore, the calculated eddy lifetime is considered as the integration time step. This parameter alongside the random sampled fluctuating fluid velocity allows the resolution of Equation 3.16, which will describe the trajectory of the particle, with further Equation 3.15 computation of the velocity at each particle position. The value of the fluctuating component of the velocity requires its computation recurring to a PDF distribution. This model assumes the turbulent flow as isotropic. However, there is the possibility of creating a cross-correlation that illustrates the anisotropic properties of the flow at every time step. These relations are first studied by Yuan and Crowe [89] and further approached in Shirolkar et al. [88]. These correlations support that will be possible to determine the velocity components $U'_{i:f}$ and $U'_{j:f}$, where U'_1 and U'_2 account for two fluctuating sampled velocities from the *PDF* distribution. The components are correlated by using the correlation coefficient R and further depicted in Equation 3.23.

$$\text{Correlations} = \begin{cases} U'_{i:f} = U'_1 \\ U'_{j:f} = R \cdot U'_1 + \sqrt{1 - R^2 \cdot U'_2} \\ R = \frac{\overline{U'_{i:c} \cdot U'_{j:c}}}{\sqrt{U'^2_{i:c} \cdot U'^2_{j:c}}} \end{cases} \quad \text{, varies between } 0 \text{ and } 1 \tag{3.23}$$

Following the physical description, there is the necessity of searching within the utilized software a model that ensures implementation of this Euler-Lagrange approach. Consequently, the Discrete Phase Model (DPM) usage is justified due to its similarities with the previously mentioned Euler-Lagrange model [99]. This model uses the discretization of the particle path alongside the stochastic path prevision. The model assumes the single droplets as a discrete particle that interacts with the continuous phase in a two-way-coupling schematic and allows the occurrence of the combustion phenomenon. Furthermore, there is the intention of explaining the modulation of combustion that is performed considering heat and mass transfer between both discrete and continuous phases.

3.2.2 Combustion Modeling

3.2.2.1 Interaction Discrete Phase and Continuous Phase

The interaction between both phases reveals its most relevant phenomenon as the evaporation process. As a consequence, the modeling of the combustion recommends the definition of a specific discrete phase as a liquid fuel. Subsequently, the evaporation process is applied in the defined discrete phase following the methodology defined in Equation 3.24. These formula models the shrinking of the liquid fuel droplet particles and the quantity converted into gaseous fuel. The applied formula is similar to the obtained in theoretical models of the droplet evaporation when considered convective environments, likewise, the model exhibited in Turns [53]. Ultimately, the product of this process will moreover react with the oxidant provided in the system originating the combustion phenomenon.

$$\frac{d(d_p)}{dt} = \frac{2}{\rho_p \Delta H_{vap}} \left[\frac{2k_g \left(1 + 0.23\sqrt{Re_p}\right)}{d_p} (T_\infty - T_p) \right] \tag{3.24}$$

3.2.2.2 Combustion Phenomenon

The combustion model employment within the numerical analysis of single droplets combustion requires considering the conditions verified in the experimental setup. The experimental procedure features that the fuel droplets and the oxidant (hot air) supplies are not provided together, implying the occurrence of a non-premixed combustion process. In a process like this, the oxidant and the fuel enter the reaction zone by different suppliers [99].

The non-premixed model relies upon certain assumptions that will be further specified. The most relevant ones focus on approximating the thermochemistry of the combustion reaction into a single parameter known as mixture fraction, f, detailed in Equation 3.25, and is considered the mass fraction originated from the fuel stream injected into the domain. In Equation 3.25, the mixture fraction parameter reveals a subscript, i, that accounts for the respective species subscript. Specifically, it is characterized as the local mass fraction of the elements of the fuel streams (C, H, and the other species) and the consequent burnt and unburnt products along with the constituents of their species (CO_2, H_2O, O_2). The approach of this model assumes the conservation of the chemical reactions while inferring that the mixture fraction is a scalar quantity that does not demand the source term in its governing equation. Hence, the combustion process is simplified to a mixing process, and subsequently, the issues involved in closing the nonlinear mean reaction rates are averted. Furthermore, once the mixture fraction is computed it is important to remark the chemistry modeling that should be considered as an equilibrium model with the chemical equilibrium.

$$f = \frac{Z_i - Z_{i:Ox}}{Z_{i:f} - Z_{i:Ox}} \quad (3.25)$$

The following step of the modeling is to define how the transport occurs for the mixture fraction. Under certain assumptions, such as the verification of equal diffusivities, the species equation is allowed to be reduced to a single equation defined from studies of Jones and Whitelaw [100], which results in the Equation 3.26. In the chemical reaction, there are chemical elements that incorporate the phenomena considered conserved throughout the event. This assumption implies that the reaction source terms in the species equation can be nullified and that the parameter f is considered a conservative value. The usage of the turbulence model to capture any turbulence indicates that the transport equation of mixture f has to account for this modeling. When considering f as the applicable general variable property per unit mass, ϕ, Equation 3.6 can be rearranged into Equation 3.26. The property k accounts for the laminar thermal conductivity of the mixture, C_p is the mixture specific heat, σ_t accounts for the Prandtl number, μ_t is the turbulent viscosity, and $\overline{f}$ is the average mixture fraction. Additionally, S_m is portrayed as the source term for the mass transfer into the gas phase from the liquid fuel droplets, and S_{user} represents a user-defined source term.

$$\frac{\partial}{\partial t}\left(\rho_c \overline{f}\right) + \nabla \cdot \left(\rho_c \overrightarrow{v}\overline{f}\right) = \nabla \cdot \left[\left(\frac{k}{c_{p:c}} + \frac{\mu_t}{\sigma_t}\right)\nabla \overline{f}\right] + S_m + S_{user} \quad (3.26)$$

In order to compute the combustion procedure, the utilized software adopts the simplest and most consensual approach [100] that specifies the transport equation of the mean f and the variance described in Equation 3.27. Regarding the newly appeared variables ε portrays a

turbulent property, f' characterizes the f variance described as f'=f-$\overline{f}$ and C_d and C_g represent turbulent constants. The employed constants σ_t, C_g and C_d possess certain default values in order for the mathematical model to work, being respectively 0.85, 2.86 and 2.0.

$$\frac{\partial}{\partial t}\left(\rho_c\overline{f'^2}\right) + \nabla\cdot\left(\rho_c\overrightarrow{v}\,\overline{f'^2}\right) = \nabla\cdot\left[\frac{k}{c_{p:c}} + \frac{\mu_t}{\sigma_t}\nabla\overline{f'^2}\right] + C_g\mu_t\cdot\left(\nabla\overline{f}\right)^2 - C_d\rho_f\frac{\varepsilon}{k}\overline{f'^2} + S_{user} \quad (3.27)$$

The chemical equilibrium model is a system that allows the computation of the thermochemical reactions computing from the mixture fraction in the assumption that chemical equilibrium is reached. The model accounts for the intermediate species and dissociation reactions. The model provides a better approximation of flames temperatures in comparison with the Eddy-Dissipation model. This model is often more accurate than the assumption that the chemical equilibrium occurs in rich mixtures, allowing a smoother prediction of the equilibrium species, which facilitates the formulation of the look-up tables. Overall, flame diffusion is determined during these conditions, whereas there are other models in this software that might be more accurate in the prevision of the flamelet diffusion and prediction of flame temperatures of the fuels. The software model also assumes a non-adiabatic nature in the simulation of the combustion phenomenon considering the chemical equilibrium model. The non-adiabatic treatment considers the discrete phase as liquid fuel particles that reacts with the continuous phase occurring heat transactions. This treatment implies the computation of the energy equation by employed software, suggesting a complex and time-consuming approach that generates an elaborated computation of the species look-up tables.

The chemical model correlates the mixture fraction with the resultant species and their various properties. This computation for all the concerned species predicts the thermochemical properties, such as specific species mass fraction, density, temperature, etc. In this case, where there is a non-adiabatic nature, the calculation of the properties in the combustion environment considers the enthalpy variation, which is represented in Equation 3.28. In this expression, ϕ_i accounts for a specific property, while H represents the instantaneous enthalpy within a single mixture fraction system.

$$\phi_i = \phi_i(f, H) \quad (3.28)$$

The experimental procedure intends to reach a laminar flow, yet the combustion simulation formulation requires the assumption of the existence of turbulence. The model employed in the utilized software presumes averaged values and fluctuating scalars in the shape of an assumed probability density function (PDF), describing a turbulence-chemistry interaction

model. This mathematical formulation is depicted as $p(f)$ in Equation 3.29. Concerning the parameters of this equation, T_ω represents the time scale of the PDF function, t_i portrays the interval of time considered in the analysis, in which the mixture fraction f is consumed throughout the respective Δf band characterized as a fraction of time. The applied characterization does not possess physical meaning besides the mathematical formulation. Essentially, the goal is to approximate the turbulence observed experimentally to a representative actual mathematical function.

$$p(f)\Delta f = \lim_{T_\omega \to \infty} \frac{1}{T_\omega} \sum_{n=i} t_i \quad (3.29)$$

The non-adiabatic nature of the experiment implies that local flow computation depends on heat loss indicating the variation of the system enthalpy, H. This premise impacts the chemical equilibrium of the system and the consequent deduction of the species derived from the combustion. Hence, the estimation of the species scalars from the mixture accounts for this variation depicted in Equation 3.28. The enthalpy applied into Equation 3.6 results in Equation 3.30 that computes the local enthalpy throughout the system. The expression estimates the enthalpy within the chemical reaction system, where S_H accounts for the source term due to the heat exchange with the dispersed phase.

$$\frac{\partial}{\partial t}(\rho\overline{H}) + \nabla \cdot (\rho \overrightarrow{v}\overline{H}) = \nabla \cdot \left(\frac{k_t}{c_p}\nabla\overline{H} + \right) + S_H \quad (3.30)$$

This diagram represented in Figure 3.2 denotes the utilized schematic by the employed software to reach the final information of the combustion products. The non-adiabatic nature of the procedure reveals the importance of the enthalpy variation information aiding the characterization of the complete chemical model that defines combustion reaction. Additionally, considering this information alongside the PDF function characterizing the turbulent interactions enables the computation of the mean scalar values of the products of the combustion defined as a standard ϕ. The coupling of this procedure is the expression that calculates the mean scalars of the combustion process considering the fluctuations of the enthalpy characterized in Equation 3.31. The model utilized by the software further calculates the look-up tables with the products of combustion and the respective mean scalar properties accounting for the dependence between turbulence-chemical interactions and the non-adiabatic nature. This model considers the turbulence occurring at a droplet level where the turbulent fluctuations are measured, and the evaluated eddies possess the length scale of the droplet diameter, thus the model enables the representation of the turbulence around the droplet surface and within the combustion process.

$$\overline{\phi_i} = \int_0^1 \phi_i(f, \overline{H}) p(f) df \quad (3.31)$$

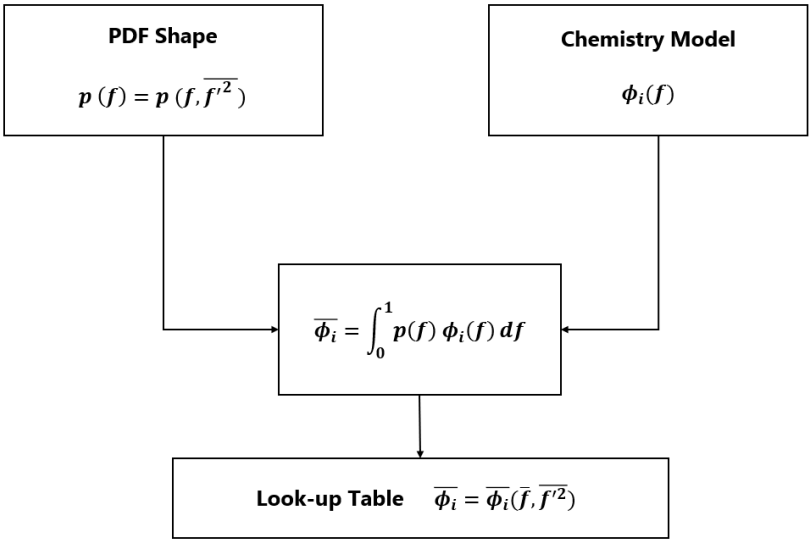

Figure 3.2: Schematic of the averaged scalars dependace and properties from the turbulence and chemistry model, adapted from [99].

Throughout this section, there was an intention of specifying the models that describe the chosen modeling approach. There was an evident explanation of the physical models employed alongside the description of the procedures. The succeeding step is the specification of the computational case and the explanation of the considered assumptions. Lastly, there is the need to specify the mathematical calculations used in the simulations.

3.3 Numerical Approach

3.3.1 Geometry and Meshing

The definition of the problem domain is one of the most relevant factors when discussing a simulation of a specific phenomenon. Consequently, the transition from the physical facility to a computational geometric domain ensures the acquisition of reliable computation results. The geometry is required then to be similar to the experiments performed.

Concerning the requirement of this case in simulating the phenomena occurring in the facility mentioned in Section 3.1, the chosen employed geometry in the numerical simulation is a two-dimensional (2D) planar configuration. This approximation has the purpose of reducing the computational cost while predicting the phenomena accurately, the low turbulence intensity revealed in the experimental procedure also allows the simplification of the 3D geometry into a 2D domain. In spite of the real problem holding a three-dimensional (3D) cylindric configuration, the simulation will consider the domain as a longitudinal rectangular plane

of the original setup as exhibited in Figure 3.3. The operating software provides CAD capabilities that allow the creation of the domain geometry. The utilized function is named *DesignModeler*, and due to the simple general interface, this tool is suitable for creating the elementary nature domain geometry.

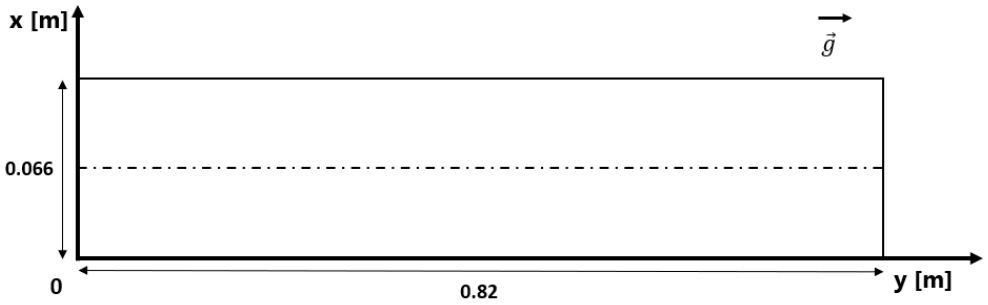

Figure 3.3: Representation of the geometry of the domain.

Considering the grid meshing of the domain, the mesh that is more suitable to the problem should be adopted. Concerning this case, the simple quadrilateral geometry suggests that the best-fitted type of mesh is a regular quadrangular mesh. In order to improve the obtained results, the mesh near the region of the inlets and the injection of the discrete phase is denser than the rest of the domain. This procedure also aids the decrease of computational power while increasing the efficacy levels with lower grid elements.

3.3.2 General Settings

This subsection describes the quality evaluation concerning the implemented mesh and the description of the general settings implemented in the simulation. Among these settings, there is an explanation of the selected solvers regarding time, pressure, and space. Lastly, throughout the domain, there is a characterization of the gravitational acceleration and respective interpretation.

The main aspects that should be accounted for, in this case, in order to ensure a good quality mesh, is the orthogonality and the aspect ratio. Regarding the orthogonality, in the case of this simulation, all the mesh elements possess a quadrilateral form ensuring perfect orthogonality. Concerning the aspect ratio, it will steadily change throughout the length of the domain due to the higher grid refinement needed in the region of the inlet and injection, yet never surpassing the reference value of $5:1$. Nonetheless, the values reported are not sufficient to affect the mesh quality. Overall due to the simplistic geometry, the chosen mesh presents no issues.

The choice of the solver used in the problem relies between a pressure-based and a density-based solver. This particular simulation considers a pressure-based solver. The density-based solver was originally conceived to solve high-speed compressible flows. On the contrary, the pressure-based solver computes incompressible flows that have not achieved supersonic velocities. This solver usually ensures reaching numerical results in accordance

with the experimental data.

The velocity formulation is crucial in achieving accurate simulations of the velocity fields throughout the domain. The equations of motion should be solved regarding the moving reference frame, while the acceleration of the fluid requires the additional terms to appear within the momentum equations. The utilized software possesses either the relative velocity formulation or the absolute velocity formulation. The relative velocity formulation expresses the momentum equations using the relative velocities as dependent variables. Meanwhile, the absolute velocity formulation expresses the momentum equations considering dependent variables. The significant detail between both formulations is the approach made in the reference of the domain. Usually, whenever the fluid is rotating it is utilized the relative velocity formulation. On the contrary, the absolute formulation is commonly employed while the fluid is not on rotation. As a result, these facts justify the selection of the absolute velocity formulation option in this simulation.

Generally, the numerical simulations differ in the employed time formulation, there are transient or steady schematics. The primary contrast between both cases relies on how the time is formulated. The steady formulation is compelling whenever the conditions reached after a relatively long time will no longer vary, achieving a uniform regime. However, in the transient formulation, time is a relevant detail meaning that the flow conditions will vary due to the advancement of the time steps. This simulation intends to replicate an experiment where the flow properties do not deviate throughout time and further implement the discrete phase within this phase, creating the evaporation of the particle and consequent combustion. The discrete particles demand a time formulation independent from the continuous phase, whereas the flow phase requires a formulation where a steady state is achieved in which the characteristics of the flow are immutable over time. These characteristics suggest the usage of a steady time formulation.

The domain geometry is a significant detail in the interpretation of the general settings in an ANSYS®Fluent 2021 R1 simulation. Initially, it was thought that the best approach would be an axisymmetric geometry where the x-axis would be the symmetry axis that is normally predefined by the software [99]. However, the axisymmetric approach carries additional problems when utilizing an Euler-Lagrange formulation. The axisymmetric approach would require the simulation of only half of the droplet. This condition reveals problematics due to characteristics of the Euler-Lagrange model, where the particle is infinitesimal and where the droplet properties are condensed within that particle. Hence, a 2D planar approach was selected, which is considered a slice in the center of the experimental setup cylinder, representing a plane with no geometric variation on the z direction of the cylinder axis system. This geometry revealed a better agreement with the employed model while not increasing the simulation complexity and computational resources. Within the center of the geometry, the dashed line represents the line where the injection of single droplets occurs. This planar representation is allowed in the CFD software, maintaining its continuous geometry through the domain, yet requires a further description of the boundary conditions to perform the

simulation. Concerning the geometry, the chosen reference of the axis defines the x-axis as the radial axis, the y-axis is the axial reference. This layout will allow improved visualization of the simulation through a geometry that lies on the positive y-axis of the x-y plane. This disposition enables the representation of the gravitational force in the axial reference throughout the y-axis, as depicted in Figure 3.3. This axis matches the vertical trajectory of the single droplet as well as being parallel to the gravitational acceleration, $||\overrightarrow{g}|| = ||\overrightarrow{g_x}|| = 9.81\ m/s^2$. This type of configuration was firstly selected due to the initial intentions of performing an axisymmetric study. The employed schematic is the standard configuration that is assumed by the CFD software to define the axisymmetric simulations with the x-axis as the reference axis. Nonetheless, this schematic represents a convenient way of problem visualization, which explains not modifying the geometry despite utilizing the planar alternative.

3.3.3 Boundary Conditions

The definition of simulation boundary conditions aims to describe the flow behavior in the domain borders. The definition of boundary conditions, coupled with the characterization of the domain geometry is especially relevant within the limits of the domain due to the consequent subjection to these conditions criteria. Poorly defined boundary conditions might represent critical accuracy issues in the problem obtained solutions. The boundary conditions of this physical problem are exhibited in Figure 3.4, alongside a representation of the expected velocity profile.

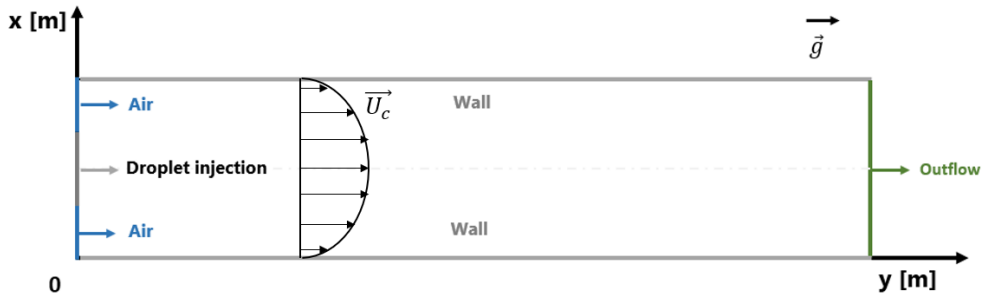

Figure 3.4: Representation of the domain boundary conditions.

Six boundary conditions are defining the domain of the problem. Firstly, the top and bottom boundaries are walls, since they represent the quartz walls that involve the drop tube furnace. These boundaries assume a constant temperature condition to account for the heat provided by the electric resistances that surround the quartz glass cylinder. Additionally, both walls are stationary and apply the no-slip shear condition. Moreover, there is an additional wall boundary defining the tip of the injector. The stationary wall assumes a no-slip condition, where the constant temperature is assumed considering a slightly lower value compared to the other wall temperatures. This boundary condition reveals assertive approximating the flow nearby the tip of the injector, where there is little experimental information.

Concerning the inlets, the mass-flow inlet option is preferable due to the provided information regarding the experimental facility. There is knowledge considering the quantity of

volumetric flow entering the experimental setup alongside its measured temperature. This information enables the estimation of the respective mass flow. Besides this, there is a demand for turbulence information of the flow. The demand accounts for the turbulent length scale. In this case, this parameter is equal to the size of the holes regarding the grid that exits in the experimental setup used to prevent turbulence. Additionally, the turbulent intensity requires its computation using Equation 3.32, which Re_{D_H} portrays the tube diameter. However, the turbulent parameters calculated seem remarkably low. This preferably occurs due to the experimental work intention in achieving a laminar flow. The specification for the mass-flow inlet is a relevant achievement. The inlet information is computed by the experimentally utilized information of the volumetric 3D mass flow and the temperature of that specific flow. Firstly, the volumetric flow is converted into a mass flow by dividing by the flow specific density at that determined temperature $\dot{m}_{3D} = \dot{V}_{3D}/\rho_{flow}$. The following step is the conversion of the flow into a 2D flow. This occurs since the model computations should be performed in a 2D geometry, and the available experimental data is meant for the 3D nature of the experimental setup. In order to realize the conversion, ANSYS®Fluent 2021 R1 recommends the usage of the Equation 3.33 to convert to a 2D geometry. In the expression, $\dot{m}_{2D:planar}$ represents the mass flow of the 2D geometry, while $\dot{m}_{3D}$ portrays the mass flow for the 3D geometry of the experimental procedure. The parameter H_I represents the height of the inlet in the 2D geometry and the L_{ref} accounts for the characteristic length. This property possesses the unity for standard rectangular geometry conversions, yet in this case, considering the reformulation of a 3D circular geometry into a 2D rectangular domain, the characteristic length, L_{ref}, is considered 2π. Lastly, A_{3D} represents the area of the 3D inlet considered to be a circular-crown geometry in the experimental apparatus. Subsequently, the transformation of the flow is needed every time the characteristics of the flow modify. This consideration is valid for different temperatures of the flow, which result in the modification of several flow properties that are further depicted in the results chapter of the dissertation.

$$I = 0.16 \cdot (Re_{D_H})^{-1/8} \quad (3.32)$$

$$\dot{m}_{2D:planar} = \dot{m}_{3D} \frac{H_I \cdot L_{ref}}{A_{3D}} \quad (3.33)$$

The last selected boundary condition was the outflow. According to the operated software manual [99], there is the possibility of computing the simulation equations while assuming that the details of the flow velocity and pressure are unknown in a specific domain position prior to the respective flow computation. At the exit of the drop tube furnace, where flow is close to a fully developed condition, the outflow option was preferred over the pressure-outlet choice. This decision might be justified due to the absence of experimental information at

this position and the assumption that the flow is fully developed.

3.3.4 Implemented Models

The software ANSYS®Fluent 2021 R1 provides several models that allow the replication of a wide variety of phenomena seen in nature. Regarding this dissertation, there are sufficient models in the software that ensure the computation of the phenomena intended to simulate.

Firstly, there is the requirement of enabling the Heat Transfer modeling. This option ensures the computation of the energy transfer throughout the domain by solving Equation 3.3. The incorporation of this model is justified since there is the need to compute the temperature of the domain alongside the combustion procedure.

Furthermore, there is the necessity of modeling the continuous phase within the CFD software. Hence, there is the necessity of selecting the viscous model option and the evident turbulence model. The operated software possesses a wide variety of different turbulence models that could model the continuous phase. However, as previously discussed the most reasonable option is the $k-\varepsilon$ turbulence model. The employment of a turbulence model can account for turbulence redundancy and trying to comprise for every form of turbulence that could occur within the system. Some procedures must be performed as a consequence of applying the turbulence model. There is the necessity to describe how coarse or fine a mesh should be for a particular flow pattern, assuming importance in the modeling of turbulence to determine the proper size of the cells in the vicinity of the domain walls. The parameter y^+ behaves throughout the domain comparing the normal turbulent flows computed in CFD analysis. Equation 3.34 exhibits this parameter depending on the characteristics of the flow, where U_T represents the flow friction velocity and, y_p, portrays the distance between a specific mesh cell center and the wall. Due to the characteristics of the flow, y^+ throughout the flow maintains relatively low values. This parameter should not be between 5 and 30 that is considered the buffer layer, typically inducing more significant errors. However, y^+ is acceptable to be between 30 and 300 for high Reynolds numbers, or below 5 for low Reynolds number flows [101]. The low turbulence levels observed in the domain reveal that the y^+ are below the margin of 5. These results demonstrate that the meshes are adequate for the simulation [101] and indicate the validation of the model in accordance with the experimental intentions of creating a laminar flow.

$$y^+ = \frac{\rho_c y_p U_T}{\mu_c} \quad (3.34)$$

The discrete phase modeling has an extensive explanation in subsection 3.2.1.2. Besides describing the physical model that depicts the phenomenon is also important to explain how to account for the procedure in CFD software. The option provided in the software to model an Euler-Lagrange phenomenon is the Discrete Phase Model (DPM). However, the discrete

phase computes the path tracking a specific dispersed particle through the calculated continuous field. The software considers different dispersed phase materials, which in this particular case should assume as a liquid fuel droplet that must evaporate. The discrete phase also allows the implementation of expressions that model exchange momentum, mass, and energy with the fluid phase. The implementation of these expressions ensures the modeling of phenomena such as droplet evaporation.

The tracking of the discrete phase occurs in either steady particle tracking or unsteady particle tracking. The unsteady particle tracking enables additional options such as the particle time step size, number of time steps, and the time of the beginning and end of the injection of the particle. This type of tracking is utterly complete in predictions more accurate with the particle injection. However, there are difficulties in gathering the information required to implement the unsteady tracking. The steady-tracking does not require as many parameters to follow. Nevertheless, the particle still demands the data of the injection of the flow of the particle to do its tracking adequately. This option was the one selected in this simulation since it was the information that could be obtained more accurately.

The referred injection property reveals relevancy within the simulation possessing the same units of a standard mass flow. Thus, was implemented a strategy to determine the quantity that should be assumed. The employed method considers 3.5 as a reference injector that provides the phenomenon of a single droplet injector stream.

Figure 3.5: Schematic of single droplet phenomenon represented as a monosize stream of droplets [71].

The mass flow of droplets, $\dot{m}_{droplet}$, is defined as a quantifier of how much droplet mass passes over a selected interval of time, possessing the units of $[Kg/s]$. In order to determine the mass flow, it is first essential to calculate the droplet mass passing through a reference location over time. The multiplication of the droplet volume with the fuel density and further

division by the time gap between droplets assures the calculation of the mass droplet considered in the computation. Noteworthy that the fuel will be changed according to the different simulations, and the droplet volume is simplified into a sphere volume assuming the diameter of the droplet. Figure 3.5 represents the distance s, which is considered in the calculation of the mass passing through the interval of time and thus determinating the interval of time between droplets. Hence, it is possible to be obtained the average velocity of the droplet, U_d, possessing relevancy to calculate the gap time between droplets. Furthermore, utilizing the velocity value and multiplying with the distance between droplets, s, it is possible to determine the gap that passes between droplets $\Delta t_{droplet}$. The assumed distance between droplets is the minimal distance that allows the single droplet phenomena. The results obtained in this section enable the analysis of this parameter in the combustion properties.

This simulation accounts for the combustion of a liquid droplet involved in a low-velocity airflow, possessing a reduced Reynolds number. There is the recommendation of modeling recurring to the coupling of the discrete phase and non-premixed models. Hence, the fuel stream considers the non-premixed combustion model to compute the fuel mixture fraction. The model assumes as the combustion fuel the gas firstly originated from the evaporation procedure of the discrete phase. The correspondent utilized gaseous species also originated from the liquid fuel specie previously defined. There is a necessity of characterizing the boundary conditions regarding species that define the chemical and thermic reaction in conformity with the CHEMKIN files, provided by the user or within the ANSYS®Fluent 2021 R1 libraries. Through this definition, it is possible to determine the products of the reaction by providing the oxidant species and the fuel evaporating species indicating the temperature of the boiling point of the liquid fuel.

Different types of n-alkanes and jet fuel are defined in this simulation. The combustion reaction of certain fuels is not available in the employed software predefined library. Thus, it is relevant to import the information of the CHEMKIN Files of additional fuel combustion and the respective library of species. Regarding jet fuel, this software possesses a vast amount of information regarding its thermochemical information and properties based on the experiments provided by Rachner [102]. Concerning the n-alkanes such as n-dodecane and n-hexadecane, there is a lack of information regarding their combustion procedures in the database provided by the utilized software. Their properties in the software also reveal unsatisfactory data, which demands the implementation of the addition of external CHEMKIN files. The thermochemical modeling of combustion requires the creation of new materials with the information of the respective liquid fuels. The utilized CHEMKIN files are implemented from the Lawrence Livermore National Library, which employs the experiments formulations supplied by Westbrook [103], Lapointe [104] and Kukkadapu [105]. The properties of the fuel and respective gaseous phase can be obtained through the information obtained from Yaws [106] and depicted in Table 3.3. The gathered information is further validated with the results obtained in the next section.

The simulation of the combustion process depends particularly on specific properties de-

scribing liquid fuel droplets and further gaseous phases. The poor definition of these parameters possibly leads to errors in the computation of information concerning the droplet fuel evaporation and its respective combustion. The properties of the liquid droplets are defined by recurring to Yaws [106]. Meanwhile, the gaseous phase mixture properties are determined recurring to the simple model of the droplet combustion enounced by Turns [53]. Similarly to what was perceptible in the evaporation problem, there is importance in defining appropriate values for the parameters $c_{p:g}$, k_g, and ρ_l. These values are calculated through Equations 2.12, 2.13, and 2.14, while considering the burning characteristics of the fuel droplet, resulting in their synthesis displayed in Table 3.3. The required modeled flame temperatures are computed utilizing an iterative process that considers the kinetic process of the combustion phenomenon. However, the flame temperatures computed in this process differ from the ones obtained in the operating CFD software. This discrepancy explains the different flamelet model utilized in the simulation, which might be too simplistic to represent the phenomena. Regardless, the chemical equilibrium model reveals a mathematical model in accordance with the physical properties and experimental data.

Liquid Fuels	ρ_l **[Kg/m^3]**	$c_{p:g}$ **[J/(Kg · K)]**	k_g **[W/(m · K)]**
n-Dodecane at 800 °C	598.0	5210	0.1446
n-Dodecane at 1000 °C	598.0	5210	0.1596
Jet-A1 at 800 °C	563.2	4762	0.1406
Jet-A1 at 1000 °C	563.2	4762	0.14760
n-Hexadecane at 800 °C	565.0	4350	0.1280
n-Hexadecane at 1000 °C	565.0	4350	0.1380

Table 3.3: Summary of physical properties for the different three fuels for each analyzed temperature: ρ_l, the density of the liquid; $c_{p:g}$, the specific heat of the evaporated gas; k_g, the thermal conductivity of the evaporated gas.

Throughout this chapter, it occurs the selection of the models and computation of the properties employed in the numerical simulation. The validity of the models and the respective accuracy of the properties are further evaluated compared with the experimental results. However, before analyzing the obtained results, there is the necessity to describe the respective solver theory and mathematical discretization of the CFD computation.

3.3.5 Solver Theory and Mathematical Discretization

The solver theory and mathematical discretization assume particular interest due to the importance of describing how the numerical equations are solved and the strategies used to compute. The utilized software possesses different solvers such as density and pressure-based solver, which support a wide variety of pressure-velocity coupling, alongside its appropriate spatial and temporal discretization.

The chosen solver is the pressure-based solver due to its broad utilization in low-speed in-

compressible flows. Firstly, updates the fluid properties based on the current solution, following the solving of the momentum equation, one after another utilizing the updated values of pressure and mass fluxes. Following this step, the algorithm computes the pressure correction equation using the newly calculated velocity field and mass flux of the flow with a further update of the mass flux. Lastly, the procedure determines the scalar equations describing the flux properties and updating the source terms needed to model the interaction between different phases. Furthermore, there is a convergence check of the equations and investigate the demand for further iterations.

The velocity-pressure coupling is a procedure involving the computation of the discretization of the Navier-Stokes system essential to define a liquid flow. This process reveals a high dependence of velocity on pressure implying inter-equation coupling. Several pressure-velocity coupling methods exist to model this interaction. Meanwhile, the Semi-Implicit Method for Pressure-Linked Equations (SIMPLE) resembles the better-balanced option. The previous studies of Silva [71], Barata et al. [107] and Rodrigues [108] assume the method as an adequate option for incompressible steady-state problems that require linear equations solved iteratively. Regarding this simulation, the employment of this method justifies the low computation processing requirements, the usage of incompressible steady-state processing, and the low computation requirements in the flow simulation.

There are several issues aggregated with the solving of Navier Stokes Averaged equations whenever solved numerically. Even though there is the same number of equations and variables, the convection term in the momentum equations is non-linear. There is no equation for pressure, and the computed velocity fields from momentum equations must satisfy the continuity equation. Essentially, there is the necessity to obtain an approximation of the velocity field from the solving of the initial momentum equation, which implies a distribution of pressure that comes from this procedure. Consequently, a newly formed pressure equation shall appear and solve accounting for the new pressure distribution, accordingly with the momentum and continuity equations. Subsequently, the computation of the velocity field requires a derivation of a corrector for this field in order to satisfy the continuity equation. The newly formed corrections of the flux and pressure are implemented in the domain discretized grid cells and update the values calculated throughout the cells.

Regarding the utilized equations, there is the necessity of representing the continuous equations in a discrete form equation at each iteration. This occurs to represent a specific property throughout the grid domain. These equations utilize the relaxation factors to correctly update scalar properties equations associated with the pressure field for each cell of the domain. The relaxation factors parameters guarantee that the solution of the simulation from a specific step to the next does not deviate in excess as it then might get unstable. These factors are associated with the different equations being computed in the numeric simulation. The adjustment of these values will also modify the representation of the residuals of the simulation for each equation. The control of these parameters increases or decreases the smoothness of the simulation under certain reference values provided by the manual of the operated soft-

ware [99]. The excess variation of these parameters can lead to errors in the computation. Throughout the simulation, minimal adjustments to some scalar values equations to diminish the deviations between iterations, yet under the reference recommended values for each equation.

There are various possibilities to formulate the discretization. In this case, it occurs utilization of one of the most complex and complete discretization methods. However, firstly simpler procedures are utilized to check primordial solutions of the computation. The employed model is the quadratic upstream interpolation for convective kinetics (QUICK) scheme firstly provided by Leonard [109]. The scheme has high-order differencing schemes, which consider the inter-dependency between neighboring nodes as represented in Figure 3.6. There are various possibilities to formulate the discretization. In this case, it occurs utilization of the most complex discretization method. However, firstly simpler procedures are utilized to check primordial solutions of the computation. The employed model is the quadratic upstream interpolation for convective kinetics (QUICK) scheme firstly provided by Leonard [109]. The model has high-order differencing schemes, which consider the inter-dependency between neighboring nodes. There is a subsequent decrease in mistakes of the process in the calculation of the upstream and downstream cell values. The scheme is highly recommended for cases of quadrilateral meshes where there are upstream and downstream faces and cells. The schematic computes a high-order value of the convected variable ϕ at a specific face while weighting the average of second-order-upwind and central interpolations of the scalar in the analysis. Hence, the value of a specific scalar ϕ is obtained through a quadratic function. The validation of the model occurs whenever the flow is towards the left to right and passes by two bracketing nodes within an upstream side node. The application of the QUICK schematic in the employed software enounces that this scheme is frequently more accurate on structured meshes aligned in the flow direction.

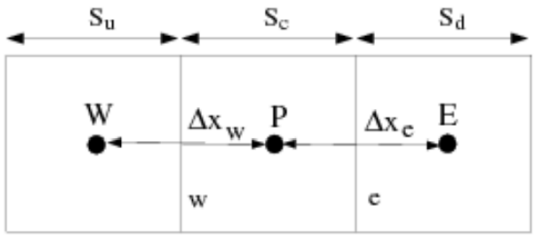

Figure 3.6: One-Dimensional control volume where it is applied the QUICK discretization

The computation of gradients constructs the values of scalars in the cell centroid alongside determining the velocity derivatives and the second diffusion terms. The discretization process for certain flow equations requires the existence of the gradients ($\nabla\phi$) of a particular variable ϕ to determine the discrete diffusion and convective terms. The utilized software possesses different methods to compute the gradients while operating distinct approaches. The software default method to calculate the gradients from the wide variety of options is the Least Squared Cell-Based method. This method reveals a good accuracy for unstructured and structured meshes along with not requiring expensive computational capability.

The pressure interpolation is relevant in order to acquire the pressure values from each mesh at the face. Similarly to the computation of the gradient, the operated software offers a wide variety of options to compute the flow field of this parameter, yet the recommended method for a normal Eulerian flow with discrete phase is the Second Order scheme. This scheme can reconstruct the face pressure utilizing a central differencing scheme and it is a robust scheme that can predict accurate results.

3.3.6 Grid Independence Study

The grid independence study has great relevance in validating CFD numerical results. It is crucial to identify for any model that is solved numerically that the solution is not affected by the grid size. It is considered the grid utilized for the numerical simulations the mesh depicted in Figure 3.7 with 10400 elements, which is further refined and coarse in order to study the grid independence.

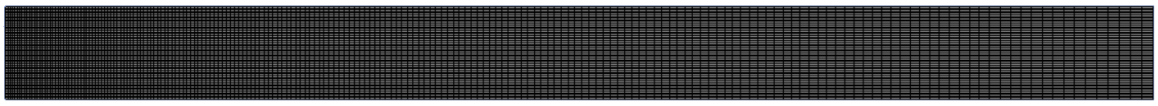

Figure 3.7: Representation of the domain grid mesh implemented in this numerical study.

It is possible to resort to different approaches to achieve grid independence. Generally, it is attempted to analyze a specific characteristic, even though maintaining the domain unalterable. When verified that the grid size does not influence the outcome of a specific parameter in the simulation, it can be stated that the simulation yields grid independence. The numerically obtained flow fields of the continuous phase are parameters considered in a grid independence study. Consequently, the study of the continuous phase of the model was performed by analyzing the influence of the grid on the velocity profiles throughout the drop tube furnace. Proceeding with this analysis, three locations in the tube were selected where the respective velocity profiles were obtained (Figure 3.8). Such data was further collected for different meshes with distinct levels of refinement. This refinement was chosen under a certain proportion throughout the analysis. This fact is due to the intention of maintaining a certain balance of the mesh elements size and elements during the increase of the number of grid points.

The 2D nature of this simulation assumes that it is just necessary to analyze the horizontal velocity profile to determine the grid independence. The study for distinct locations in the drop tube furnace allows the investigation of the grid influence for different points throughout the domain. This analysis is justified to prove that the calculation of the continuous phases is performed in an adequate mesh for distinct locations of the domain. Regarding the velocity analysis at the $0.125\ m$ below the tip of the injector, it was simulated the conditions for different grids with 5400, 10400, and 21300 elements.

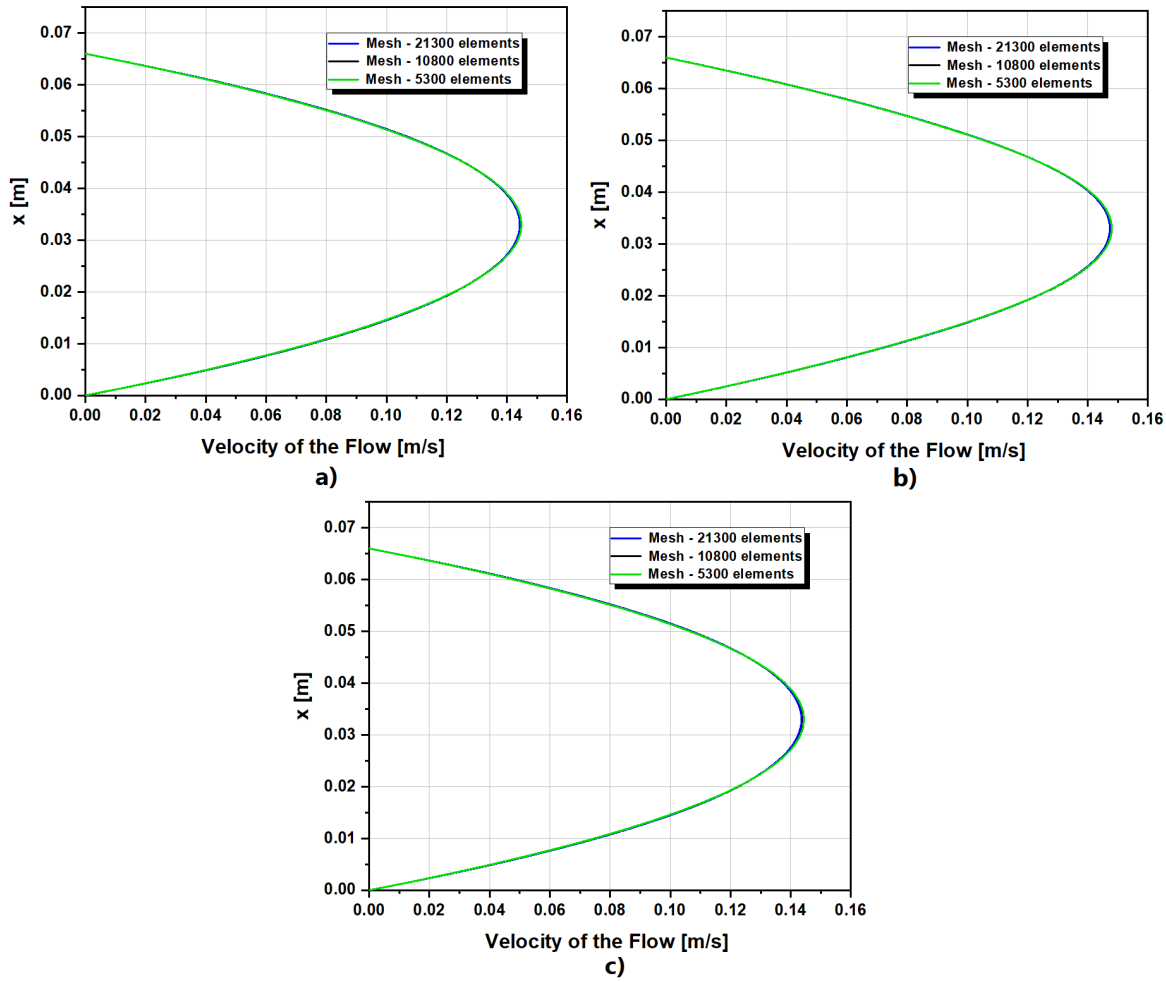

Figure 3.8: Comparison of the different horizontal velocity profiles between the distinct mesh refinements while varying the distances of the tip of the injector: a) $0.5\ m$ below the tip of the injector; b) $0.25\ m$ below the tip of the injector; c) $0.125\ m$ below the tip of the injector.

The respectively obtained velocities are $0.10258\ m/s$, $0.10406\ m/s$, and 0.10820 m/s which reveal relative error between the higher refined mesh and the intermediate of $1.44\ \%$ and a relative error of $3.86\ \%$ for between the intermediate and the lower refined mesh. Concerning the obtained velocities at $0.25\ m$ below the tip of the injector, it was simulated the same referred meshes. This distance reveals lower velocities which reveal that respectively it is obtained $0.10455\ m/s$, $0.10336\ m/s$, and $0.10726\ m/s$. The evident relative error between the finner mesh and the intermediate is $1.15\ \%$ and the relative error among the intermediate and the most rudimentary mesh is $3.63\ \%$. Lastly, there was an analysis of the velocities at the position 0.5 m below the tip and it was also simulated for the different referred distances. Concerning this distance, it was obtained respectively $0.10250\ m/s$, $0.10453\ m/s$ and $0.10828\ m/s$. The correspondent relative error between the finner mesh and the intermediate is around $1.88\ \%$ and regarding the analysis between the intermediate and the most rudimentary mesh is $3.46\ \%$. These obtained results and the visualization of Figure 3.8 suggests that the difference between the different velocities possess a negligible error below $10\ \%$. This evidence indicates that the grid independence is obtained and the number of elements of the mesh does not influence the obtained value of the velocity [10, 71].

Chapter 4

Results and Discussion

This chapter aims to introduce the obtained numerical outcomes and resultant discussion. The simulation demands the replication of the DTF conditions, yet it is intended a variation of ambient temperature enabling the analysis of distinct combustion environments. The validation of the flow conditions for the different temperatures requires employing experimental researches data.

Concerning the numerical combustion of the dispersed phase, it is expected to reproduce the injection of various fuels within the DTF while analyzing the influence of the ambient temperatures. Therefore, it is investigated the impact of the ambient temperature variation and molecular properties of the fuel in the combustion characteristics and dynamics of the fuel droplet. Furthermore, the discussion of the results verifies the accuracy of this numerical approach in simulating this physical phenomenon, with a further comparison with experimental outcomes and literature research.

4.1 Primary Visualization of the Setup Flow

In the experimental setup, the fuel droplets are injected within a heated drop tube furnace where the air is heated and further supplied recurring to flow inlets. The replication of these conditions requires a computation of the flow attributes, demanding a previous study of the characteristics of the flow and its respective properties. Furthermore, current numerical research intends to replicate the different ambient temperatures inside the DTF, aiming to analyze the effects on the combustion phenomenon of the droplets. Consequently, it is relevant to simulate the flow under distinct conditions while achieving the intended ambient temperatures since the flow properties depend on the temperature that achieves. Resulting in a formulation where the flow attributes change and require a renewed computation for each simulated possibility. The primary flow parameters that describe the temperature modifications are summarized in Table 4.1. Such parameters are further employed in the flow equations and turbulence model, allowing the determination of the stream characteristics. The obtained information intends to be identical to the conditions encountered in the experimental setup of Ferrão et al. [7–9], and the correspondent air properties result from the calculation utilizing the information available in the literature. Ultimately, the validation of the obtained continuous phase requires comparison with experimental data. Due to the goal of analyzing the temperature influence in the combustion procedure, there is experimentally obtained information regarding the temperature evolution in the DTF [7–9]. The data examines the temperature evolution since the flow is injected into the furnace throughout the

apparatus and might ensure an adequate comparison between numerical and experimental outcomes, verifying the accuracy of the mathematical approach.

Temperature [ºC]	$\dot{m}_{2D}$ **[Kg/s]**	ρ_c **[kg/m^3]**	μ_c **[Pa.s]**	$c_{p:c}$ **[J/(kg K)]**	k_c **[W m ·k]**	**I [%]**
500	3.2×10^{-3}	0.49	3.6×10^{-5}	1080	0.056	0.086
600	2.7×10^{-3}	0.40	3.9×10^{-5}	1051	0.061	0.090
800	2.1×10^{-3}	0.33	4.3×10^{-5}	1154	0.071	0.096
900	2.0×10^{-3}	0.31	4.6×10^{-5}	1171	0.076	0.098
1000	1.8×10^{-3}	0.27	4.8×10^{-5}	1185	0.081	0.099
1100	1.6×10^{-3}	0.25	5.0×10^{-5}	1197	0.086	0.100

Table 4.1: Summary of the air properties for different ambient temperature

Subsequently to the calculation of the flow parameters, it is essential to include these characteristics within the equations that solve the continuous phase. This phase of the domain utilizes mathematical means to be computed and allows the solving of the flow equations, as previously mentioned. The consequent result of the computation is the velocity field associated with several temperature fields throughout the drop tube when tested at different ambient temperatures. Concerning the velocity magnitude field, the result of computing the flow equations is the scheme represented in Figure 4.1. This figure exhibits the different velocity lines throughout the domain when T= 900 °C, selected due to portraying the intermediate value of the tested temperature environments. Generally, the shape registered of the velocity profiles will be similar to what is depicted in Figure 4.1, for the different temperatures intended to simulate, achieving a steady condition after an irregular beginning due to the airflow inlet, yet varying in the obtained magnitudes. This value is revealed similarly in each computed simulation, performed considering a steady solver, suggesting a negligible variation of this parameter with the employed range of temperatures. The mean velocity magnitude computation reveals accordance with the experimental data obtained by Ferrão et al. [7], which coupled with the temperatures information aids to validate the obtained continuous phase.

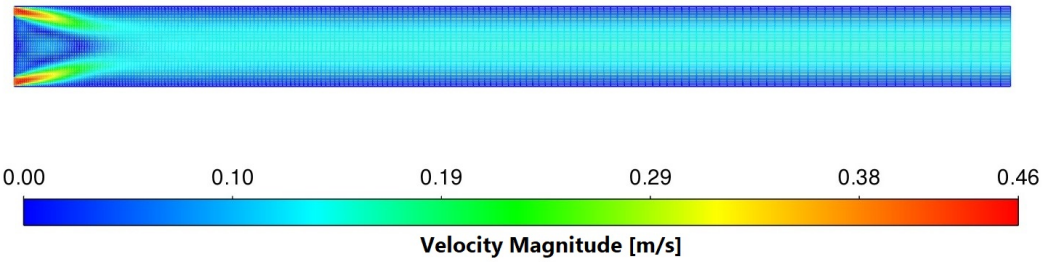

Figure 4.1: Exemplification of the obtained velocity profile when it is verified T = 900 °C.

Figure 4.2 shows the comparison between the experimental and numerical results at different ambient temperatures. The temperature profiles are acquired throughout the centreline shown in Figures 3.1 and 3.4, which is as well the path followed by the fuel droplets. Pri-

marily the data visualized in Figure 4.2 suggests accordance between the numerical curves and the experimentally obtained outcomes for each analyzed condition. Concerning the temperature evolution tendency for both outcomes, it is possible to visualize that after the flow heating period, since the injection of air, the simulation achieves the intended temperature for each simulation. However, the location where it is reached the arranged temperature is variable, revealing a farther stabilization location from the injector tip alongside a decrease of the considered ambient temperature. This phenomenon is more prominent in the experimental data and might have an explanation related to the variation of the flow properties according to the intended temperature modifications and subsequent influence on the stabilization of the injected air. Lastly, the ignition region of each computation is just when the temperature is stabilized with the intended simulated temperature. Therefore, the ignition region will also vary in the various simulations, approximating the tip of the injector with the increase of the considered ambient temperature. However, the range of distances does not vary considerably, allowing standing within the distance regarded in the visualization window of the setup of the experimental work. This DTF window allows both qualitative and quantitative evaluation of the droplets combustion.

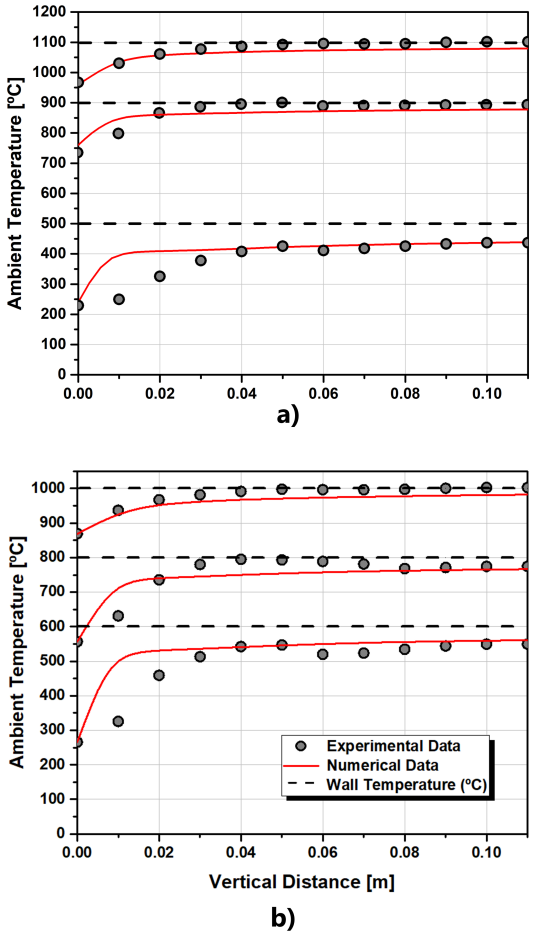

Figure 4.2: Comparison between experimental and numerical data following the pretended behavior: a)T= 500, 900, 1100 C b) T= 600, 800, 1000 C.

4.2 Implementation of the Combustion Model

After the computation and interpretation of the continuous phase and consequent implementation and research of the discrete phase evaporation model, it is crucial to upgrade the approach to allow the combustion phenomenon to occur within the intended conditions. The combustion approach is extensively discriminated in the methodology section alongside the literature research on the evaporation approaches. The validation of the continuous phase and comparison of data with experimental data allows further analysis. Consequently, it is implemented a discrete phase within the domain ensuring evaporation of the phase and consequent combustion process for the distinct fuels. The combustion of the employed software utilizes the CHEMKIN files that describe the combustion procedures. The first implemented fuel is n-dodecane. The employment of this fuel is justified since there is various well-defined information regarding its properties throughout the literature.

4.2.1 Combustion of n-dodecane

The usage of n-dodecane is related to the diverse available information in the literature regarding its properties and combustion characteristics, such as specific heat at constant pressure, fuel density, and thermal conductivity, among others. Additionally, the n-dodecane is already a widely employed and known fuel in various combustion researches [79]. Additionally, n-dodecane is considered a surrogated fuel from jet fuel, which is relevant since jet fuel is multicomponent, and its comparison with a surrogated single component, likewise n-dodecane, enables an intriguing analysis [83]. The operated mathematical computation is further validated by utilizing experimental outcomes of n-dodecane tested in the experimental setup used in the researches of Pacheco et al. [6] and Ferrão et al. [7, 8].

The analysis of combustion characteristics, such as d^2 law, burning rate, heating time, and droplet lifetime, allow a proper analysis of the combustion performance of the fuel, likewise performed in the literature studies [65, 79, 80]. Additionally, these parameters ensure appropriate comparison with experimental data. While the d^2 law is conceivable to obtain by employing the mathematical model, the burning rate is obtained from further analysis of the d^2 law. Figure 4.3 shows the square of the normalized droplet diameter as a function of the normalized time for n-dodecane. In addition, the black line portrays the numerical results while the experimental data is accounted by the symbols. The numerical analysis is performed by tracking one single particle, and the employed model and approach suffer a validation by comparing the numerical outcomes with the experimental data. On the contrary to the experimental data, the numerical results possess two distinct phases: which are the initial heating phase and the steady phase, similar to Figure 2.11 exhibited in the literature [79]. The heating phase is considered the time interval until the fuel reaches the boiling point. The droplet heating phase increases with the decrease of the ambient temperature, which is under the physical phenomenon enounced by Wang et al. [64]. Concerning the steady phase beginning at $t/D_0^2 = 0\ s/mm^2$ instant, is characterized by the linear decrease of normalized square diameter with time, with a nearly constant slope, defined as the burning rate (K). This

phase allows comparison between the experimental and numerical information since the experimental data, is sustained on a qualitative analysis of the droplet diameter decrease.

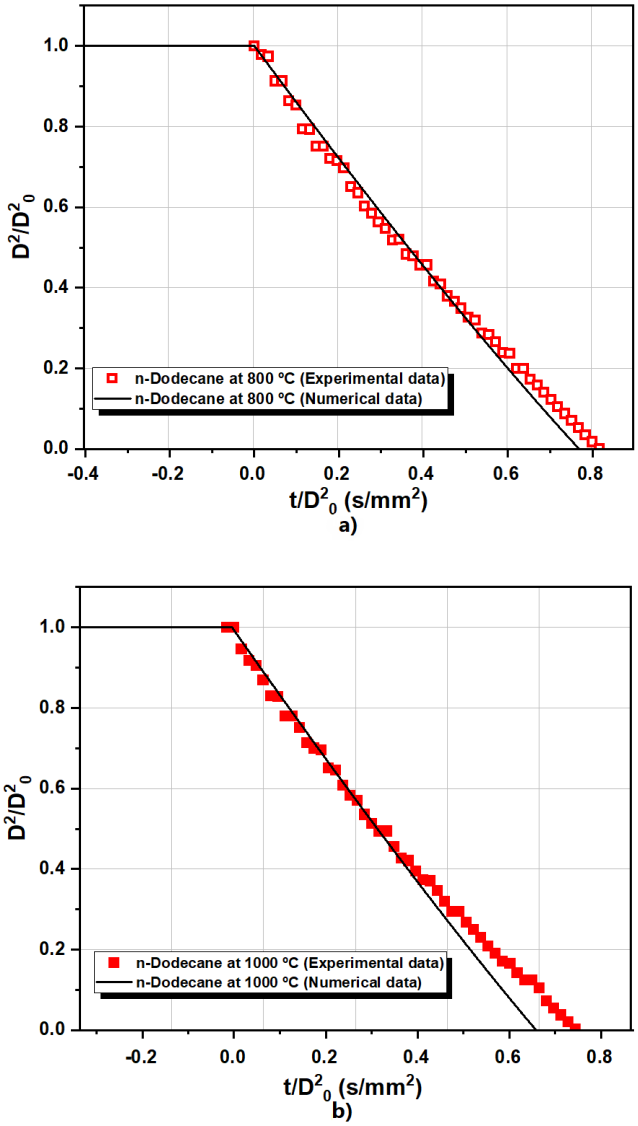

Figure 4.3: Square of the normalized droplet diameter as a function of the normalized time: a) T = 800°C and b) T = 1000 °C for n-dodecane.

Generally, there is an accordance between the experimental and numerical data for both temperatures considering the qualitative analysis of the steady phase of the d^2 law (Figure 4.3) where the experimental and numerical data are fitted to be analyzed jointly. Regarding the burning rate (K) investigation, the droplets that react at a higher ambient temperature reveal a higher burning rate. These results suggest accuracy with the literature where [65, 66] demonstrated an increase of the burning rate of the fuel droplets with the consequent increment of ambient temperature. Therefore, the n-dodecane tested at T = 1000 °C ambient temperature will possess a shorter lifetime when compared with the droplets at T = 800°C ambient temperature. The differences in the droplet lifetime are highly associated with the previously mentioned droplet heating phase, which is more preeminent at higher heat en-

vironments as revealed in [67]. The results indicate that the increase in the ambient temperature enhances the burning event and related combustion properties for the n-dodecane droplets.

Once it is analyzed several burning characteristics for n-dodecane droplets for T $= 800$ °C and T $= 1000$ °C temperatures, it is relevant to study other properties significant in the combustion. The droplet velocity and its variation represent a parameter prone to analysis since it enables the comprehension of the droplet physics dynamics during the combustion phenomenon. Firstly, it is assumed an initial droplet velocity is based on the videotape interpretations performed in the analysis of the experimental data, suggesting flaws in the utilized values. The acquired information, represented in Figure 4.4, relates the droplet velocity during the combustion event with the decrease of the normalized square droplet diameter. Specifically, this data is gathered throughout both evaporation phases.

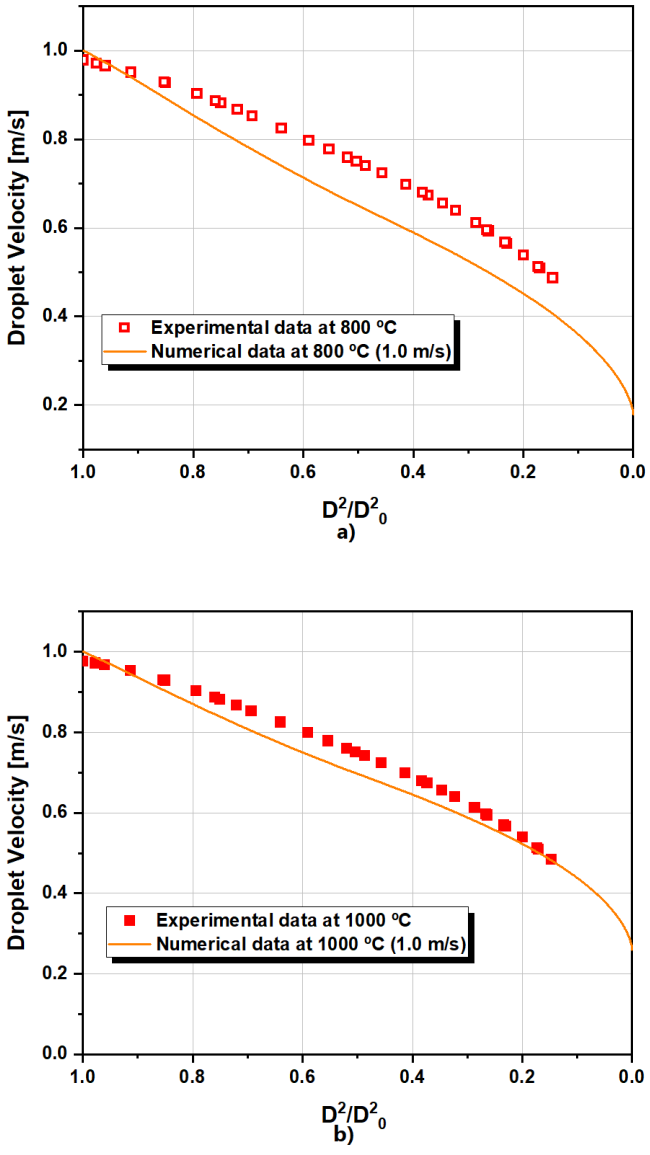

Figure 4.4: Droplet velocity as a function of the square of the normalized droplet diameter for $1m/s$: a) T $= 800$ °C and b) T $= 1000$ °C for n-dodecane.

The information is thus compared with the experimentally obtained outcomes, that after being acquired, suffer a scrutinized process adapting a polynomial function that defines a tendency line of experimental results. It is visible that the droplet velocity diminishes with the decrease of the droplet diameter. These results are in accordance with the literature visualized data suggesting a relationship between the droplet diameter reduction and the consequent reduction of the droplet velocity in the evaporation/combustion phenomena, associated with the loss of mass phenomenon of the droplet as explained in the literature review chapter [72–74]. This tendency is intensified at smaller diameters in the numerically obtained curve, suggesting an acceleration at the end of the evaporation process. The experimental reports concerning smaller diameter indicate problems in its calculation due to the lack of data at the final part of the evaporation procedure. Generally, the numerical data captures the tendency experienced by the experimental data with $16\ \%$ of relative error for T $= 800$ °C and $9\ \%$ of relative error for T $= 1000$ °C, revealing acceptable divergence. However, at higher ambient temperatures the errors are less evident, which suggests a better approximation of the experimental data, that might be explained by the improvement of the temperature profiles visualized in the numerical simulation of the DTF, as depicted in Figure 4.2.

Furthermore, it is crucial to analyze the sensibility of the droplet initial velocity adjustment in the evolution of droplet velocity during the presence of the combustion procedure for the ambient temperatures of T $= 800$ °C and T $= 1000$ °C . Figure 4.5 depicts the analysis of the variance of the initial velocity, with the decrease of the diameter and consequent droplet velocity. The investigation of Figure 4.5, demonstrates a relationship between the decline of the droplet velocity and the reduction of its diameter for each elaborated curve, revealing accordance with the literature [72–74]. This analysis is justified by the apparent discrepancies of the experimental data tendency line and the numerically obtained curves for the $1.0\ m/s$, suggesting the further implementation of additional velocity traces. Generally, the tendency of the graph is identical for each simulated initial velocities inputs in the droplet.

After an initial period where is noticed a clear divergence, the experimental data line begins to follow a trend visualized in the simulations of $1.2\ m/s$ for the experiment at T $= 800$ °C. Concerning the T $= 1000$ °C experiment, the experimental data in the intermediate part of the procedure aligns with the curve of $1.1\ m/s$ simulation. However, throughout the remnant of the depicted curve, the experimentally obtained results tendentially follow the numerical simulation considering $1.0\ m/s$ as initial velocity. Ultimately, it is detectable conformity between experimental and numerical in capturing the physical phenomenon of droplet deceleration throughout the combustion and evaporation procedure. Regardless, it is noticeable the presence of modeling complications due to divergence of experimental outcomes and the 1.0 m/s initial velocity curve. This is the assumed experimentally calculated initial velocity, yet the experimentally obtained results are in some instants in accordance with distinct curves ($1.1\ m/s$ and $1.2\ m/s$), suggesting that the experimentally computed droplet initial velocity might differ from this value.

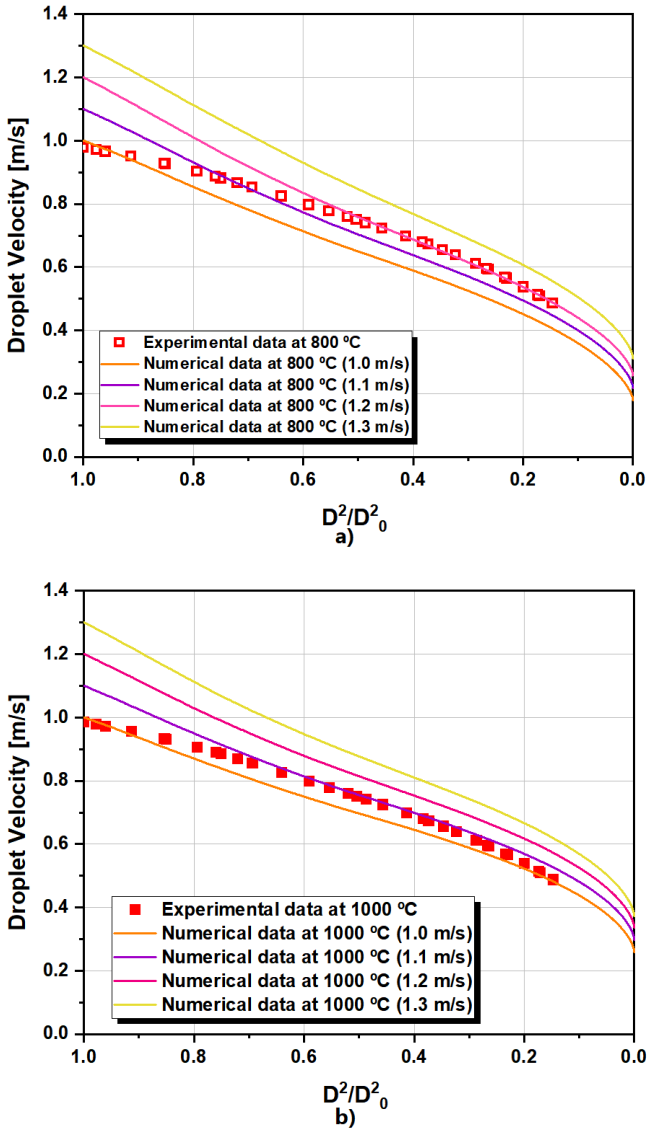

Figure 4.5: Droplet Velocity as a function of the square of the normalized droplet diameter for different droplet velocities: a) T = 800 °C and b) T = 1000 °C for n-dodecane.

Following the research computation, it is relevant to analyze the dependency of the initial droplet velocity to the burning characteristics of the fuel droplet. Therefore, the intention is to implement a study of the d^2 law for each analyzed initial droplet velocity and further investigate the dependency on this characteristic. In order to proceed with this investigation for each situation, it is required the evaluation of the square of the normalized droplet diameter as a function of the normalized time as shown in Figure 4.6. Each depicted curve in the graph represents s d^2 law study considering a specific initial droplet velocity simulation. As previously mentioned, the n-dodecane droplets possess a higher lifetime at lower ambient temperatures. Examining the different curves regarding the variation of the initial droplet velocity is possible to achieve the conclusion that the variation of the d^2 for each initial velocity is negligible. This is certified by the d^2 curves for each initial droplet velocity possessing a maximum of $2\ \%$ of relative error in reference with the $1.0\ m/s$ curve in the simulation that considers $1.4\ m/s$ of initial droplet velocity. These results reveal accordance with the study

enounced in the literature, yet in different employed ambient conditions and distinct velocity variations, suggesting some corroborating information that can support this study [75]. Similarly to the study in the literature, a deviation of the initial velocity of 30% is not enough to affect the droplet d^2 law and respective lifetime.

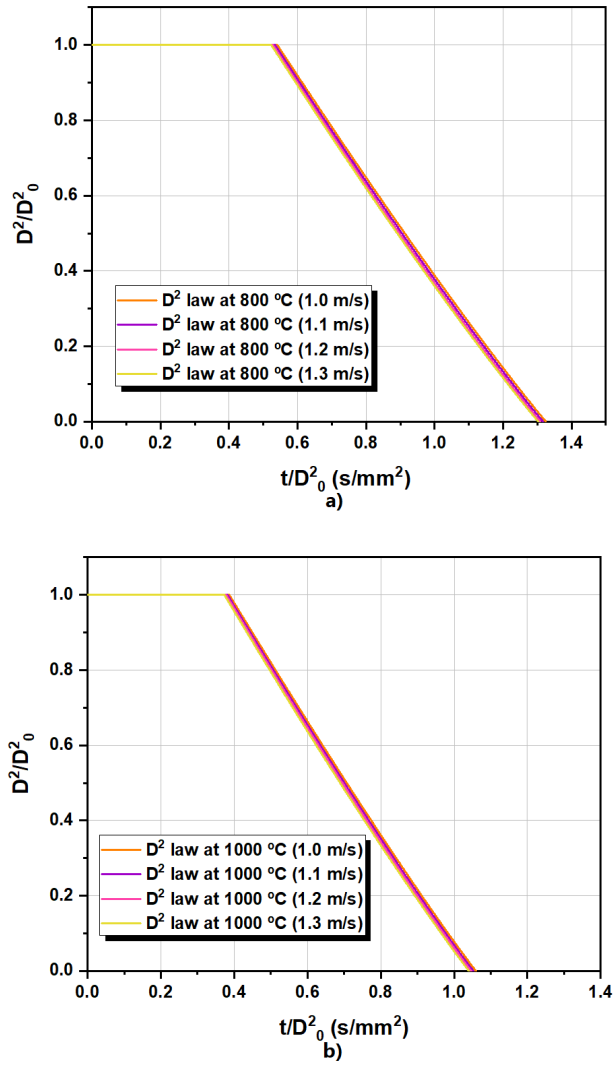

Figure 4.6: Square of the normalized droplet diameter as a function of the normalized time for different initial droplet velocity: a) T $= 800$ °C and b) T $= 1000$ °C for n-dodecane.

The analysis of the combustion enables as well the study of the droplet distance path in the domain in order to research the location where the droplet ignites and the droplet heeating time ($\Delta\ t_{ig}$). Therefore, it is possible to obtain the path performed by the single injected droplet throughout the combustion domain until reaching the end of its lifetime. This study relies on the development of a schematic of the DTF where the droplet stream is injected and suffers the droplet diameter reduction and generated combustion following a specific centerline such as the model specified in Figures 3.3 and 3.4. There are two distinct phases of this procedure, initially, the droplet receives the heat from the hotter environment until reaching the boiling point. Subsequently, it starts the evaporation procedure defined by the reduction of the droplet diameter and the consequent combustion process of the gaseous

product of the fuel. The combustion is always guaranteed within the domain because at the distance and instant that the droplet starts to shrink, the software initializes the calculation of the equations that define the combustion process [99]. This premise ensures that the droplet heating time is considered the ignition time of the fuel droplet. Figure 4.7 shows the path of the droplet resulting from the numerical study, describing the distance from the tip of the injector in centimeters and the variation of the droplet diameter in adimensional time.

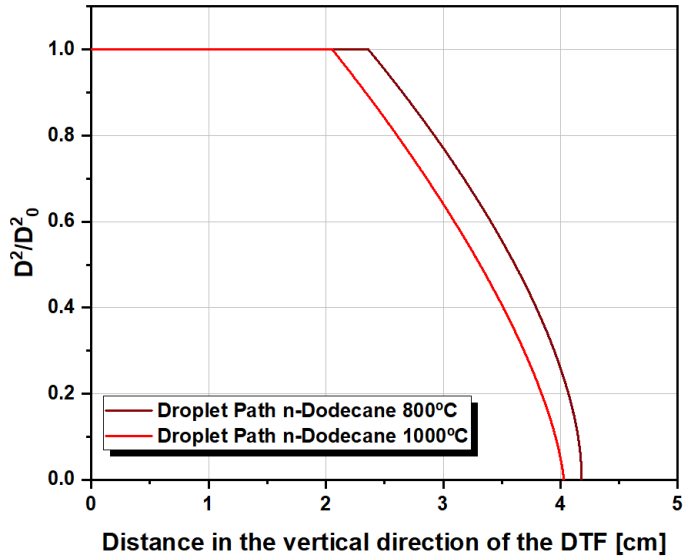

Figure 4.7: Comparison between the different ambient temperatures, T= 800 °C and T = 1000 °C and the respective droplet path within the domain for n-dodecane.

Noteworthy that the experimental facility works of Ferrão et al. [7–9], and Pacheco et al. [6] possess two windows where the visualization of the droplet combustion is acquired and further analyzed. This procedure allows collecting information of the decrease of the diameter since it considers that the evaporation starts when the fuel ignites. Consequently, the positioning of the window is within the region where most of the fuel droplets are predicted to begin the ignition. This region can be assigned as the ignition region. An accurate position of these windows ensures the acquisition of reliable data. The visualization windows are rectangular, with $2\ cm$ width and $20\ cm$ height. Specifically, after analyzing the droplet path results, there is a region around $2.5\ cm$ below the tip of the injector where exists evidence of occurring droplet ignition. Figure 4.7 demonstrates that the droplet starts to reduce diameter at the end of the heating phase igniting for both analyzed temperatures after $2\ cm$ being in accordance with the information of the simulated experimental facility [6–9]. Regarding the location of the window fits with the numerically obtained ignition location. The ignition experiment was conducted for T = 800 °C and T = 1000 °C, and the obtained diameter reducing curves are similar for each analyzed temperature. This fact alongside, the numerically obtained ignition being within the experimental data realm of visualization validates the employed numerical model. Another relevant detail is that as expected, the experiments conducted at higher temperatures enhance the ignition of the fuel as demonstrated in the literature [64–66]. This is verified since the ignition of the fuel occurs more near the injector

tip and subsequently fully evaporates at an earlier position when compared with the smaller ambient temperature.

After analyzing the development of several combustion characteristics, it is relevant to study how the droplet temperature evolves until achieving the boiling point and allowing the ignition time ($\Delta\ t_{ig}$) analysis. The boiling point of n-dodecane is T $= 489.7$ K which is a relevant parameter in this analysis. Figure 4.8 shows the droplet temperature evolution correlated with the adimensional time. This analysis considers that the combustion occurs after the droplet reaches the boiling point of n-dodecane, and the ignition time is the timeframe demanded to allow this procedure. Figure 4.8 depicts that the boiling points are achieved for both experiments, through a linear function since the droplet injection at T $= 300$ K. These mathematical curves reveal the same tendency of temperature evaluation for both ambient temperatures. Concerning the boiling point, the simulation for T $= 800$ °C achieves the boiling point after t/D_0^2 = $0.4\ s/mm^2$, while the simulation for T $= 1000$ °C reaches the boiling point after t/D_0^2 = $0.35\ s/mm^2$. These times followed the results obtained in previous computations suggesting evidence that the increase of the ambient temperature enhances combustion. This happens since the simulation at higher ambient temperature achieves the boiling point earlier, diminishing the heating time of droplet and thus igniting earlier than the experiment at T $= 800$ °C. This phenomenon influences the droplet lifetime, suggesting that the droplet requires less time to completely disappear in a combustion process when considered higher temperatures environments. This information reveals conformity with the literature data that enounces that the ignition delay and consequent total lifetime decreases with the increment of the combustion ambient temperature [67].

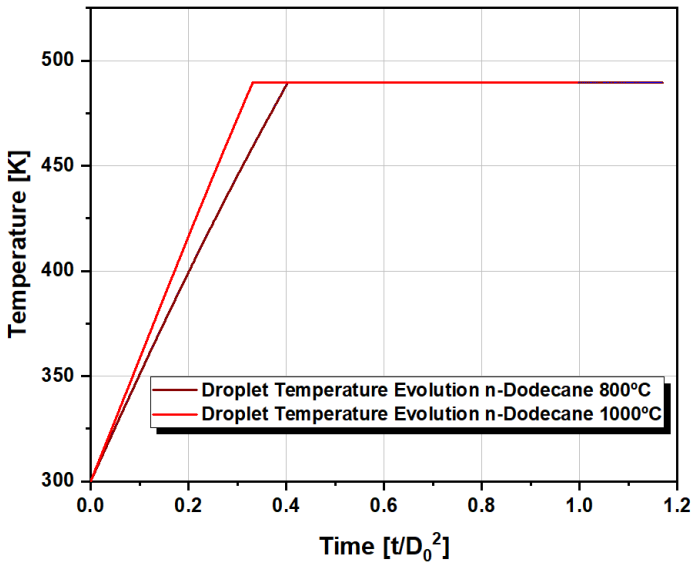

Figure 4.8: Comparison between the different ambient temperatures, T= 800 °C and T $= 1000$ °C and the respective droplet temperature evolution within the domain for n-dodecane.

4.2.2 Combustion of jet fuel

The utilization of jet fuel assumes relevancy for being the primary source of nowadays air fleet. Besides this, there is an abundance of information available in the literature on fuel properties, as depicted in the previous chapter. However, the combustion of jet fuel is complicated to model due to its multicomponent nature and the difficulties of modeling the different chemical kinetics mechanisms of the different components during the combustion procedure. Such an issue is surpassed since the operating software possesses a library that includes the combustion chemical kinetics of this fuel alongside the different mechanisms of their components. After the respective validation of the model with the n-dodecane, there is optimism that the model is also successful with jet fuel. Regarding the experimental data employed to asset the accuracy of the model, the respective equipment was already previously utilized with n-dodecane validation.

Similarly to n-dodecane precise burning characteristics are correlated with experimental data. Figure 4.9 displays the square of the normalized droplet diameter as a function of the normalized time for jet fuel.

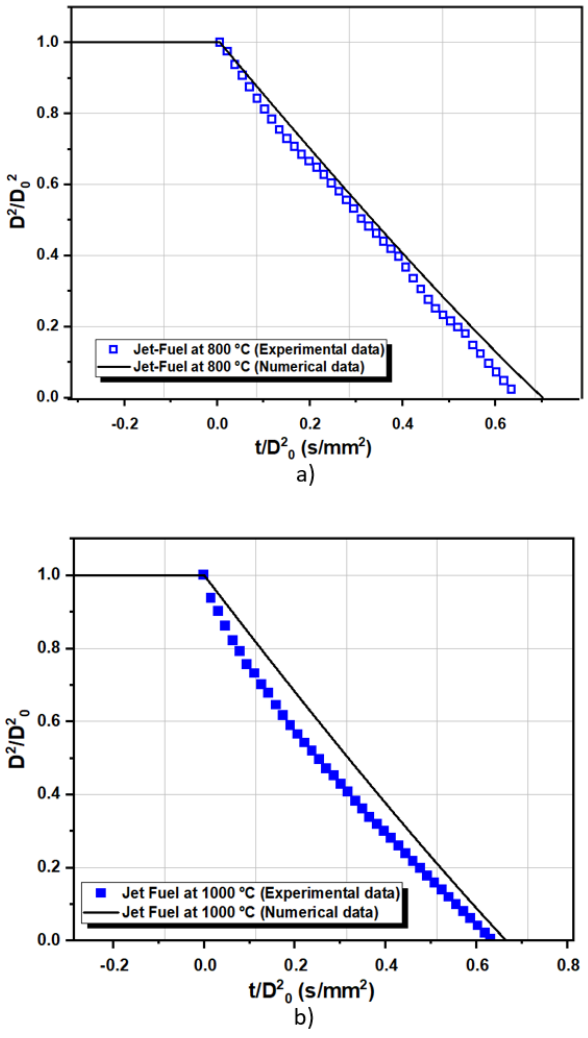

Figure 4.9: Square of the normalized droplet diameter as a function of the normalized time: a) T = 800 °C and b) T = 1000 °C for Jet-A1.

In the same way as the analysis of the n-dodecane, the experimental data for jet fuel does not possess the heating phase visible in the numerical information. The correspondent steady-state commences as well at the t/D_0^2 = 0 s/mm^2 instant, then the correspondent analysis among numerical and experimental outcomes are conceivable. It is relevant to highlight that for both T $= 800$ °C and T $= 1000$ °C, the numerical simulated outcomes follow the known d^2 law. Through an analysis of the respective d^2 law schematics in Figure 4.9, it is as well possible to obtain the burning rate (K), corresponding to the linear decrease of the normalized square diameter with time assuming a nearly constant slope. Generally, the numerical simulations are in accordance with the experimental data. The increase of the ambient temperature enhances the combustion process. This is visible since once again there is an increment from T $= 800$ °C to T $= 1000$ °C. This modification reveals effects on the droplet lifetime and respective burning rate. While the droplet lifetime diminishes with the increment of the temperature the burning rate enhances with this occurrence. These results comply with the obtained results with n-dodecane, and the literature [64–66] that indicate an enhancement of the burning event with the increment of the combustion temperature conditions for different fuels, specifically with jet fuel as noticed in Pacheco et al. [6]. Ultimately, the jet fuel droplets exhibit smaller droplet lifetimes in comparison with the n-dodecane, whereas the burning rate determined from the jet fuel experiments is higher than the n-dodecane burning rate. The justification of this evidence might be due to the different molecular natures of the fuels, yet these comparisons are further analyzed in this chapter.

Following the analysis of the burning characteristics of the d^2 law for jet fuel droplets, it is also relevant to study the behavior of the droplet velocity during combustion. Likewise the previous study analysis, there is the assumption of initial droplet velocity based on experimental information. The obtained data relates the droplet velocity in the combustion event with the decrease of the normalized square droplet diameter. There is evidence that the droplet velocity diminishes with the droplet diameter reduction, such tendency is also more preeminent at smaller diameters. The correlation of the decrease of droplet velocity with the shrink provoked by the evaporation/combustion procedure is supported by the information obtained with the combustion of n-dodecane and the prior enounced literature [72–74]. The analysis is completed with the results exhibited in Figure 4.10. Generally, the numerical data captures the tendency of the literature, yet there is a higher discrepancy at $1\ m/s$ initial velocity with the tendency line computed from the experimentally obtained data for jet fuel. The experimental data tendency line is computed to each considered simulation through the same process initially mentioned in the n-dodecane combustion analysis. This difference is visible at both tested temperatures and is more pronounced when compared with n-dodecane, suggesting the complications of modeling these characteristics in this fuel. The multicomponent nature of jet fuel and correspondent impact in the droplet modeled behavior might justify the obtained differences between the numerical and experimental outcomes.

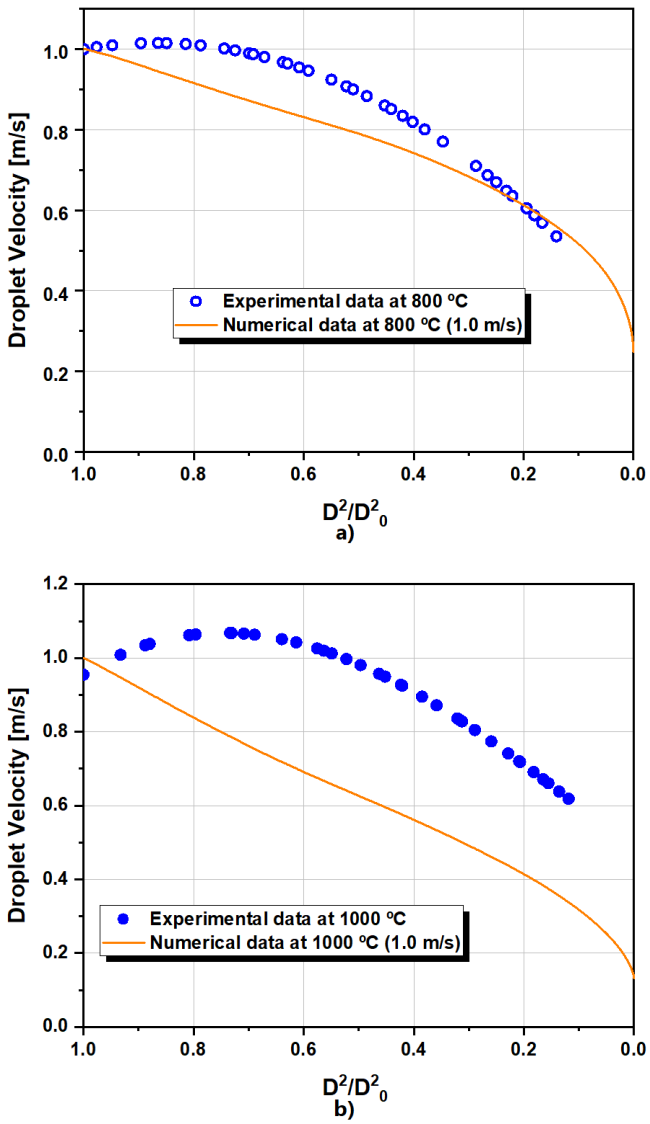

Figure 4.10: Droplet Velocity as a function of the square of the normalized droplet diameter for $1\ m/s$: a) T $= 800$ °C and b) T $= 1000$ °C for Jet-A1.

The observed discrepancies intensify the demand to analyze the influence of the adjustment of the initial droplet velocity. Once again, Figure 4.11 exhibits the variance of the initial velocity and how the reduction of the droplet diameter influences the droplet velocity. In the jet fuel analysis, the tendency line of the experimental data and the numerically obtained curves for the $1m/s$ speed depict noticeable discrepancies in comparison with n-dodecane. The employed initial droplet velocity sensibility study intends to capture the experimental data tendency with other initial droplet velocity computations. Likewise, in the n-dodecane experiments, the trend of the graph is identical for all initial velocities inputs of the droplet following the data suggested in the literature [72–74]. Tendentially the droplet velocity reduces throughout the combustion process and evident decline of droplet diameter. However, in the case of jet fuel, the experimental data is in better conformity with higher initial velocity curves. Concerning the experiment at T $= 800$ °C, there is a resemblance that follows the trend of the $1.1\ m/s$ curve numerical in the midpoint of its lifespan, while at T $= 1000$ °C

experiment, it is noticeably the analysis that diverges more pronounceable from the numerical information only marginally approximating to the trend visible in the $1.3\ m/s$ numerical curve. Throughout all the cases, droplets at the beginning of the lifespan suggest a discrepancy between numerical and experimental outcomes. Ultimately, these jet fuel simulations achieved the aimed literature trend while displaying disparity with the experimental data tendency line.

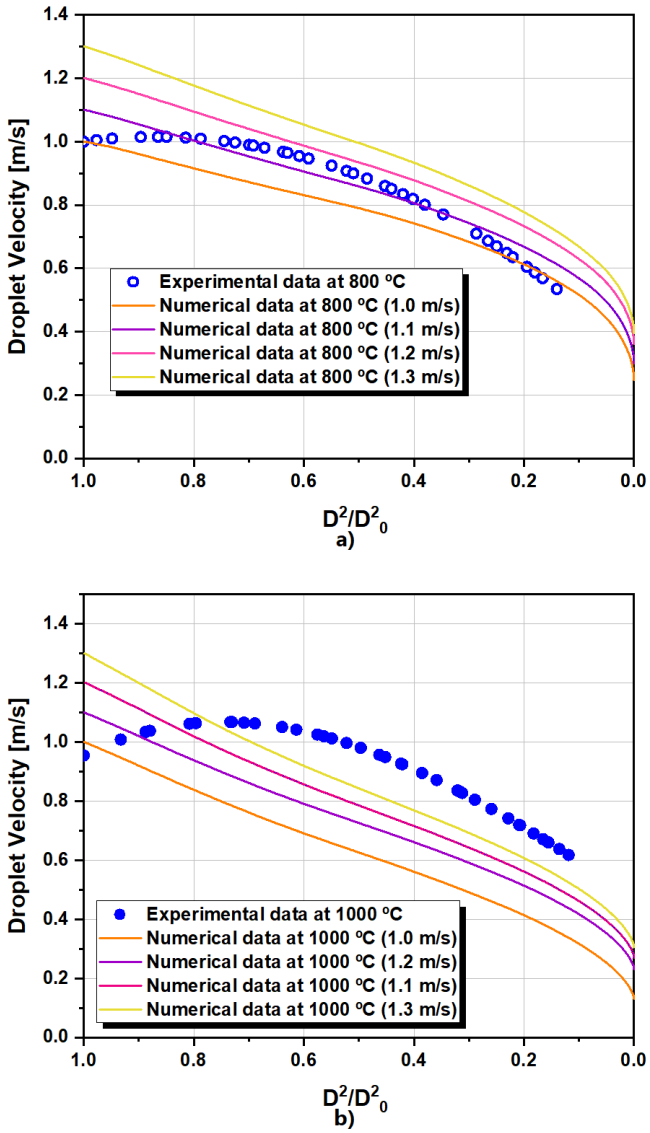

Figure 4.11: Square of the normalized droplet diameter as a function of the normalized time for different droplet initial velocities: a) T = 800 °C and b) T = 1000 °C for Jet-A1.

Additionally, there is a study of the d^2 law to each corresponding velocity conditions, as shown in Figure 4.12. Likewise the previous fuel, there is the exposure of a graph visualizing the square of the normalized droplet diameter as a function of the normalized time. In the previous analysis, the jet fuel droplets possess a higher lifetime in lower temperatures of the drop tube furnace. The initial droplet velocity variation assumes a respective d^2 curve, and the correspondent graph reveals that the different d^2 curves are coincident, indicating

identical lifetimes. Similar to the n-dodecane, the computed error between the various d^2 obtained curves, exhibits a negligible value of $2\ \%$. It was notified that the variation of the initial velocity results in similar outcomes to the n-dodecane research, exposing agreement with the literature interpretations [75].

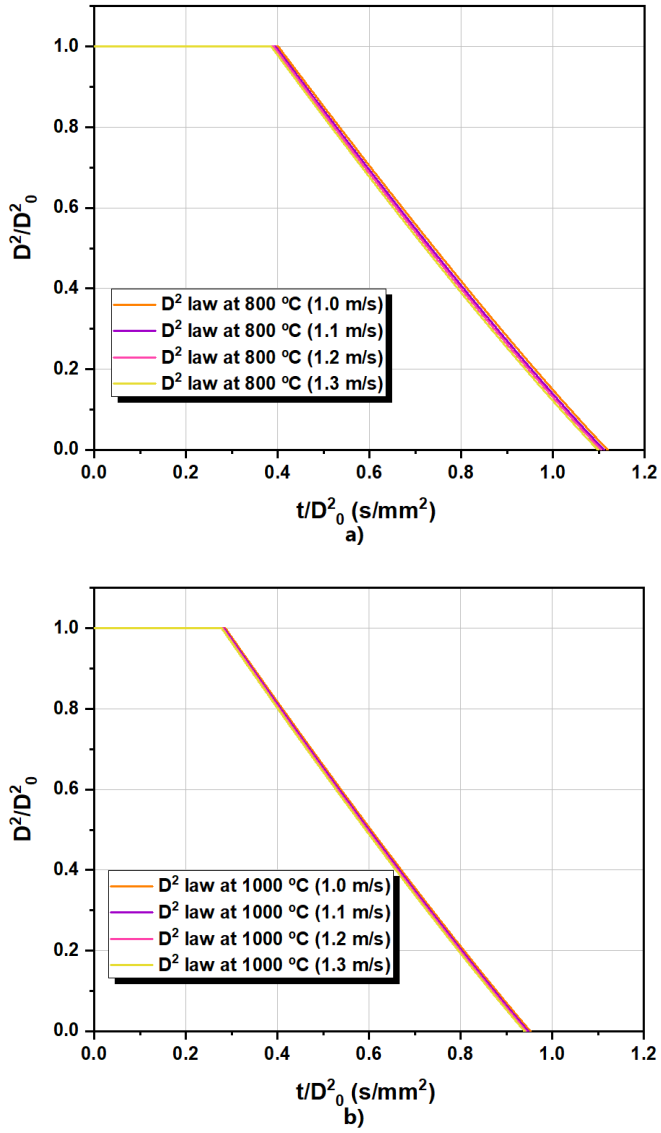

Figure 4.12: Square of the normalized droplet diameter as a function of the normalized time for different initial droplet velocities: a) T = 800 °C and b) T = 1000 °C for Jet-A1.

Regarding the n-hexadecane combustion characteristics, there is also a study about the path followed by these droplets. Likewise the previous fuels the procedure is represented by Figure 4.19 depicting the trajectory performed by n-hexadecane droplets correlated with the reduction of the droplet diameter. Analogous to the previous fuels simulations, there is a phase where the droplet achieves the boiling point and an additional phase describing the evaporation process alongside the conducted distance. The Figure 4.19 exhibits the ignition of the droplet, for T = 800 °C occurs approximately 3.5 cm below the injector tip, and for T = 1000 °C the ignition region occurs at $2.5\ cm$. This evidence reveals that this n-alkane

possesses a notable discrepancy between the two distinct temperature cases. However, the region where the ignition occurs is within the visualization window described in the experimental works of Ferrão et al. [7–9] and Pacheco et al. [6]. The obtained ignition regions reveal accordance with experimental results validating the numerical approach. Concerning the curves, a similar tendency for the different temperatures is expected. Even though the n-hexadecane curve for 800 °C reveals a more extensive performed path in the domain. This occurs due to the increase of time achieving the boiling point provoking the droplet to ignite farther from the tip of the injector. The result regarding this fuel also reveals agreement with the enhancement of combustion characteristics alongside the increment of the ambient temperature [64–66].

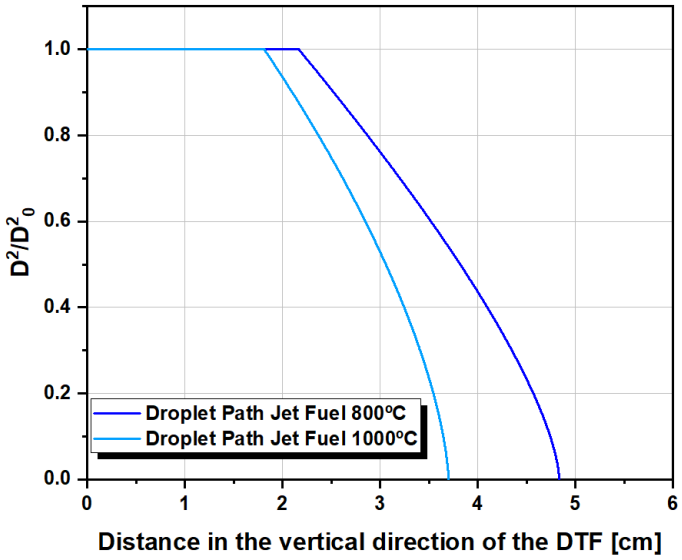

Figure 4.13: Comparison between the different ambient temperatures, T= 800 °C and T = 1000 °C and the respective droplet path within the domain for Jet-A1.

Similarly to the previous analysis, the study of the temperature evolution and ignition time ($\Delta\ t_{ig}$) requires testing and interpretation for jet fuel. The boiling point of jet fuel is rather complicated to obtain due to its multicomponent nature, yet the employed software assumes 479.15 K. As previously performed, the required schematic is exhibited in Figure 4.14 where the temperature of the droplet evolves throughout the adimensional time. The boiling points are achieved through a linear function since the droplet injection, revealing the same tendency of temperature evaluation for both cases. Regarding the reaching of the boiling point to both temperature environments for both cases T = 800 °C and T = 1000 °C the adimensional time is near being around $t/D_0^2 = 0.35\ s/mm^2$. However, as expected the amount of time to arise to the boiling point for the ambient with lower temperature is greater when analogized with the experiment at 1000 °C. This suggests that the phenomenon is anew enhanced with the increase of temperature. Hence, this data indicates the increase of the droplet total lifetime in lower ambient temperatures causing the droplets to delay the ignition time, which is once again in agreement with what is reported throughout the literature [67]. Conversely to n-dodecane, the differences between the two ambient temperatures are less prominent. This

indicates the influence of the jet fuel nature within the temperature where the combustion is occurring.

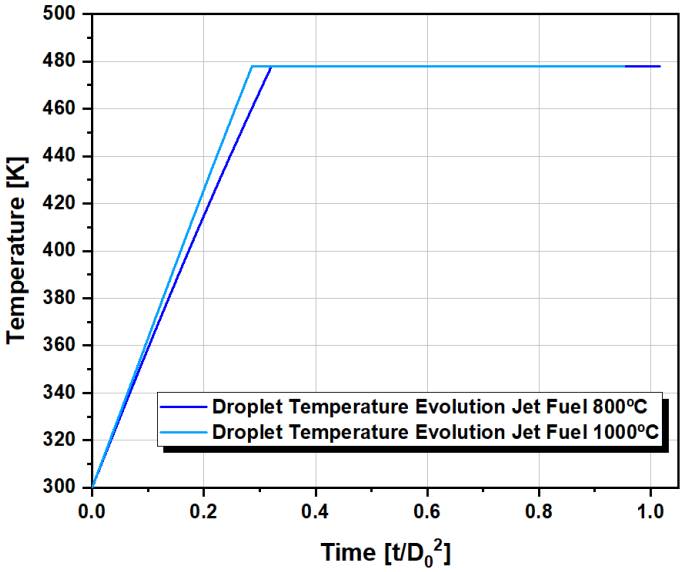

Figure 4.14: Comparison between the different ambient temperatures, T = 800 °C and T = 1000 °C and the respective temperature evolution within the domain for Jet-A1.

4.2.3 Combustion of n-hexadecane

The HVO is nowadays a biofuel with the potential to overcome the current domain of jet fuel in the air transport fleet. This information requires further study to unveil the potential of this fuel, which justifies the intent to model the burning characteristics. The combustion of HVO is complex to model since it is a multicomponent fuel. This concern is conceivable to overcome since the literature appoints simplifications in the multicomponent nature, employing specific approaches, simplifying the modeling complexities. Hence, the goal of this research concerns the feasibility of assuming the HVO combustion considering only a single component, standing in this study as the n-hexadecane. The choice of n-hexadecane is justified since is known as one of the heaviest components [85]. Besides that, there is information regarding its combustion in a CHEMKIN file further acquired. The implemented model is more likely to achieve corresponding errors in this fuel. Such fact is due to the single component assumption that simplifies the physical phenomenon. The experimental data employed to asset the accuracy of the model is obtained from the experimental equipment previously mentioned [6–9]. Figure 4.15 depicts the square of the normalized droplet diameter as a function of the normalized time, in this case for n-hexadecane. Similar to the previous analysis, the experimentally obtained HVO does not possess the heating phase visible in the numerical information. The comparison between experimental data and the numerical outcomes is thus entirely feasible after the $t/D_0^2 = 0\ s/mm^2$ instant. Noteworthy that the numerical information is considering the n-hexadecane an assumption of the experimental HVO results. The results show a generally good agreement between experimental and numerical results. In spite of the good agreements, this fuel reveals more noticeable discrepancies in the d^2 analysis of experimental and numerical data. These effects are justified

by the simplification of the simulation. Likewise, in the previous cases, the increase of the furnace temperature stimulates the combustion of the fuel, following what stated [64–66]. This observation is revealed due to the decrease of the droplet heating phase and evident total droplet lifetime with the increment from T = 800 °C to T = 1000 °C.

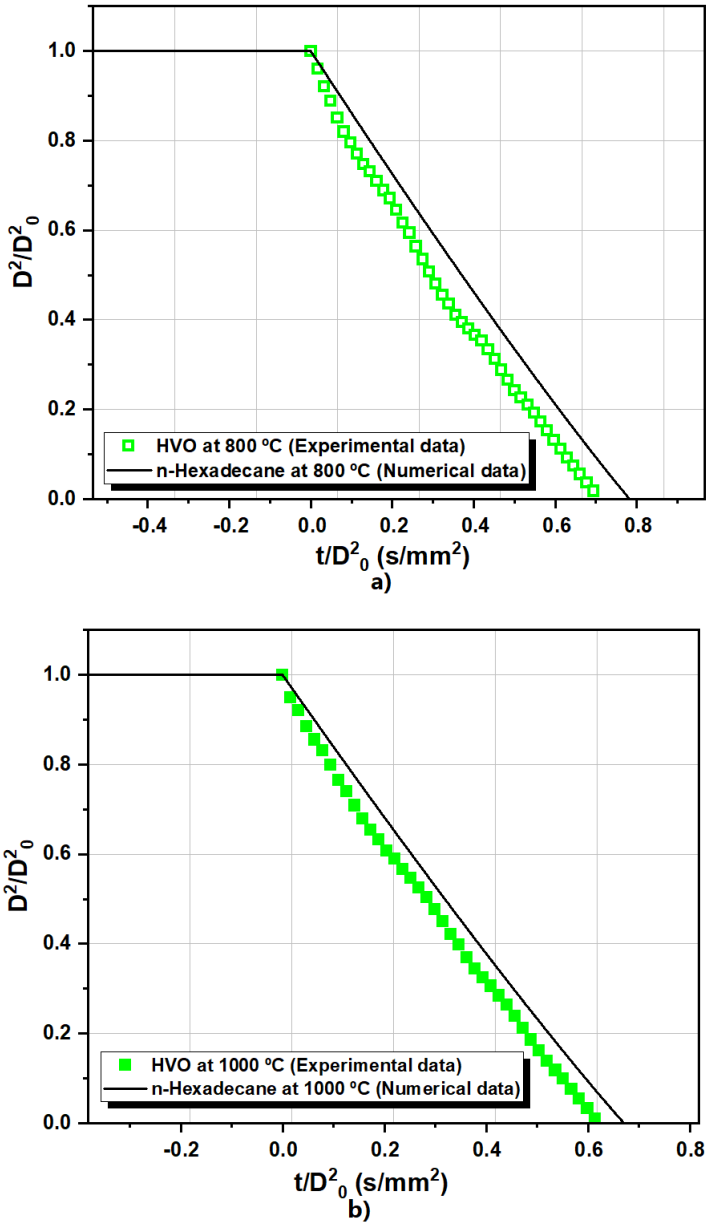

Figure 4.15: Square of the normalized droplet diameter as a function of the normalized time: a) T = 800 °C and b) T = 1000 °C for n-hexadecane.

The increase of ambient temperature also increases the droplet burning rate alongside revealing that at each temperature and in both experimental and numerical results, the n-hexadecane droplets are the ones that reveal a higher lifetime. Concerning the burning rate, it is visible in experimental and numerical data a decrease in the burning rate of this fuel for both conditions in comparison with the jet fuel, similar to what was obtained in [6].

The n-hexadecane simulations also require a study on the velocity of the droplet throughout the domain. Once again, for n-hexadecane, the assumption of initial droplet velocity is according to the experimentally obtained information. This parameter is then employed in the combustion model and verified the droplet velocity throughout the reduction of the droplet diameter. As noted, the droplet velocity reduction alongside the decrease of the droplet diameter reveals tendencies identical to the other tested fuels and the literature [72–74]. This information is visible in Figure 4.16 where is seen the numerical data regarding the simulation considering $1\ m/s$ as initial velocity compared with the tendency line developed from the HVO experimental outcomes. There is an evident disparity between the experimentally obtained data trend line and the numerical curve of $1\ m/s$, which was visible for both ambient temperatures, similar to what was obtained with jet fuel. These discrepancies may be justified due to the performed approximations.

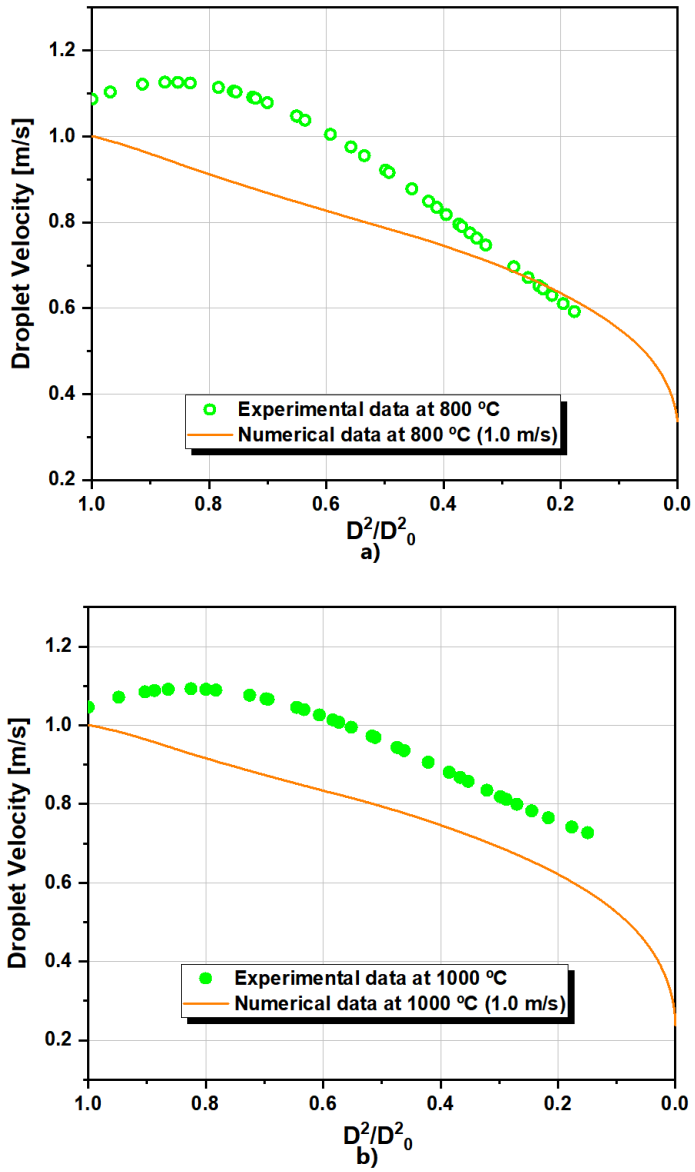

Figure 4.16: Droplet Velocity as a function of the square of the normalized droplet diameter for $1\ m/s$: a) T $= 800$ °C and b) T $= 1000$ °C for n-hexadecane.

The observed discrepancies between the experimental trend line and the numerical outcomes require the same procedure performed in other fuel simulations. Similarly to other fuels, Figure 4.17 displays different initial velocities curves and the corresponding decrease of the droplet diameter influencing the droplet velocity. Throughout the different simulations, the tendency of the curves reveals similarities for the various initial droplet velocities simulations. Likewise, in the jet fuel investigation, the experimental trend line data admit better accordance with higher initial velocity curves. Concerning the T $= 800$ °C experiment, after a divergent beginning, there is a resemblance following the trend of the $1.2\ m/s$ curve, yet the experimental trend line starts to follow the tendency observed by the $1\ m/s$ numerical curve at the end of the droplet lifetime. Regarding the T= 1000 °C experiment, the experimental trend line tends to approximate to the $1.2\ m/s$ numerical curve after beginning, where diverges from the numerically obtained curves. Generally, there is good agreement with the other fuels intends and the literature, where the droplet velocity reduces alongside the reduction of diameter at each considered initial velocity [72–74].

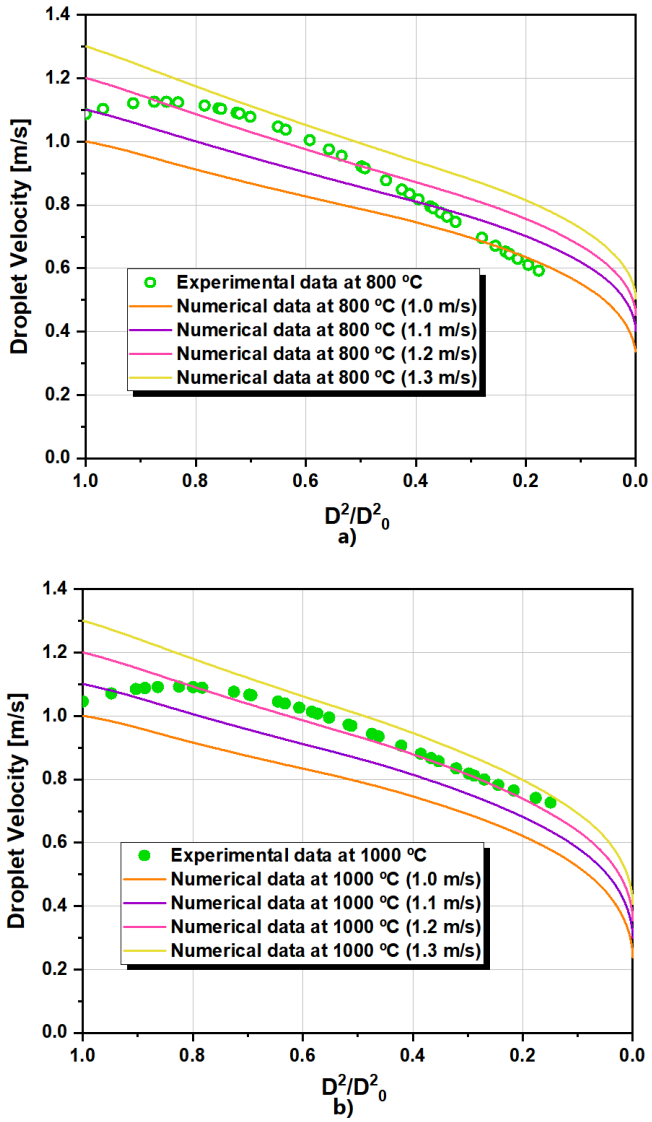

Figure 4.17: Square of the normalized droplet diameter as a function of the normalized time for different droplet initial velocities: a) T= 800 °C and b) T $= 1000$ °C for n-hexadecane.

As performed to other fuels, there is the necessity of analyzing the d^2 law and its dependence on the initial velocity visible in Figure 4.18. Figure 4.18 exposes the square of the normalized droplet diameter as a function of the normalized time. In conformity with other simulations, the fuel droplets possess a higher lifetime in lower temperatures of the DTF. The modification of the initial velocity of the fuel droplet implemented in the model creates different curves, its definition reveals insignificant differences between the defined curves ($2\ \%$ of computed relative error). This evidence is visible in all the tested fuels, which implies that this variation of the initial velocity of the droplet is insignificant concerning certain burning characteristics of the fuel droplet, in agreement with the interpretation of [75]. The parameters that are included in this category are the heating phase of the droplet, droplet lifetime, and the burning rate of the droplet.

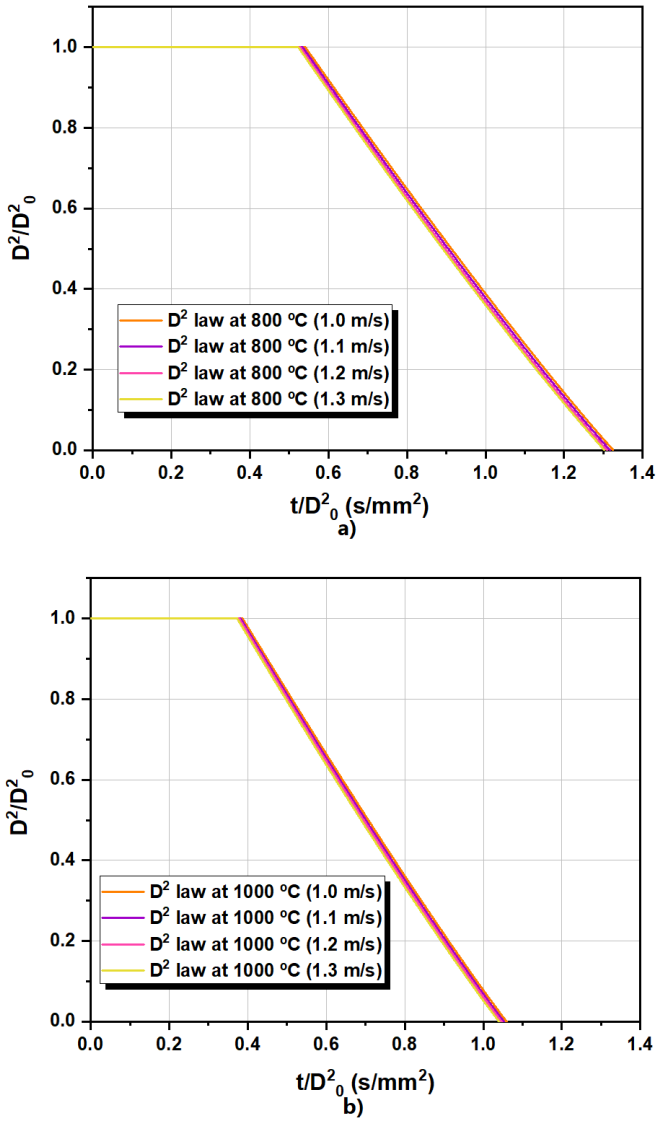

Figure 4.18: Square of the normalized droplet diameter as a function of the normalized time for different initial droplet velocities: a) T= 800 °C and b) T= 1000 °C for n-hexadecane.

Regarding the n-hexadecane combustion characteristics, there is also a study about the path followed by these droplets. Likewise the previous fuels the procedure is represented by Fig-

ure 4.19 depicting the trajectory performed by n-hexadecane droplets correlated with the reduction of the droplet diameter. Analogous to the previous fuels simulations, there is a phase where the droplet achieves the boiling point and an additional phase describing the evaporation process alongside the conducted distance. The Figure 4.19 exhibits the ignition of the droplet, for T = 800 °C occurs approximately 3.5 cm below the injector tip, and for T = 1000 °C the ignition region occurs at $2.5\ cm$. This evidence reveals that this n-alkane possesses a notable discrepancy between the two distinct temperature cases, which might be explained by the points that will be further specified about the different alkanes properties. However, the region where the ignition occurs is within the visualization window described in the experimental works of Ferrão et al. [7–9], and Pacheco et al. [6]. The obtained ignition regions reveal accordance with experimental results validating the numerical approach. Concerning the curves, a similar tendency for the different temperatures is expected. Even though the n-hexadecane curve for 800 °C reveals a more extensive performed path in the domain. This occurs due to the increase of time achieving the boiling point provoking the droplet to ignite farther from the tip of the injector. The result concerning this fuel also reveals agreement with the enhancement of combustion characteristics alongside the increment of the ambient temperature [64–66].

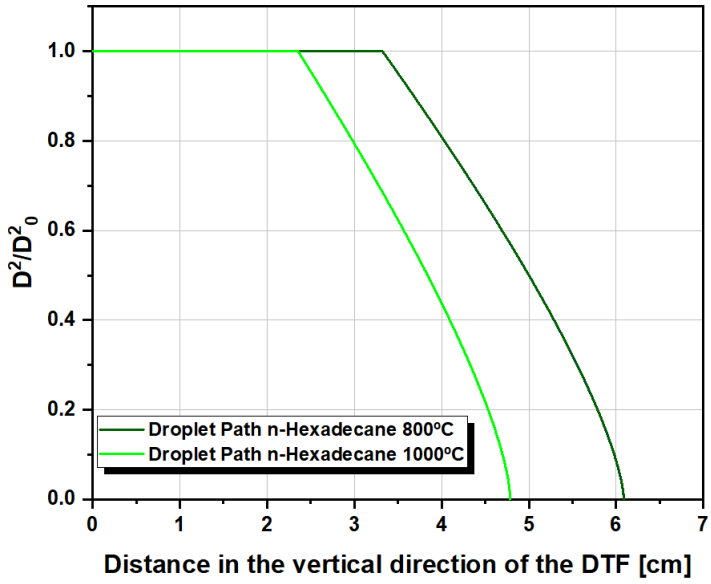

Figure 4.19: Comparison between the different ambient temperatures, T = 800 °C and T = 1000 °C and the respective droplet path within the domain for n-hexadecane.

The temperature evolution and ignition time ($\Delta\ t_{ig}$) analysis is also performed for the n-hexadecane simulation. The boiling point considered for n-hexadecane is 573.15 K which is the higher temperature for the tested fuels. Figure 4.20 shows the representation of the temperature evolution with the passage of adimensional time for the tested circumstances. The evolution of temperature until reaching the boiling point is through a linear function since the injection of the droplet. Regarding the simulation considering T = 800 °C, the droplet requires $t/D_0^2 = 0.5\ s/mm^2$ to reach the boiling point, while in T = 1000 °C the droplet achieves the boiling point after $t/D_0^2 = 0.4\ s/mm^2$. Expectedly, the adimensional time required to

reach the boiling point at T = 800 °C is larger than what evidenced for the T = 1000 °C simulation. This anew supports the idea of the increase of temperature will enhance the combustion properties, specifically in this case, the heating required time of the droplet to ignite [67]. The differences between heating times for both temperatures are notable for n-hexadecane compared to other fuels [6,79]. This evidence implies what is visible in other burning characteristics that suggest a less volatile molecular display for this fuel, which is analyzed further in this chapter.

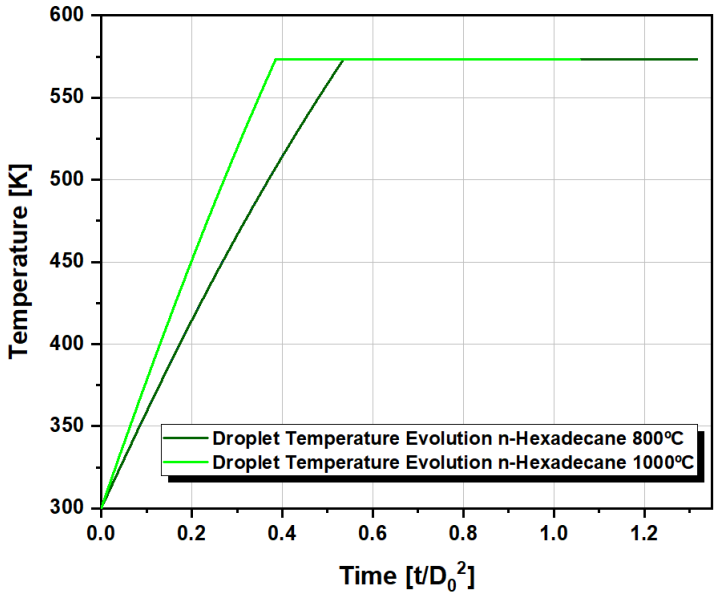

Figure 4.20: Comparison between the different ambient temperatures, T = 800 °C and T = 1000 °C and the respective temperature evolution within the domain for n-hexadecane.

The analysis of the temperature evolution and ignition time ($\Delta\, t_{ig}$) considering n-hexadecane allows further comparison with experimental data in the literature. The data is adapted from the performed researches of Faeth and Olson [80]. This work intends to study different combustion attributes for various n-alkanes and further formulation of an analytical model. One of the characteristics that are analyzed is the time that the fuel droplet takes to ignite. In this specific case, it is relevant to employ the information of the ignition time-correlated with the droplet size. Considering the researched information, it was developed a graph depicted in Figure 4.21 where there is a correlation between the ignition time of the analyzed droplet and the correspondent droplet size. Figure 4.21 adapted from the work of Faeth and Olson [80] depicts two different regions that characterize the presence of ignition considering the ignition time and the droplet size. The implementation of the study developed by [80] assumes that the ignition time for a droplet size of 215 μm is 0.0330 s for T= 800 °C and 0.0239 s for T = 1000 °C. Allocating this information to the developed Figure 4.21 , enables the creation of two points representing the combustion characteristics of both simulated temperatures. The observable dots are inside the combustion region, suggesting the presence of ignition in the conditions of this simulation, identical to the obtained numerical outcomes. Noteworthy that the operating conditions regarding the pressure and internal flow are distinct from the simulated outcomes in this dissertation.

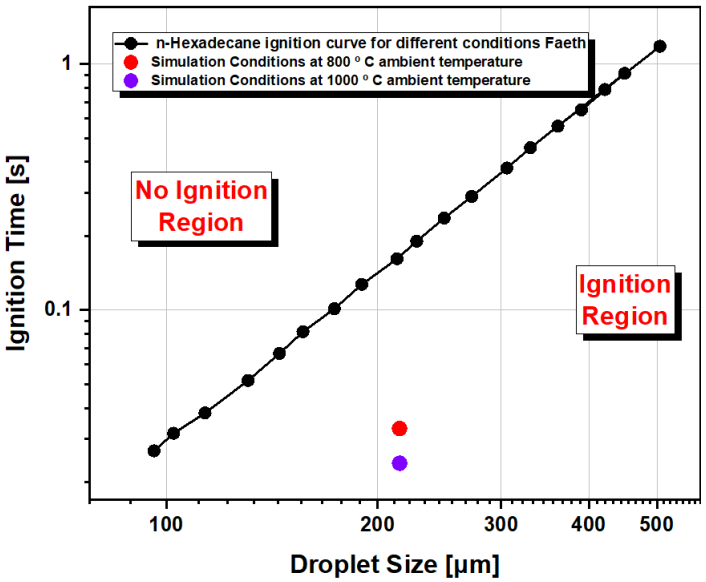

Figure 4.21: Adaption of the schematic depicted in Faeth and Olsen [80] including the conditions evaluated in the present work.

4.3 Comparison of combustion characteristics concerning the distinct fuels

Succeeding the implementation of the combustion model for each intended fuel it is relevant to examine specific characteristics within each other. This fact is justified since the dissertation aims to compare the burning behavior of traditional fossil fuels and alternative biofuels. The comparison of the burning properties of the various fuels guarantees the prudent employment of these fuels in transportation and reveals the ones who ensure better performances. In this specific study, there is the possibility to compare the d^2 law for different fuels and consequent fuel consumption. The computation of the d^2 law allows the determination of the droplet ignition time, correspondent lifetime, and the droplet burning rate.

Concerning the d^2 law curves, the information gathered from the implementation of the combustion model to the analyzed fuels is depicted in Figure 4.22, exhibiting good agreement with the equivalent experimental research portrayed in Figure 2.11 [79]. The various curves display different droplets lifetimes likely influenced by the differences regarding the heating time. The n-hexadecane fuel droplets present longer lifetimes in opposition to jet fuel having a smaller lifetime. There is a relationship between the droplet lifetime and the number of fuel carbons, and the consequent size of the molecular chain size. The lower boiling point alongside a higher vapor pressure in the fuels with lower carbons within their molecular chains may justify a faster heating phase for these fuels and consequent diminishing of the droplet lifetime. The average molecular chain of jet fuel, exhibited in Table 3.1, suggests a less apparent existence of carbons in the molecular chain in comparison with n-hexadecane, indicating that the obtained results in this study are in accordance with the studies performed by Shang et al. [79]. Noteworthy that the differences between the droplet lifetimes at the T $= 1000$ °C

experiment are less significant than at the T = 800 °C. This fact may be justified since the combustion at higher temperatures fuels tends to behave more similarly, despite the distinct presence of carbons in the molecular chains.

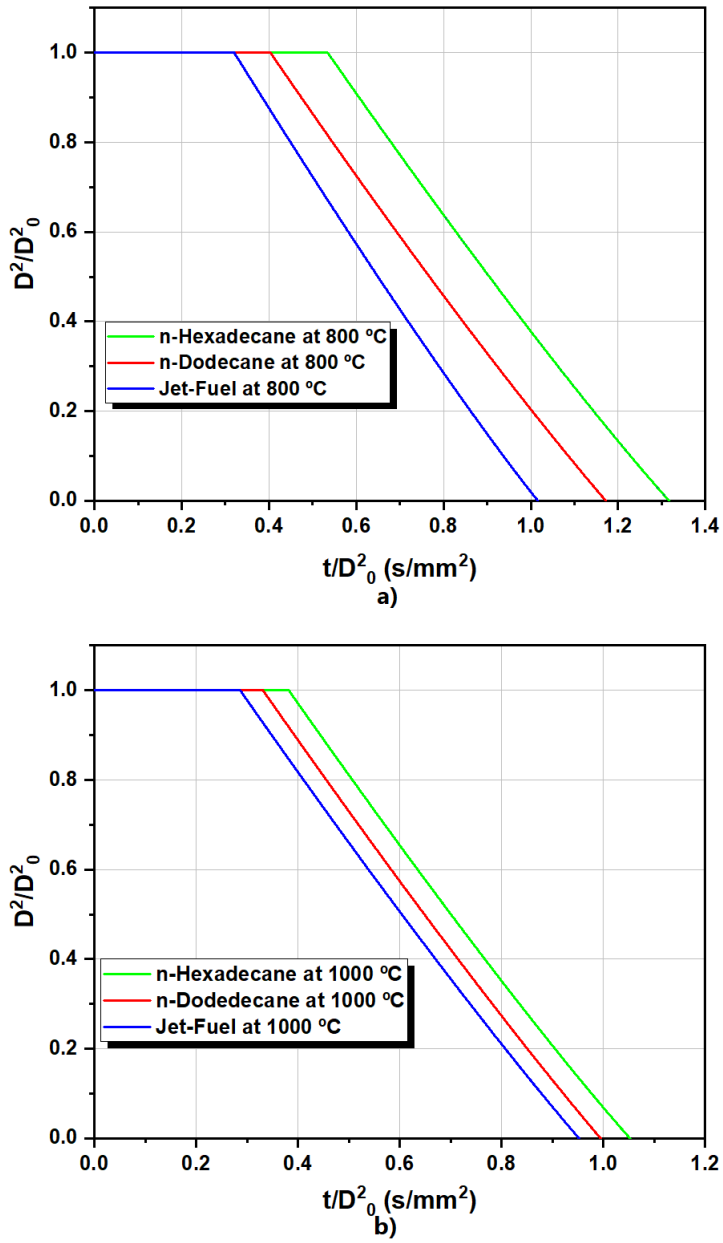

Figure 4.22: Square of the normalized droplet diameter as a function of the normalized time for the different fuels: a) T = 800 °C and b) T = 1000 °C.

The development of graphics of the d^2 law for different fuels allows the analysis of the respective burning rates. Such burning rate is the result of the decrease of the droplet diameter which permits its calculation by determinating the slope of the steady curve of the graph. This is valid for the numerically computed curve that is further compared to the experimental burning rates outcomes. Table 4.2 depicts the burning rates for the different fuels submitted to different temperatures adding the relative error between experimental and numerical results. Generally, there is a tendency between the increased temperature and the

enhancement of the burning process. This is justified since for each fuel, for experimental and numerical results, the burning rate increases whenever the ambient temperature increments from 800 °C to 1000 °C. As previously mentioned, there is a relationship between the droplet lifetime and the respective number of the carbons in the fuel chain. This evidence is also visible in the analysis of the burning rate. The numerical results validate the premise that the burning rate for single component n-alkanes decreases with the increment of the number of carbons within the molecular chain [25, 79]. In this simulation, the n-dodecane droplets for each temperature analyzed possess a higher burning rate in comparison with the n-hexadecane. The tendency is not followed with jet fuel, which is justified due to its high multicomponent nature. Lastly, the combustion model is again validated when there is a comparison between experimental and numerical data. Globally, for the fuels employed there is an acceptable margin of relative error between the experimentally calculated burning rate and the numerically obtained. The most significant error is around 11 % while the less notable is 6 %, which clarifies the accuracy of the employed model. Comparing the different fuels, it is evident that jet fuel reveals higher precision in the obtained results, this may be justified due to the detailed information provided by the utilized software regarding this particular fuel.

Fuels	**Temperatures [°C]**	**Approach**	**Burning Rates [mm^2/s]**	**Relative Error [%]**
Jet Fuel	800	Experimental	1.58	6.0
		Numerical	1.48	
	1000	Experimental	1.70	9.0
		Numerical	1.54	
n-Dodecane	800	Experimental	1.26	10.8
		Numerical	1.33	
	1000	Experimental	1.39	8.2
		Numerical	1.54	
n-Hexadecane	800	Experimental	1.47	6.1
		Numerical	1.31	
	1000	Experimental	1.66	10.9
		Numerical	1.53	

Table 4.2: Summary of the different burning rates obtained accounting for distinct fuels and conditions.

Furthermore, Figure 4.23 exhibits a comparison of the fuels utilized, respective development of the burning rate alongside a function of the normalized droplet lifetime. The comparison between T $= 800$ °C of ambient temperature and T $= 1000$ °C implies that the tendencies of behavior for both properties are similar for different conditions. Firstly, as previously noted, there is an evident decrease in the burning rate along with the increment of the number of carbons within the molecular chain. On the contrary, respecting droplet lifetime is visible an increase in the droplet lifetime alongside the same circumstances. This information reveals compliance with the studies performed by Shang et al. [79] and in Figure 2.12 adapted from this research. Additionally, throughout the simulation, it is remarked that the increase in temperature influences these properties. The burning rate will decrease with the increment

of temperature while the droplet lifetime will diminish. Figure 2.12 notably possesses evidence that yet these tendencies are visible for higher temperatures the differences between the different fuels are less significant. The distinct fuels, notify less notable differences in the combustion characteristics and thus justify the premise that the increase of temperature suggests a standardization of the combustion behavior of the distinct analyzed fuels.

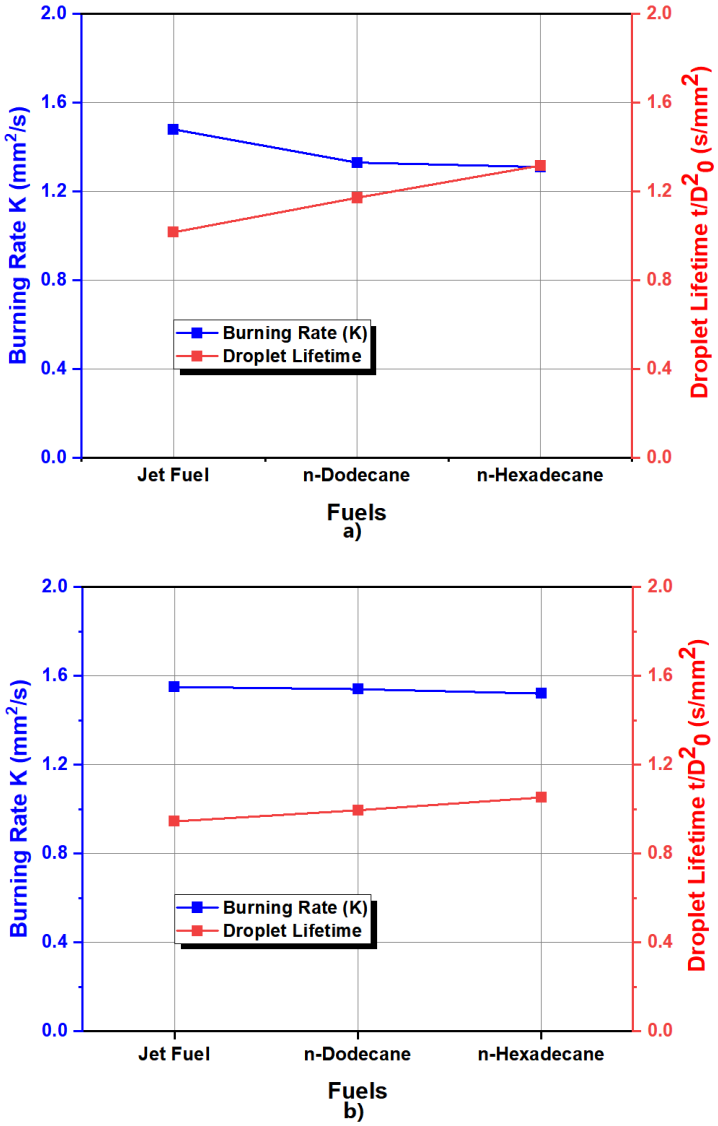

Figure 4.23: Evolution of the mean burning rates (left, blue) and normalized combustion duration (right, red) with jet fuel and the different n-alkane droplets : a) T = 800 °C and b) T = 1000 °C.

Chapter 5

Conclusions and Future Work

The final chapter of this dissertation possesses two distinct sections. The first section portrays the delineated conclusions generated throughout the research performed in the dissertation. The conclusions regard the numerical approach utilized to model the single droplet combustion phenomenon of different alkanes. Furthermore, the second section is dedicated to enumerating the recommendations for future work that are feasible to be performed to improve the knowledge concerning this theme.

5.1 Conclusions

The performed simulations accurately predict single droplet combustion under high ambient temperature. The obtained outcomes ensure the validation of this mathematical approach to correctly replicate the combustion intended phenomena. The Euler-Lagrange approach reveals a precise replication of the intended event inducing to several conclusions when analysed the obtained results of both continuous and discrete phases. In order to correctly scrutinize the results it is relevant the comparison between experimental and numerical data.

Concerning the continuous phase, it was obtained velocities and temperature fields of the flow. The comparison with the experimental data reveals that the temperature profiles of the simulation are similar to the temperatures gathered from the experimental apparatus. This data is further validated by the numerical results of fuel combustion that suggest that the droplets ignite in the stabilization region of the temperature profiles, as visualized and feasible for comparison in Figure 4.2 and Figure 4.3. This information reassembles the outcomes from the velocity magnitude throughout the domain that reveals similarities to the experimentally intended flow disposition. The simulation information regarding the continuous phase and respective comparison with the experimental data concludes that the Euler-Lagrange approach and corresponding utilization of the k-ε to model the domain turbulence is accurate to the physical event. Additionally, the analysis of the y^+ and the discretization displays exactness in predicting the conditions of the DTF when comparing the obtained data with the experimental information.

The discrete phase simulation information concerns mainly the outcomes of the droplet fuel combustion further compared to the experimentally acquired data. The data concerning the decrease of the diameter correlated with the droplet lifetime suggests an accurate simulation following the d^2 law that further reveals conformity with the experimentally obtained data. This notification demonstrates the precision of this method in accurately predicting the com-

bustion characteristics of the burning fuel droplets. The results indicate that for each tested fuel and condition, the simulation fits with the experimental data and the literature widely researched d^2 law.

The droplet velocities are possible to be modeled throughout the domain and correlated with the decrease of the droplet diameter. This information is then validated with experimental data and reveals acceptable accuracy. The droplet velocity tendentially decreases with the reduction of the droplet diameter conforming with experimental data, yet some factors might influence the analysis. The initial droplet velocity was revealed to affect the droplet velocity versus the droplet reduction, which will possess a decline of the droplet velocity at higher values. On the contrary, the variation of the initial velocity does not reveal modifications in the droplet lifetime. These results were verified for distinct temperature conditions and fuels and further compared with experimental data, which suggests the credibility of these findings.

An increase in air temperature has crucial relevance within the combustion characteristics of the fuel droplets. The increase of the air temperature revealed for each tested fuels a decrease of the droplet lifetime. In addition, the increment of the ambient temperature indicated an increase in the droplet burning rate and a reduction in the ignition time. This information is further coupled with the evidence that at higher ambient temperatures the droplet ignites nearer the tip of the injector and achieves the boiling point faster. The knowledge is then certified by realizing additional comparisons with experimental data to the accuracy of the acquired information. The obtained outcomes suggest that the increment of the environment temperature enhances the combustion of the fuel droplets for each tested fuel.

The type of fuel and its chemical composition possess significant relevancy in acknowledging the improvement of the combustion performance and respective enhancing of the fuel burning characteristics. For the same involved ambient conditions, the n-hexadecane reveals lower burning rates and higher droplet lifetimes when compared with jet fuel and n-dodecane. This information aligns with the ignition time that is higher for n-hexadecane and alongside the outcomes of the time required to achieve the boiling point. These results are similar to the information of the ignition location for n-hexadecane being farther from the tip of the injector. The outcomes reveal that the chemical composition of the fuel influences the burning characteristics, which are also observed with the experimental data. Additionally, these characteristics require evaluation for different temperatures, revealing the burning occurring at higher temperatures and suggesting a less notorious difference between the distinct employed fuels. The information gathered, suggests an influence in the increment of temperature has a role in uniformizing combustion.

5.2 Future Work Recommendations

The results obtained in this dissertation provide an initial workplace for the numerical analysis of the phenomenon of single droplet fuel combustion through an Euler-Lagrange approach for Jet Fuel and Alkanes. Nevertheless, several points can be specialized and improved to increase the precision of the simulations.

Firstly, it is relevant to remark that the system utilized by the ANSYS Fluent that computes the flamelet diffusion and the consequent emissions and products of combustion is rather rudimentary whenever compared to the complexity of the phenomena. Hence, the development of a model that can predict accurately the flamelet diffusion as well as the flame temperature and emission of the combustion process would be a beneficial point to increment the accuracy of the simulation. The model employed has good agreement with the experimental data since most of the information obtained experientially is related to the discrete phase that is less influenced by the problematics of the model. However, a more complex model would be required for extra analyses regarding the flame occurrence and the flame diffusion associated with combustion phenomena and the continuous phase.

Secondly, the HVO (Hydrotreated Vegetable Oil) as stated, is approximated to n-hexadecane. However, the employed software enables the modeling of multicomponent evaporation and respective combustion. Perhaps, the accounting for the multicomponent nature of the HVO for the elements that possess a higher percentage of its composition would represent even greater accordance between experimental and numerical data.

Lastly, the implementation of the nanoparticles of aluminum in the HVO fuel droplets is the next logical step for future work. The work developed by Ferrão et al. [7–9] in the field of the addition of nanoparticles of aluminum in order to improve the combustion characteristics of the HVO has been mesmerizing, and the existence of additional numerical data comparable with the experimental results could possess paramount importance. The implementation of these attributes has already been studied before with the addition of radiation models that account for the droplet alteration of emissivity due to the incorporation of the particles. These procedures ensure the simplification of the complexity of the model and require further study and implementation.

Bibliography

[1] D. S. Lee, D. W. Fahey, P. M. Forster, P. J. Newton, R. C. Wit, L. L. Lim, B. Owen, and R. Sausen, "Aviation and global climate change in the 21st century," *Atmospheric Environment*, vol. 43, no. 22-23, pp. 3520–3537, 2009.

[2] V. Smil, *Energy transitions: global and national perspectives*, 2nd ed. ABC-CLIO, 2016.

[3] S. Blakey, L. Rye, and C. W. Wilson, "Aviation gas turbine alternative fuels: A review," *Proceedings of the Combustion Institute*, vol. 33, no. 2, pp. 2863–2885, 2011.

[4] A. H. Lefebvre, *Gas turbine combustion*, 2nd ed. CRC press, 1998.

[5] L. Peskett, R. Slater, C. Stevens, A. Dufey *et al.*, "Biofuels, agriculture and poverty reduction," *Natural resource perspectives*, vol. 107, pp. 1–6, 2007.

[6] G. Pacheco, A. Silva, and M. Costa, "Single-Droplet Combustion of Jet A-1, Hydroprocessed Vegetable Oil, and Their Blends in a Drop-Tube Furnace," *Energy & Fuels*, vol. 35, no. 9, pp. 7232–7241, 2021.

[7] I. Ferrão, A. R. Silva, A. S. Moita, M. A. Mendes, and M. M. Costa, "Combustion characteristics of a single droplet of hydroprocessed vegetable oil blended with aluminum nanoparticles in a drop tube furnace," *Fuel*, vol. 302, pp. 121 – 160, 2021.

[8] I. Ferrão, M. A. Mendes, A. Moita, and A. Silva, "Single droplet combustion of aluminum nanoparticles added to a biofuel: effect of particle concentration and ambient temperature," in *International Conference on Liquid Atomization and Spray Systems (ICLASS)*, vol. 1, no. 147, 2021.

[9] I. Ferrão, A. S. Moita, M. A. Mendes, and A. R. Silva, "The influence of aluminum particles in a Hydroprocessed Vegetable Oil combustion," *European Combustion Meeting (ECM)*, vol. 1, 2021.

[10] D. de Almeida Vasconcelos Rodrigues, "VOF Method: Numerical Analysis of Single Droplets Impinging upon Liquid Films," Master's thesis, Aerospace Science Department, University of Beira Interior, Covilhã, 2018.

[11] I. Abrantes, "Sustainable aviation fuels and imminent technologies - CO2 emissions evolution towards 2050," Master's thesis, Aerospace Science Department, University of Beira, Covilhã, 2021.

[12] D. Ribeiro, “Experimental Study of a Single Droplet Impinging upon Liquid Films: Jet Fuel and Biofuel Mixtures,” Master’s thesis, Aerospace Science Department, University of Beira Interior, Covilhã, March 2018.

[13] Pedro Pinto, “Collision Dynamics of a Single Droplet onto a Heated Dry Surface: Jet Fuel and HVO Mixtures,” Master’s thesis, Aerospace Science Department, University of Beira Interior, Covilhã, 2021.

[14] João Cardoso, “Design and Fabrication of a Low Cost, Push Mode Piezoelectric Stream Droplet Generator with Interchangeable Nozzle,” Master’s thesis, Aerospace Science Department, University of Beira Interior, Covilhã, 2021.

[15] P. Forster, A. Jain, M. Ponater, U. Schumann, W. Wang, T. Wigley, D. Wuebbles, and D. Yihui, “Potential Climate Change from Aviation,” *Aviation and the Global Atmosphere: A Special Report of the Intergovernmental Panel on Climate Change*, vol. 185, 1999.

[16] International Air Transport Association, “IATA Sustainable Aviation Fuel Roadmap,” International Air Transport Association, 2015.

[17] B. Tam and C. Neumann, “A human health assessment of hazardous air pollutants in Portland, OR,” *Journal of Environmental Management*, vol. 73, no. 2, pp. 131–145, 2004.

[18] H. A. Shahad and S. K. Wabdan, “Effect of operating conditions on pollutants concentration emitted from a spark ignition engine fueled with gasoline bioethanol blends,” *Journal of Renewable Energy*, vol. 2015, 2015.

[19] N. Radovan, H. Michal, and P. Štefan, “Emission Controls Using Different Temperatures of Combustion Air,” *The Scientific World Journal*, vol. 2014, 2014.

[20] S. W. Kim, A. Heckel, S. A. McKeen, G. J. Frost, E. Y. Hsie, M. K. Trainer, A. Richter, J. P. Burrows, S. E. Peckham, and G. A. Grell, “Satellite-observed U.S. power plant NOx emission reductions and their impact on air quality,” *Geophysical Research Letters*, vol. 33, no. 22, 2006.

[21] ScienceDaily, “Ocean carbon uptake widely underestimated,” *https://www.sciencedaily.com/releases/2020/09/200904090312.htm*, September 4,2020 , acess. April,2021.

[22] U. of Concerned Scientists, “CO2 and Ocean Acidification: Causes, Impacts, Solutions,” *https://www.ucsusa.org/resources/co2-and-ocean-acidification*, January 30,2019, acess. April,2021.

[23] G. L. Stephens and S. A. Tjemkes, “Water vapour and its role in the earth’s greenhouse,” *Australian Journal of Physics*, vol. 46, no. 1, pp. 149–166, 1993.

[24] Y. Liu, X. Sun, V. Sethi, D. Nalianda, Y.-G. Li, and L. Wang, “Review of modern low emissions combustion technologies for aero gas turbine engines,” *Progress in Aerospace Sciences*, vol. 94, pp. 12–45, 2017.

[25] P. Coelho and M. Costa, *Combustão*, 2nd ed. Orion, 2012.

[26] M. Uchida and Y. Akasaka, “A Comparison of Emissions from Clean Diesel Fuels.” *SAE transactions*, vol. 108, pp. 483–488, 1999.

[27] R. Sadeghbeigi, “Chapter 3 - FCC Feed Characterization,” in *Fluid Catalytic Cracking Handbook*, 3rd ed. Oxford: Butterworth-Heinemann, 2012, pp. 51–86.

[28] Council of European Union, “Council regulation (EU) no 836/2011,” 2011, https://eur-lex.europa.eu/legal-content/EN/TXT/?uri=CELEX

[29] K. Abed, M. Gad, A. El Morsi, M. Sayed, and S. A. Elyazeed, “Effect of biodiesel fuels on diesel engine emissions,” *Egyptian Journal of Petroleum*, vol. 28, no. 2, pp. 183–188, 2019.

[30] EASA - European Union Aviation Safety Agency, “SULPHUR - Reduction of sulphur limits in aviation fuel standards,” 2010,acess. February,2021, https://www.easa.europa.eu/document-library/research-reports/easa2008c11.

[31] V. Poloczek and H. Hermsmeyer, “Modern gas turbines with high fuel flexibility,” *Power-Gen Asia, Kuala Lumpur, Malaysia*, vol. 200, no. 8, 2008.

[32] B. Sen and E. M. Goodger, “Alternative fuels, chemical energy resources,” *Journal of Chemical Education*, vol. 58, no. 12, p. A382, 1980.

[33] European Biofuels Technology Platform, “Biofuel Fact Sheet-Fatty Acid Methyl Esters (FAME),” 2011, Biofuel Fact Sheet - EN14214.

[34] G. Hemighaus, T. Boval, C. Bosley, “Aviation Fuels Technical Review,” 2005, Chevron Corporation Technical Report.

[35] A. de Klerk, “Fischer–Tropsch fuels refinery design,” *Energy & Environmental Science*, vol. 4, no. 4, pp. 1177–1205, 2011.

[36] Ø. Vessia, “Biofuels from Lignocellulosic Material,” 2005, Norwegian University of Science and Technology Project Report.

[37] E. F. Sousa-Aguiar, L. G. Appel, and C. Mota, "Natural gas chemical transformations: The path to refining in the future," *Catalysis Today*, vol. 101, no. 1, pp. 3–7, 2005.

[38] M. C. Vasquez, E. E. Silva, and E. F. Castillo, "Hydrotreatment of vegetable oils: A review of the technologies and its developments for jet biofuel production," *Biomass and Bioenergy*, vol. 105, pp. 197–206, 2017.

[39] T. K. Hari, Z. Yaakob, and N. N. Binitha, "Aviation biofuel from renewable resources: Routes, opportunities and challenges," *Renewable and Sustainable Energy Reviews*, vol. 42, pp. 1234–1244, 2015.

[40] J. G. Speight, *The chemistry and technology of petroleum*, 1st ed. CRC press, 1999, vol. 5.

[41] ASTM D 1655, " Standard Specification for Aviation Turbine Fuels, American Society for Testing and Materials," 2015.

[42] B. International, "Jal to fly on camelina," *https://biofuels-news.com/news/jal-to-fly-on-camelina-2/*, Dec 17, 2008, acess. February,2021.

[43] G. Godsave, "Studies of the combustion of drops in a fuel spray—the burning of single drops of fuel," *Fourth Symposium (International) on Combustion*, vol. 4, no. 1, pp. 818–830, 1953.

[44] D. Spalding, "The combustion of liquid fuels," *Symposium (International) on Combustion*, vol. 4, no. 1, pp. 847–864, 1953.

[45] A. Williams, "Combustion of droplets of liquid fuels: A review," *Combustion and Flame*, vol. 21, no. 1, pp. 1–31, 1973.

[46] G. Faeth, "Evaporation and combustion of sprays," *Progress in Energy and Combustion Science*, vol. 9, no. 1-2, pp. 1–76, 1983.

[47] C. K. Law, "Heat and mass transfer in combustion: Fundamental concepts and analytical techniques," *Progress in energy and combustion science*, vol. 10, no. 3, pp. 295–318, 1984.

[48] W. A. Sirignano, "Fuel droplet vaporization and spray combustion theory," *Progress in Energy and Combustion Science*, vol. 9, no. 4, pp. 291–322, 1983.

[49] A. H. Lefebvre, "Properties of sprays," *Particle & Particle Systems Characterization*, vol. 6, no. 1-4, pp. 176–186, 1989.

[50] W. E. Ranz and W. R. Marshall, "Evaporation from Drops. Part I," *Chemical Engi-*

neering Progress, vol. 48, no. 3, pp. 141–146, 1952a.

[51] W. Ranz and W. R. Marshall, "Evaporation from Drops. Part II," *Chemical Engineering Progress*, vol. 48, no. 3, pp. 173–180, 1952b.

[52] W. A. Sirignano, *Fluid Dynamics and Transport of Droplets and Sprays*, 2nd ed. Cambridge University Press, 1999.

[53] S. R. Turns, *Introduction to combustion*. McGraw-Hill Companies, 1996, vol. 287.

[54] F. A. Williams, "On the Assumptions Underlying Droplet Vaporization and Combustion Theories," *The Journal of Chemical Physics*, vol. 33, no. 1, pp. 133–144, 1960.

[55] A. Hall, "Experimental temperature gradients in burning drops," *Symposium (International) on Combustion*, vol. 7, no. 1, pp. 399–406, 1958.

[56] H. Hiroyasu, T. Kadota, and T. Senda, "Droplet evaporation on a hot surface in pressurized and heated ambient gas," *Bulletin of JSME*, vol. 17, no. 110, pp. 1081–1087, 1974.

[57] R. Matlosz, S. Leipziger, and T. Torda, "Investigation of liquid drop evaporation in a high temperature and high pressure environment," *International Journal of Heat and Mass Transfer*, vol. 15, no. 4, pp. 831–852, 1972.

[58] C. Law and F. Williams, "Kinetics and convection in the combustion of alkane droplets," *Combustion and Flame*, vol. 19, no. 3, pp. 393–405, 1972.

[59] G. Hubbard, V. Denny, and A. Mills, "Droplet evaporation: Effects of transients and variable properties," *International Journal of Heat and Mass Transfer*, vol. 18, no. 9, pp. 1003–1008, 1975.

[60] J. L. Gregg and E. Sparrow, "An Engineering Approach to the Variable Fluid Property Problem in Free Convection," 1956, NASA Technical Reports.

[61] S. Basu and A. Miglani, "Combustion and heat transfer characteristics of nanofluid fuel droplets: A short review," *International Journal of Heat and Mass Transfer*, vol. 96, pp. 482–503, 2016.

[62] A. G. Merzhanov and I. P. Borovinskaya, "A new class of combustion processes," *Combustion Science and Technology*, vol. 10, no. 5-6, pp. 195–201, 1975.

[63] C. E. Brennen, *Fundamentals of multiphase flow*, 1st ed. Cambridge university press, 2005.

[64] C.-H. Wang, K.-H. Shy, and L.-C. Lieu, "An experimental investigation on the ignition delay of fuel droplets," *Combustion science and technology*, vol. 118, no. 1-3, pp. 63–78, 1996.

[65] S. Kotake and T. Okazaki, "Evaporation and combustion of a fuel droplet," *International Journal of Heat and Mass Transfer*, vol. 12, no. 5, pp. 595–609, 1969.

[66] I. Awasthi, D. N. Pope, and G. Gogos, "Effects of the ambient temperature and initial diameter in droplet combustion," *Combustion and flame*, vol. 161, no. 7, pp. 1883–1899, 2014.

[67] T. Saitoh, S. Ishiguro, and T. Niioka, "An experimental study of droplet ignition characteristics near the ignitable limit," *Combustion and Flame*, vol. 48, pp. 27–32, 1982.

[68] L. Chen, G. Li, and B. Fang, "Droplet evaporation characteristics of aviation kerosene surrogate fuel and butanol blends under forced convection," *International Journal of Multiphase Flow*, vol. 114, pp. 229–239, 2019.

[69] N. Froessling, "On the evaporation of falling drops," Gerlands Beitr. Geophys, Tech. Rep., 1938.

[70] G. Faeth, "Current status of droplet and liquid combustion," *Energy and combustion science*, pp. 149–182, 1979.

[71] A. Silva, "Experimental and numerical study of physical aspects of fuel processes," Ph.D. dissertation, Aerospace Science Department, University of Beira Interior, Covilhã, 2007.

[72] N. Roth, J. Wilms, and B. Weigand, "Technique for measurements of the evaporation rate of single, freely falling droplets," in *Proceedings of the 12th international symposium on application of laser techniques to fluid mechanics, Lisbon, Portugal*. Citeseer, 2004, pp. 1–10.

[73] X. Xie, Y. Li, A. Chwang, P. Ho, and W. Seto, "How far droplets can move in indoor environments–revisiting the Wells evaporation-falling curve." *Indoor air*, vol. 17, no. 3, pp. 211–225, 2007.

[74] N. Sharma, W. D. Bachalo, and A. K. Agarwal, "Spray droplet size distribution and droplet velocity measurements in a firing optical engine," *Physics of Fluids*, vol. 32, no. 2, p. 023304, 2020.

[75] Q. Chen, K. Thu, T. Bui, Y. Li, K. C. Ng, and K. Chua, "Development of a model for spray evaporation based on droplet analysis," *Desalination*, vol. 399, pp. 69–77, 2016.

[76] A. Makino and C. Law, "On the controlling parameter in the gasification behavior of multicomponent droplets," *Combustion and Flame*, vol. 73, no. 3, pp. 331–336, 1988.

[77] H. Ghassemi, S. W. Baek, and Q. S. Khan, "Experimental study on evaporation of kerosene droplets at elevated pressures and temperatures," *Combustion science and technology*, vol. 178, no. 9, pp. 1669–1684, 2006.

[78] P. Bhattacharya, S. Ghosal, and S. Som, "Evaporation of multicomponent liquid fuel droplets," *International journal of energy research*, vol. 20, no. 5, pp. 385–398, 1996.

[79] W. Shang, S. Yang, T. Xuan, Z. He, and J. Cao, "Experimental Studies on Combustion and Microexplosion Characteristics of N-Alkane Droplets," *Energy & Fuels*, vol. 34, no. 12, pp. 16 613–16 623, 2020.

[80] G. M. Faeth and D. R. Olson, "The ignition of hydrocarbon fuel droplets in air," *SAE Transactions*, pp. 1793–1802, 1968.

[81] Y. Xu, J. D. Brunson, C. T. Avedisian, Y. Shen, I. Keresztes, A. M. Condo Jr, and D. Phillips, "Burning of Algae-Derived Biofuel Droplets and Their Mixtures with Jet Fuel," *Energy & Fuels*, vol. 34, no. 1, pp. 929–935, 2019.

[82] Á. Muelas, P. Remacha, and J. Ballester, "Combustion characteristics of isolated free-falling droplets of Jet A blended with ethanol and butanol," in *Turbo Expo: Power for Land, Sea, and Air*, vol. 51067, no. 76841. American Society of Mechanical Engineers, 2018.

[83] T. Edwards and L. Q. Maurice, "Surrogate Mixtures to Represent Complex Aviation and Rocket Fuels," *Journal of Propulsion and Power*, vol. 17, no. 2, pp. 461–466, 2001.

[84] M. Lapuerta, M. Villajos, and A. Boehman, "Key properties and blending strategies of hydrotreated vegetable oil as biofuel for diesel engines," *Fuel and Energy Abstracts*, vol. 92, pp. 2406–2411, 12 2011.

[85] G. Yejun, O. Kaario, A. Tilli, M. Larmi, and F. Tanner, "A computational investigation of hydrotreated vegetable oil sprays using RANS and a modified version of the RNG k-epsilon model in OpenFOAM," *SAE*, vol. 2010-01-0739, 04 2010.

[86] B. Pizziol, M. Costa, M. O. Panão, and A. Silva, "Multiple impinging jet air-assisted atomization," *Experimental Thermal and Fluid Science*, vol. 96, pp. 303–310, 2018.

[87] D. Caudwell, J. Trusler, V. Vesovic, and W. Wakeham, "The viscosity and density of n-dodecane and n-octadecane at pressures up to 200 MPa and temperatures up to 473

K," *International Journal of Thermophysics*, vol. 25, no. 5, pp. 1339–1352, 2004.

[88] J. Shirolkar, C. Coimbra, and M. Queiroz McQuay, "Fundamental aspects of modeling turbulent particle dispersion in dilute flows," *Progress in Energy and Combustion Science*, vol. 22, no. 4, pp. 363–399, 1996.

[89] Y. Yuan and C. T. Crowe, "Particle Dispersion in Anisotropic Homogeneous Turbulence," *Particulate Science and Technology*, vol. 7, no. 3, pp. 129–137, 1989.

[90] N. Markatos, "The mathematical modelling of turbulent flows," *Applied Mathematical Modelling*, vol. 10, no. 3, pp. 190–220, 1986.

[91] B. E. Launder and D. B. Spalding, "The numerical computation of turbulent flows," in *Numerical prediction of flow, heat transfer, turbulence and combustion*. Pergamon, 1983, pp. 96–116.

[92] A. D. Gosman and E. loannides, "Aspects of Computer Simulation of Liquid-Fueled Combustors," *Journal of Energy*, vol. 7, no. 6, pp. 482–490, 1983.

[93] J. S. Shuen, L. D. Chen, and G. M. Faeth, "Evaluation of a stochastic model of particle dispersion in a turbulent round jet," *AIChE Journal*, vol. 29, no. 1, pp. 167–170, 1983.

[94] R. L. Wasserstein, "Monte Carlo Methods, Volume 1: Basics," *Technometrics*, vol. 31, no. 2, pp. 269–270, 1989.

[95] L.-P. Wang and D. E. Stock, "Stochastic trajectory models for turbulent diffusion: Monte Carlo process versus Markov chains," *Atmospheric Environment. Part A. General Topics*, vol. 26, no. 9, pp. 1599–1607, 1992.

[96] A. B. Basset, *A treatise on hydrodynamics: with numerous examples*. Deighton, Bell and Company, 1888, vol. 2.

[97] J. Boussinesq, *Théorie analytique de la chaleur mise en harmonic avec la thermodynamique et avec la théorie mécanique de la lumière: Tome I-[II]*. Gauthier-Villars, 1903, vol. 2.

[98] P. Mazur and A. Weisenborn, "The Oseen drag on a sphere and the method of induced forces," *Physica A: Statistical Mechanics and its Applications*, vol. 123, no. 1, pp. 209–226, 1984.

[99] *ANSYS® Fluent Theory Guide (Release 2021 R1)*, Ansys, Inc., 2021.

[100] W. Jones and J. Whitelaw, "Calculation methods for reacting turbulent flows: A review," *Combustion and Flame*, vol. 48, pp. 1–26, 1982.

[101] D. Kang and R. K. Strand, "Modeling of simultaneous heat and mass transfer within passive down-draft evaporative cooling (PDEC) towers with spray in FLUENT," *Energy and Buildings*, vol. 62, pp. 196–209, 2013.

[102] M. Rachner, "Die stoffeigenschaften von kerosin Jet A-1," *DLR-Mitteilungen 98-01*, no. 1, 1998, LIDO - Berichtsjahr = 2002.

[103] C. K. Westbrook, W. J. Pitz, O. Herbinet, H. J. Curran, and E. J. Silke, "A comprehensive detailed chemical kinetic reaction mechanism for combustion of n-alkane hydrocarbons from n-octane to n-hexadecane," *Combustion and Flame*, vol. 156, no. 1, pp. 181–199, 2009.

[104] S. Lapointe, K. Zhang, and M. McNenly, "Reduced chemical model for low and high-temperature oxidation of fuel blends relevant to internal combustion engines," *Proceedings of the Combustion Institute*, vol. 37, no. 1, pp. 789–796, 2019.

[105] G. Kukkadapu, S. W. Wagnon, M. Mehl, K. Zhang, C. K. Westbrook, W. J. Pitz, M. Mcnenly, S. Sarathy, A. Rodriguez, O. Herbinet *et al.*, "An updated comprehensive chemical kinetic model of C8-C20 n-alkanes." Lawrence Livermore National Lab.(LLNL), Livermore, CA (United States), Tech. Rep., 2017.

[106] C. L. Yaws, *Chemical Properties Handbook*. McGraw-Hill Education, 1999.

[107] J. Barata and A. Silva, "Numerical study of impinging droplets through a crossflow," in *40th Thermophysics Conference*, 2008, p. 3923.

[108] C. M. G. Rodrigues, "Modelling of spray-wall impingement," Ph.D. dissertation, Aerospace Science Department, University of Beira Interior, Covilhã, 2016.

[109] B. P. Leonard, "A stable and accurate convective modelling procedure based on quadratic upstream interpolation," *Computer methods in applied mechanics and engineering*, vol. 19, no. 1, pp. 59–98, 1979.